Doctoral Dissertation

Study of Antenna Analysis by Using Non-Uniform Mesh FDTD

(不等間隔メッシュのFDTD法によるアンテナ解析の研究)

December 20, 2001

Under the Supervision of

Assosiate Professor Hiroyuki Arai

Presented by

Huiling Jiang (蒋　恵玲)

Division of Electrical and Computer Engineering,
Faculty of Engineering,
Yokohama National University, Japan

Abstract

In recent years, with the proceeding of antenna's miniaturization, numerical analysis of antennas which have electrically complicated geometry is increasing. The time-domain finite-difference method (FDTD) has become the most popular numerical method for the solution of problems in electromagnet.

Numerical modeling of realistic engineering problems using the FDTD technique often requires smaller cell than that of using a uniform mesh FDTD code.

In this paper, we describe a three-dimension FDTD code by using non-uniform mesh that improves the accuracy by an assumed magnetic field component and interpolation. In second chapter of this paper, we explain the detailed formulation and algorithm of Non-Uniform Mesh.

In chapter 3, we first examine the reflection error from fine-coarse boundary because of the discontinuity. In papers be published before on subcell technique, investigation of dependence of computation error on the mesh size ratio and the fine mesh region haven't be carried out yet. In this paper, some test geometry are solved using both a uniform mesh and the non-uniform mesh FDTD scheme to validate the results and check the accuracy of the solution. We first examine the calculation accuracy due to mesh size ratio, and then investigation of how to determine the fine mesh region surrounding the object for a most small computation error will be carried out.

In chapter 4, we apply our approach to some problem, for example, analysis of monopole antenna, notch antenna which was loaded with high dielectric constant material, a top-loaded antenna which have very small structure compare to the other part of antenna, are carried out by the proposed method. By modeling antenna's fine structure compare to other part of antenna by using smaller mesh size, precise simulation is achieved by less computation resource. Non-uniform mesh FDTD algorithm is suitable for simulation of antenna that have fine structure partly.

In chapter 5, investigation of antenna-radome interaction is carried out. By using non-uniform mesh FDTD, analysis of antenna include sorrounding dielectric radome is achieved by less computation resource. Simulation and measurement of 2GHz band base station antenna is investigated. From measurement and simulation results, antenna-radome interaction become a factor that can't be ignored in antenna's design. Optimum parameter of dielectric radome for antenna's best performance is also proposed.

Contents

Chapter 1

Introduction

In recent years, the need for smaller antennas has become increasingly important because the effect of large scale integration of electronic components generally isolates the antenna as the most bulky, heavy and obtrusive part of the equipment. But it is an accepted fact that electrically smaller antennas have narrower bandwidths and poorer efficiencies than their larger counterparts. This would incur significant power losses and reduce the general efficiency of the receiver as well as increasing equipment costs. In design of small antennas, optimization of parameters by using numerical simulation is necessary.

In this chapter, we will first introduce some numerical methods that are used mainly in antenna's design and optimization. Then we will bring out a survey of the FDTD(Finite Difference Time Domain) method, about what has contributed to the popularity of the FDTD method, and some limitation in simulation of electromagnetic phenomena. In last section of this chapter, we will look back to some early work about subcell technique in FDTD analysis.

1.1 Numerical Methods for Antenna's Design and Optimization

Numerical simulation is a supplementary means in antenna's design and optimization. Usually, antenna's input characteristics(return loss and input impedance), radiation pattern, band width, current distribution, which are main characteristics of an antenna, can be obtained through numerical analysis.

About antenna's numerical simulation, many methods are used till now. For example, the geometrical theory of diffraction(GTD Method) which is suitable for parabola antenna, the moment method(MoM Method) and Induced Electromotive Force method(EMF) which are famous for wire antenna's analysis. Finite Element method(FEM) and resonant cavity method, etc. also can be given. As small antennas and low-profile antennas

increased, an simulation method that can deal with a complicated structure, problems which include multiple materials is required.

1.2 A Survey of FDTD Simulation

The finite-difference time-domain (FDTD) method is arguably the most popular numerical method for the solution of problems in electromagnetic. Although the FDTD method has existed for over 30 years, its popularity continues to grow as computing costs continue to decline. In addition, extensions and enhancements to the method are continually being published, which further broaden its appeal.

The FDTD method, as first proposed by Yee in 1966[1], is based on an explicit time-domain solution of Maxwell's equations via a volume discretization. Yee used an electric-field (E) grid offset both spatially and temporally from a magnetic-field (H) grid to obtain update equations that yield the present fields throughout the computational domain in terms of the past fields. The update equations are used in a leapfrog scheme to incrementally march the E and H fields forward in time.

Elegance of the FDTD method is in it's simplicity and its computational efficiency. The FDTD method is a highly robust technique for simulation of electromagnetic phenomena. The FDTD method has been used to solve a plethora of applications in electromagnetic. For example, electromagnetic scattering, electromagnetic pulse (EMP) simulation, bio-electromagnetic (hyperthermia, MRI, bio-hazards), antenna modeling, microwave circuit devices(linear and non-linear), EMC/EMI, electronic packaging and non-linear optics. We summarized good points, also the reason of popularity of the FDTD method as follows.

- Robustness and ease of implementation
- Computational efficiency on high performance computers
- Broad range of direct applicability
- Inhomogeneous media is inherently modeled
- Lossy, non-linear and anisotropy media supported
- Boundary conditions are inherently represented
- Broad band response obtained with single simulations

To sum up the major characteristics of FDTD analysis, several points can be given as follows:

Central Difference Approximation, 2nd order accuracy

In FDTD method, the finite-difference techniques provide a very efficient way of solving Maxwell's equations. In a finite-difference method, a space-time mesh is introduced and Maxwell's equations are replaced by a system of finite-difference equations on the mesh. The central difference approximation shown as follows is used in the FDTD analysis.

$$f'(x) = \frac{f(x + \frac{\Delta x}{2}) - f(x - \frac{\Delta x}{2})}{\Delta x} - \frac{\Delta x^2}{24} f''(x) + \cdots \tag{1.1}$$

And the Δx in formula is the space increment on x-axis. From the formula, we can note that when the Δx is small enough, the second term of formula (1.1) will become a negligible quantity. By using the central difference approximate in spatial and time domain, the second order accuracy can be maintained in the simulation. And using a smaller cell size can reduce the dispersion error.

Leap-frog Algorithm

In FDTD analysis, by positioning the field components of E and H on the mesh in the way that is depicted in Fig. 1.1 and evaluating E and H at alternate half-time steps, this is the "Leap-flog algorithm". The process of FDTD simulation is shown in Fig. 1.2.

YeeCell

Another characteristic of FDTD method is that the whole computation region is divided by Cartesian grids shown in Fig. 1.1. Therefore, when solving problems that have an arbitrary shape, for example, objects which have curve shape or taper structure, it is necessary to use the "staircases approximation" to model the target.

In this case, to maintain the FDTD numerical accuracy, the cell size be used in simulation is required to be small enough. But an increase of mesh density will cause a rapid increase of computation memory and CPU time be required in simulation.

To overcome this problem, a thin wire method for wire structures that are smaller than mesh size is proposed. And FVTD method which use an arbitrary shape grid instead of Yee cell, Contour Integral method which can deal with some complicated structure are also reported in many papers.

Broad band response obtained with single simulation

Be different from some other numerical methods, FDTD method first obtain the pulse response in time domain. Then fourier transformation is used to obtain the fre-

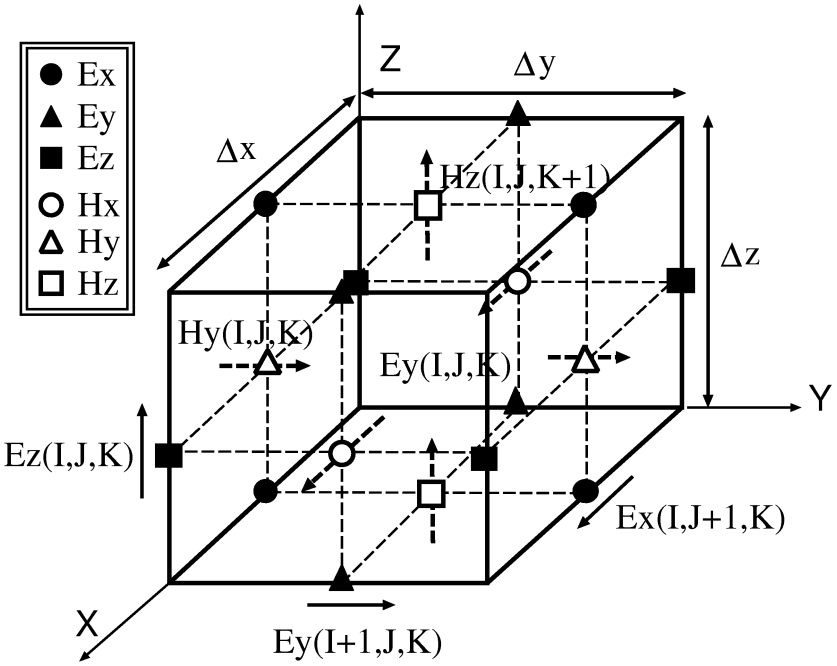

Figure 1.1: Yee cell

quency response. Therefore, it is possible for get the broad band response with a single simulation.(Fig. 1.3)

Of course, FDTD method is certainly not suitable for all application. Some of the limitations of the FDTD method include:

- Volume based discretization (as opposed to surface based discretization) can be memory intensive.
- Due to the explicit algorithm, time step is bound by the smallest spatial discretization.
- Large problems require high performance computing
- High Q structures(For example, microwave filter, etc.) may require extensive computation to reach steady state
- Discretization error grows with problem size

And FDTD result depends on the cell size be used in simulation, especially in the case of wire antenna. In order for a numerical computation to yield accurate results, the spatial cell size used in the FDTD, is taken to be much smaller than the scattering objects.

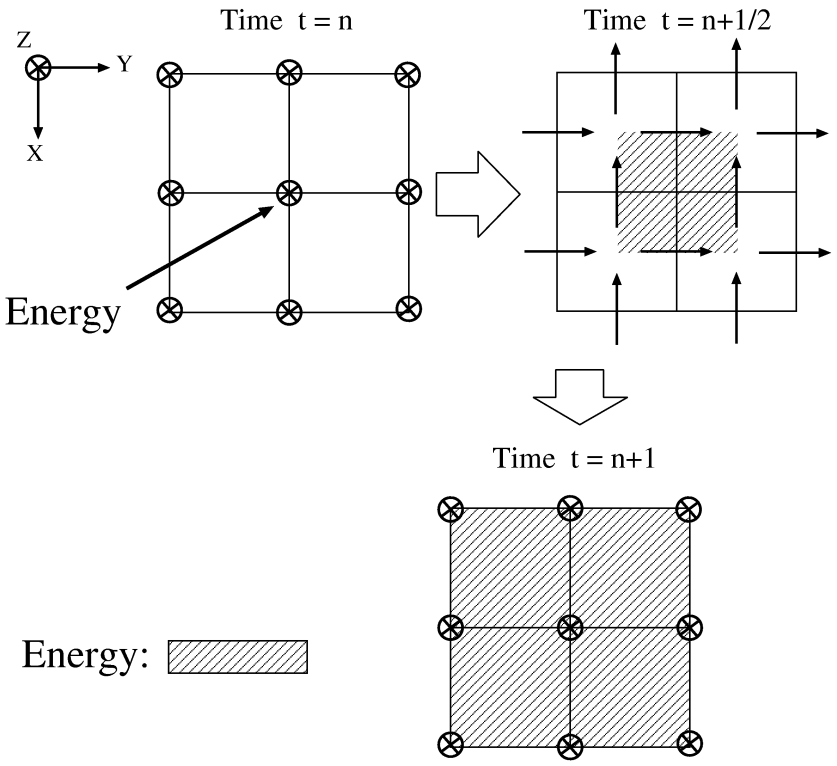

Figure 1.2: Process of electromagnetic field's calculation (2D model)

Figure 1.4 shown a computation model of patch antenna. By changing the density of division in thickness and width of patch antenna, we note that the return loss characteristic will change due to difference of mesh size.

The another issue of FDTD analysis of antennas is that small antennas usually has complicated structures. If an object under consideration has small-scale structure such as a narrow slot or thin wire, that is very small compared to the main body of target, the original method would have to use an excessively fine grid to accurately model the structure.

However, if an uniform cell size is used throughout this problem, the cells in all the analysis region to be relatively small, which may greatly increase the total number of cells. Computer memory requirements limit the number of mathematical cells and simulation model are impractical to achieve due to limited computer resources.

Another issue of FDTD method is in case of solving antennas that have an arbitrary shape. As originally formulated, the Cartesian grids used in the FDTD method dictate that a smoothly varying surface must be approximated by one that is "staircased". This approximation may lead to significant errors in certain problems.

In addition to problems caused by staircasing, if an object under consideration has small-scale structure such as a narrow slot, the original method would have to use an excessively fine grid to accurately model the associated fields.

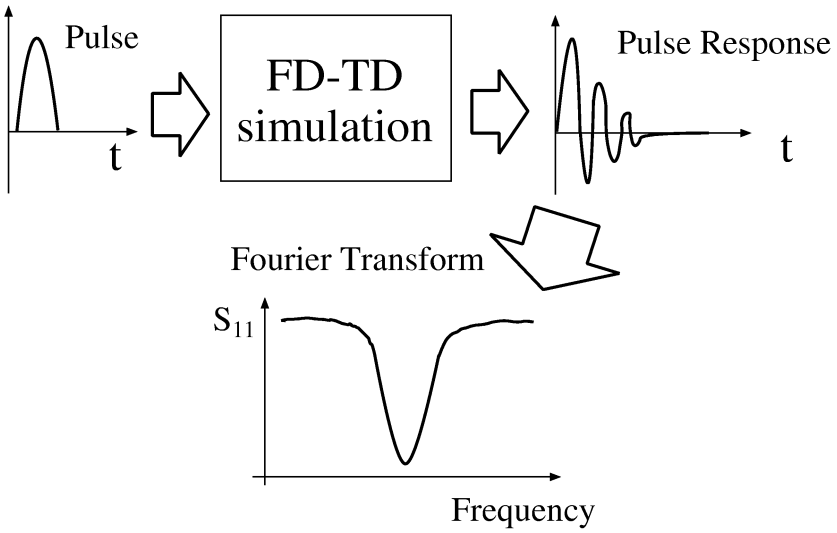

Figure 1.3: Broad band response obtained with single simulation

1.3 Early works in subcell technique

In order to keep the run time short and use as few nodes as possible, FDTD scheme which incorporates sub-cell regions is required to adequately perform the desired simulations.

To reduce the cell size and avoid the increase of arrays in computation, a number of papers have been published before on this subject[5]–[11]. The sub-gridding is achieved by local refinement of mesh based on an integer factor. Subdomains are gridded more finely than the rest of the problem space. But it is also reported that a stability problem will happen in case of large mesh ratio be used in simulation.

The key issue in these techniques is the coupling of the fine and coarse grids.(Away from the boundary between these two grids, the standard FDTD update equations are used.). Changing the size of neighboring lattices continuously and simultaneously (with arbitrary mesh ratios) in all three-space directions introduces a first order error term.

To overcome this problem, S.Xiao[9] proposed a special mesh arrangement without changing the algorithm for the uniform mesh arrangement. The merit of this approach is a second order accuracy can be maintained by very simple algorithm, but the special mesh arrangement is valid only for certain mesh ratios.

This paper presents the FDTD method by using different mesh sizes of arbitrary ratio. By using an assumed magnetic field component and interpolate components between fine and coarse meshes, its accuracy can be improved by simple algorithm. The algorithm is demonstrated for several different antenna geometries .

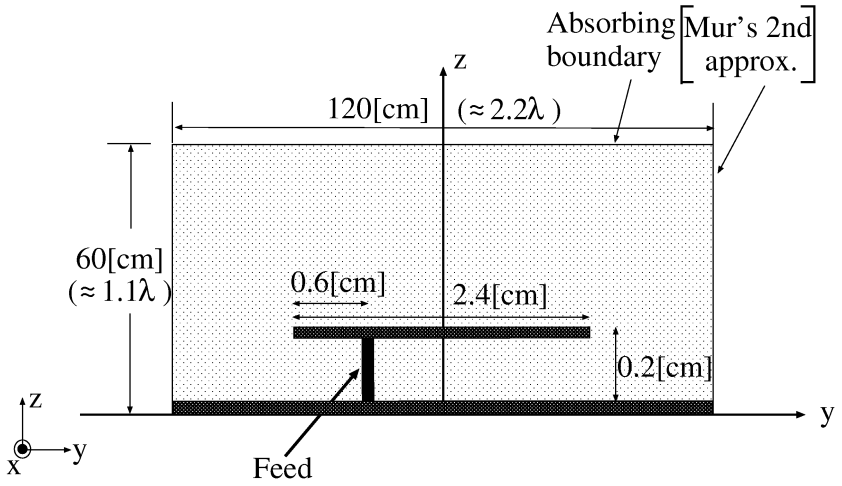

Figure 1.4: Patch Antenna

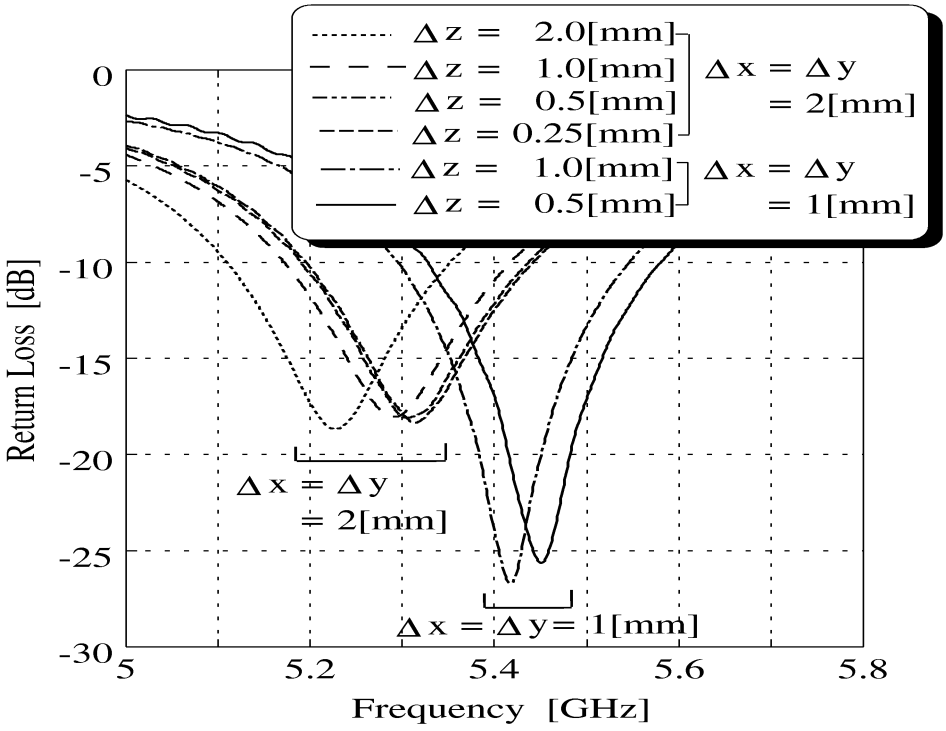

Figure 1.5: Return Loss Characteristic due to Density of Division in Thickness of Substrate

Chapter 2

Non-Uniform Mesh FDTD Analysis

2.1 Non-uniform Mesh

As mentioned in preceding chapter, the non-uniform mesh FDTD code was developed to improve the efficiency of the FDTD calculation and help focus a large number of cells in regions of interest. FDTD analysis by using non-uniform mesh shown in Fig. 2.1 is based on the finite-difference representation of Maxwell's curl equations using a central-difference formulation and the Yee-cell notation. In general, the fine mesh is used to divide a part of object[6] such as the vicinity of feed point and antenna edge. The demerit of this method is that small antenna usually has a complicated structure, it is necessary to predict the part which will influence the characteristics of antenna before computation.

In our research, the whole computational space is divided to fine mesh region and coarse mesh region. Fine mesh is used to model the region including the object, and coarse mesh is used to divide computed space between antenna and absorbing boundary. Because a fine mesh is used in the whole region of object be simulated, small antenna with complicated structure also can be modeled as usual. The size of time step is primarily determined by the smallest mesh size. A stable computation can be achieved by a very simple algorithm. For simplicity, the variable time step implementation is not used[4]. By using coarse mesh with high ratio to fine mesh at space between object and absorbing boundary, calculation can be performed with a little computing resources.

2.2 Solution for Discontinue Junction

When using FDTD method with non-uniform mesh, the major problem was always that changing the size of neighboring lattices continuously and simultaneously in all three directions introduces a first order error term. It is very important to investigate how to deal with electric and magnetic field components near boundary surface between

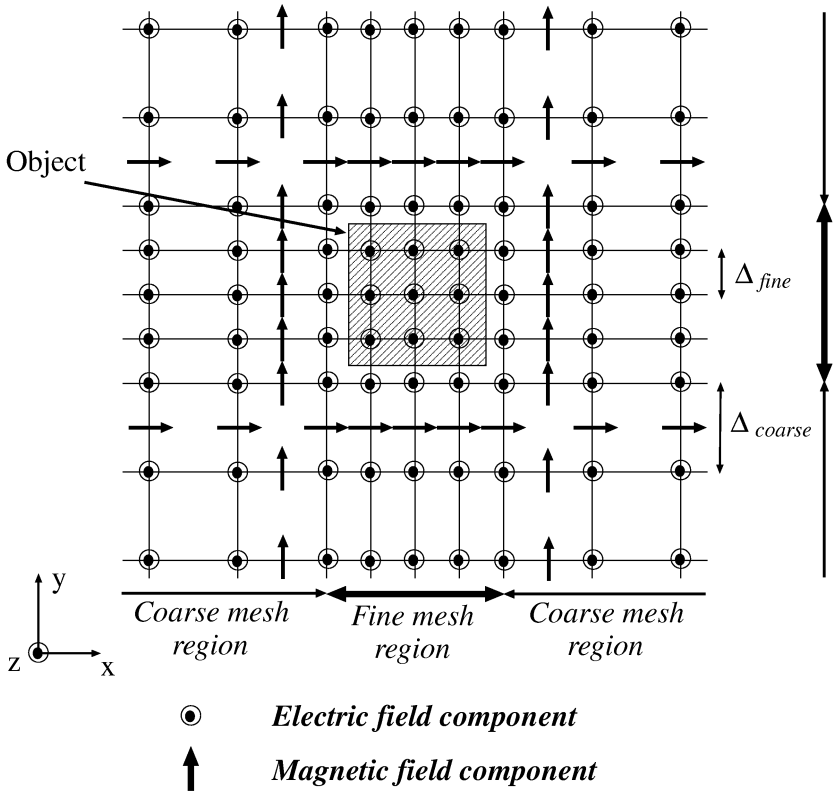

Figure 2.1: Non-uniform mesh

the fine and coarse meshes. In conventional analysis method, calculation of electric and magnetic field components is based on the difference formulation from node's position. But computation error occurred here because a central-difference formulation is used in FDTD method. The electric field component of next half step will swerve from the position we simulated.(Fig. 2.2) And the next half step later, the magnetic field component obtained from electric field component will swerve from the right position, too. As computation iterated, the difference become bigger and bigger, and bring about computation errors finally.

To avoid this discrepancy and improve the computation accuracy, an interpolation around the boundary of different meshes is required. In this section, we will introduce formulation of two kinds of interpolations: linear interpolation and quadratic interpolation.

2.2.1 Linear Interpolation

In this section, an interpolation on the coarse-fine boundary in space is utilized to reduce the reflection error due to the discontinuity. At first, we use an assumed magnetic field component $H'_y(I, J, K)$(Fig. 2.4) at a distance of half fine mesh interval from coarse-fine boundary. The value of $H'_y(I, J, K)$ component is obtained based on linear

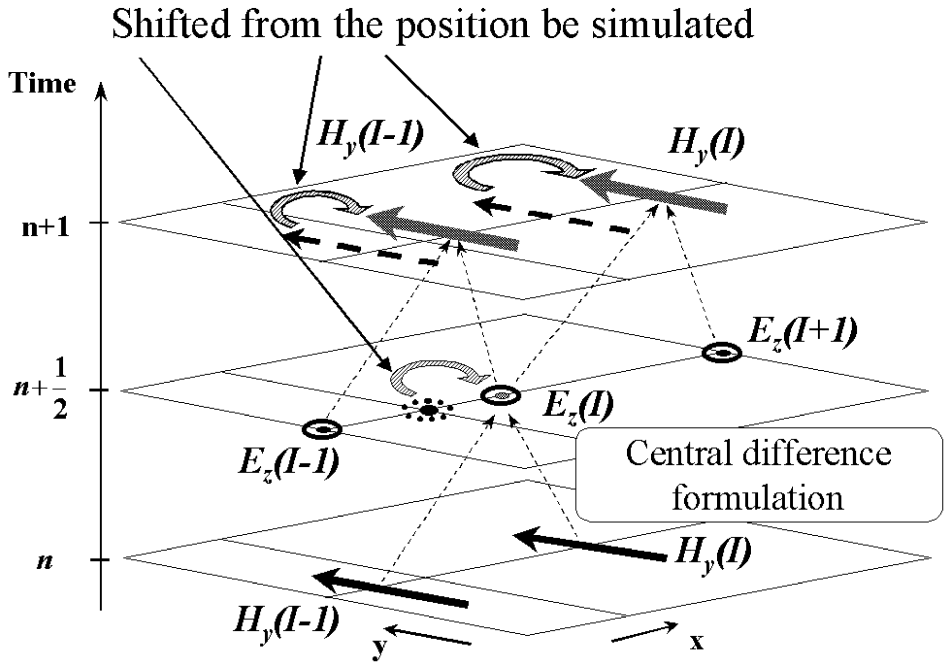

Figure 2.2: Shift of E and H Components due to Discontinue Junction

interpolation from $H_y(I-1,J,K)$ and $H_y(I,J,K)$ components. The linear interpolation is used here because cell size be used in realistic problem is much smaller than wavelength, so a linear interpolation is considered enough to obtain the accurate value.

At the next half step, when we update electric field, component on the coarse-fine boundary $E_z(I,J,K)$ is obtained from $H_y(I-1,J,K)$ and assumed component $H'_y(I,J,K)$. And components next to the boundary, $E_z(I+1,J,K)$ and $E_z(I-1,J,K)$ are obtained from the original magnetic components. Computation accuracy is therefore improved everywhere.

Formulation of linear interpolation is shown as follows.

1) In case of boundary of right side of feed point

From Figs. 2.4 and 2.5, assumed component $H'_y(I,J,K)$ is given as

$$\begin{aligned} H'_y(I,J,K) &= \frac{a-1}{a+1}H_y(I-1,J,K) \\ &\quad +\frac{2}{a+1}H_y(I,J,K) \end{aligned} \tag{2.1}$$

where a is the ratio of two kinds of mesh sizes. Using $H(I-1,J,K)$ and $H'(I,J,K)$, the electric field component $E(I,J,K)$ is evaluated. And electric and magnetic components away from the boundary can be obtained by the standard FDTD update equations.

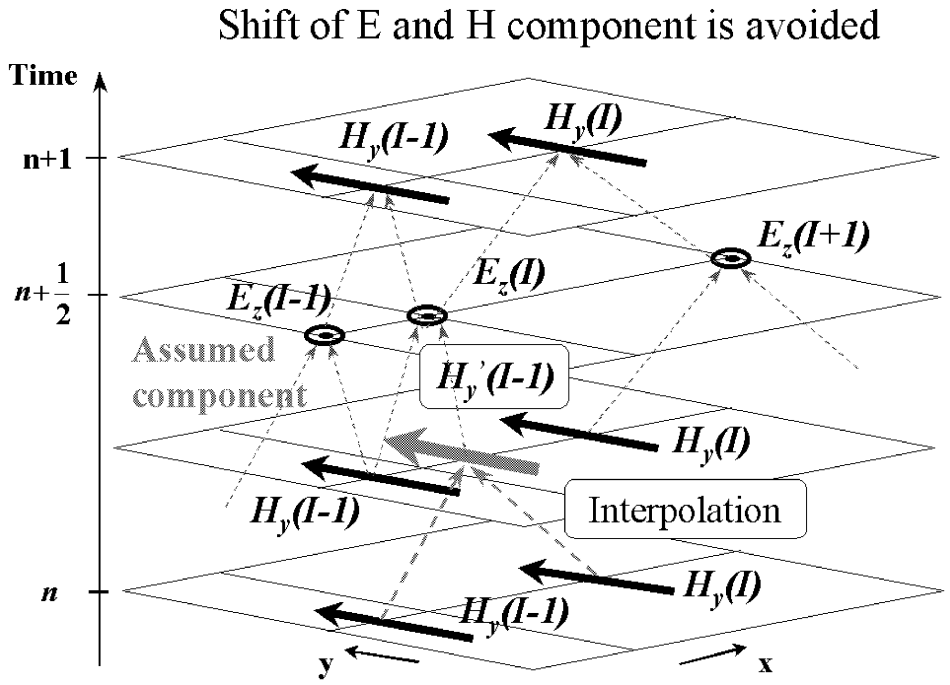

Figure 2.3: FDTD algorithm of linear interpolation

The reflection error due to center difference formulation can be reduced here because the discrepancy is avoid by using the assumed component.

2) In case of boundary of left side of feed point

From Figs. 2.6 and 2.7, assumed component $H'_y(I,J,K)$ is given as

$$\begin{aligned} H'_y(I,J,K) &= -\frac{a-1}{2a}H_y(I-2,J,K) \\ &\quad +\frac{3a-1}{2a}H_y(I-1,J,K) \end{aligned} \tag{2.2}$$

In this formulation, we have a special reason to use $H_y(I-2,J,K)$ and $H_y(I-1,J,K)$ to obtain $H'_y(I,J,K)$. In our FDTD code, we calculate electric and magnetic component in order of I, J and K. The interpolation is performed after update the magnetic component. If we express $H'_y(I,J,K)$ with $H_y(I,J,K)$ and $H_y(I-1,J,K)$, because magnetic component $H_y(I,J,K)$ and $H_y(I-1,J,K)$ are values of one time step before, numerical error will occurred at this time. To avoid this problem, we use the latest value, $H_y(I-2,J,K)$ and $H_y(I-1,J,K)$ to obtain the assumed component $H'_y(I,J,K)$. Reasonable accuracy is maintained due to the fact that the spatial variation of the fields is relatively small and that all cell sizes remain a fraction of the smallest wavelength.

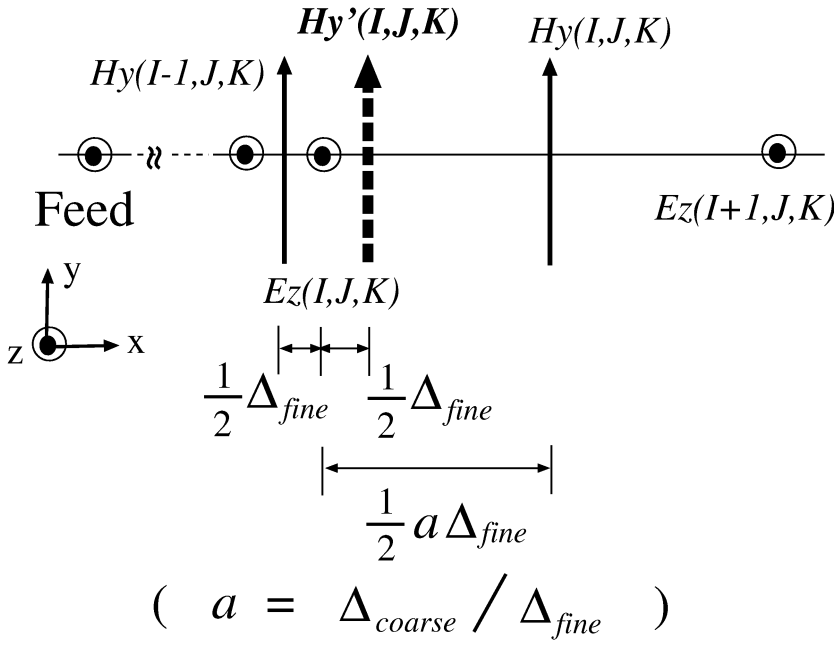

Figure 2.4: Assumed magnetic field component $H'_y(I, J, K)$

2.2.2 Quadratic Interpolation

In previous section, to obtain the assume component value, the linear interpolation formulation has been introduced. Because the electric and magnetic field are decreasing in proportion to $\frac{1}{r^2}$ in near field of antenna, and a 2nd order accuracy is maintained in FDTD analysis. It is necessary to investigate how reflection error from discontinue junction will change if we use the quadratic interpolation. In this section, we will introduce the detail formulation of quadratic interpolation.

In linear interpolation which was introduced in previous section, to obtain the assumed component$H_{y_{assume}}(I, J, K)$, two components next to the discontinue junction $(H_y(I-1, J, K) and H_y(I, J, K))$ were used. In the quadratic interpolation, components be mentioned above$(H_y(I-1, J, K) and H_y(I, J, K))$ and another two components in the fine mesh region $(H_y(I-3, J, K) and H_y(I-2, J, K))$ are used in the formulation(Fig. 2.8). And here, we will introduce the detail formulation of quadratic interpolation for discontinue junction:

1) In case of *ratio* >= 3:

$$\begin{aligned} Hy_{assume}(I, J, K) \;=\; & \frac{1}{4}H_y(I-3, J, K) \\ & -H_y(I-2, J, K) \\ & +\frac{7a+3}{4(a+1)}H_y(I-1, J, K) \\ & +\frac{1}{a+1}H_y(I, J, K) \end{aligned} \tag{2.3}$$

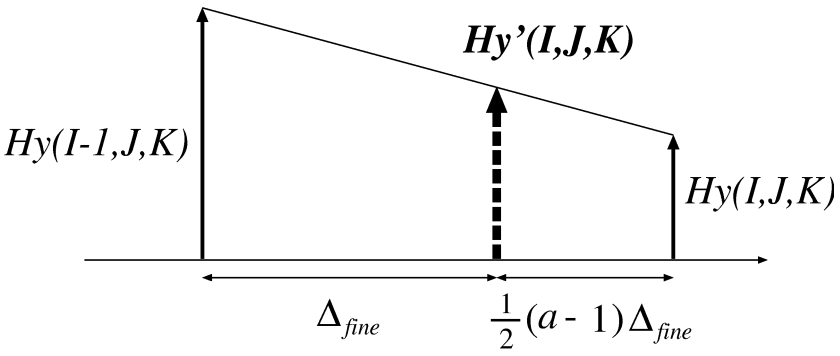

Figure 2.5: Linear interpolation for $H'_y(I,J,K)$

2) In case of $ratio = 1$ or 2:

$$\begin{aligned} Hy_{assume}(I,J,K) &= \frac{a-1}{4a}H_y(I-3,J,K) \\ &\quad -\frac{a-1}{a}H_y(I-2,J,K) \\ &\quad +\frac{7(a-1)}{4a}H_y(I-1,J,K) \\ &\quad +\frac{1}{a}H_y(I,J,K) \end{aligned} \tag{2.4}$$

The difference between formula (2.3) and (2.4) is that in the process of finding the value of $H'_{y_{assume}}$, formula (2.3) is based on the central difference approximation from components $H_y(I-1,J,K)$ and $H_y(I,J,K)$. When ratio of different mesh sizes is less than 3, assumed component $H'_{y_{assume}}$ is at same position or fairly close to the component $H_y(I,J,K)$. Less numerical error can be obtain if we use the forward difference approximation from $H_y(I,J,K)$ and $H_{y_{assume}}(I,J,K)$ instead of central difference approximation. Of course, when ratio of mesh sizes is 3, the assumed component $H_{y_{assume}}(I,J,K)$ is just in the center between components $H_y(I-1,J,K)$ and $H_y(I,J,K)$, numerical error due to the difference approximation can be kept up at the most small level. And the quadratic interpolation is based on the combination of formula (2.3) and (2.4).

2.3 FDTD Algorithm

In brief the algorithm can be described as follows

1) Time t=n: update magnetic field component using standard FDTD equations.

- Obtain assumed magnetic field component $H'_y(I,J,K)$ from $H_y(I-1,J,K)$ and $H_y(I,J,K)$ by linear interpolation.

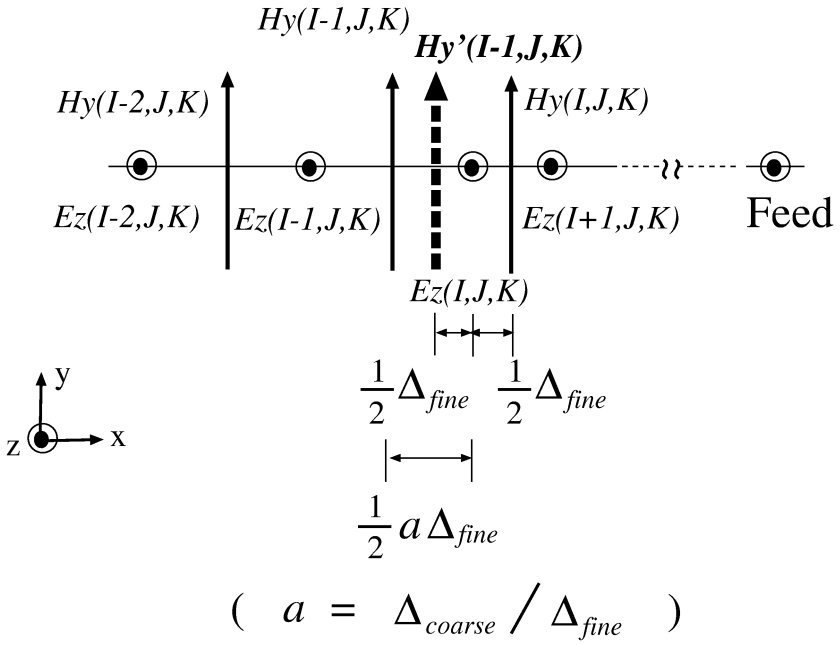

Figure 2.6: Assumed magnetic field component $H'_y(I, J, K)$

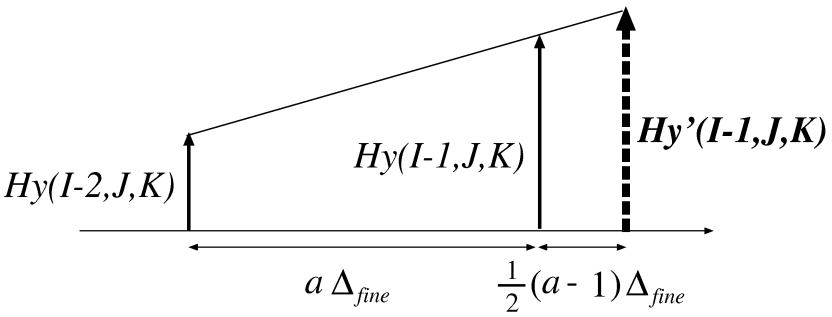

Figure 2.7: Linear interpolation for $H'_y(I, J, K)$

2) Time t=n+$\frac{1}{2}$: update electric field component using standard FDTD equations.

- Calculate electric field component on the boundary $E_z(I, J, K)$ from $H_y(I-1, J, K)$ and assumed component $H'_y(I, J, K)$.
- Update the rest electric components using standard FDTD equations.

3) Return to (1).

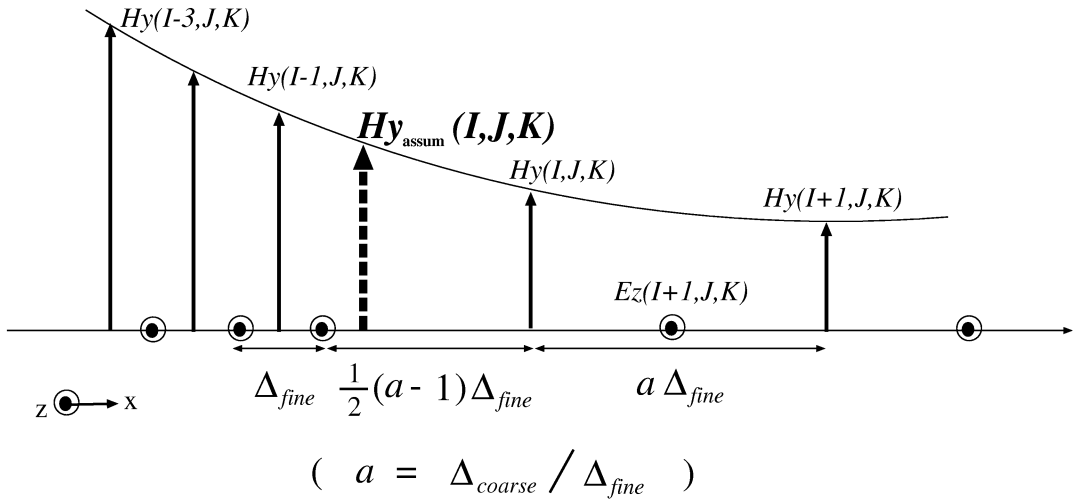

Figure 2.8: Quadratic interpolation for assumed component Hy_{assume}

2.4 Conclusions

This chapter summarized the primary elements involved in Non-uniform mesh FDTD analysis, namely:

- Assumed magnetic field component;
- Linear interpolation;
- Quadratic interpolation;

By using an assumed magnetic component and linear interpolation, the simple algorithm can be used to reduce computation resources and to improve its accuracy simultaneously.

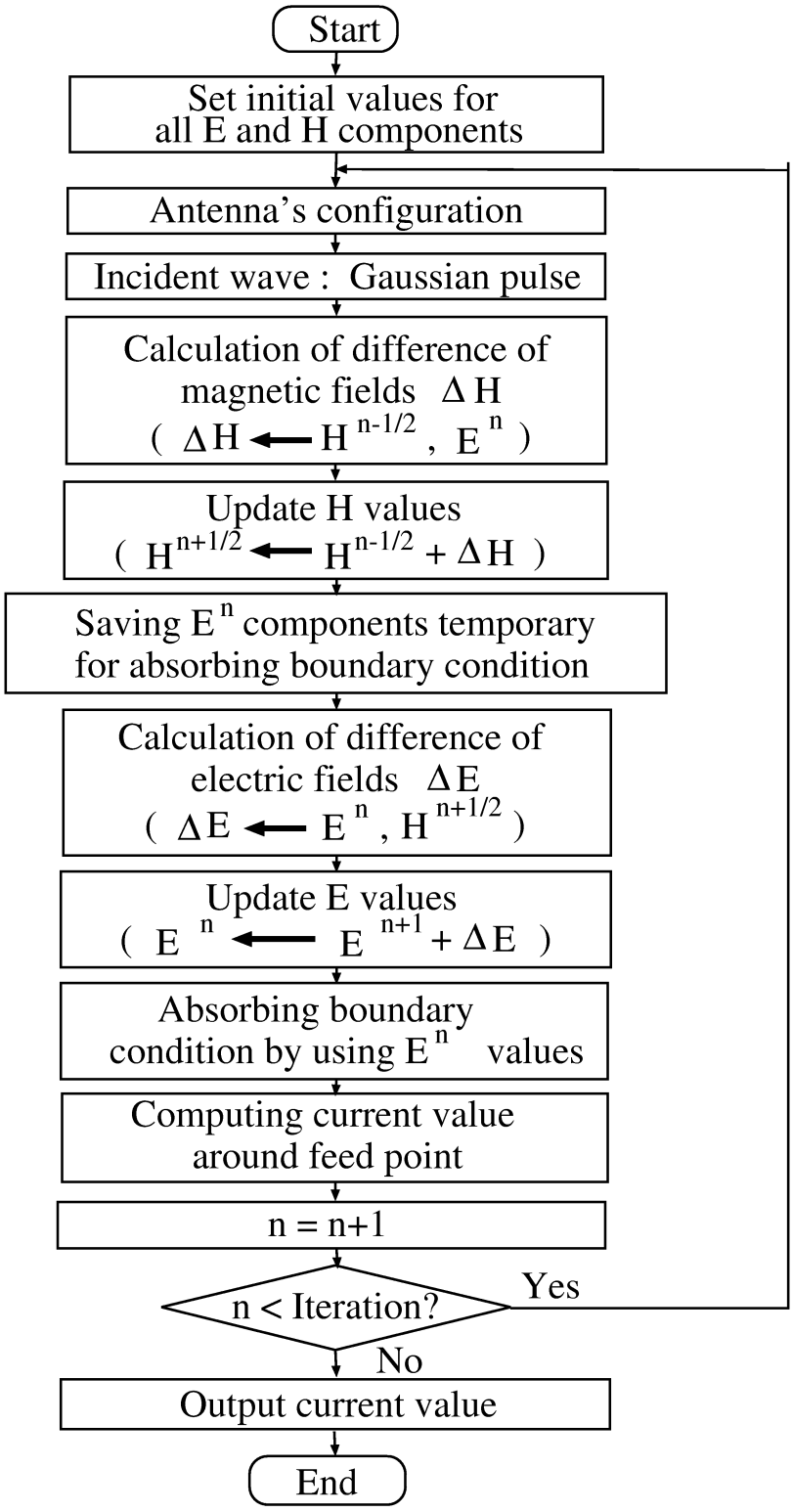

Figure 2.9: Flow chart of FDTD simulation

Chapter 3

Error Investigation of NUM-FDTD

Before we use the non-uniform mesh, in order to confirm the availability of use large mesh ratio, it is necessary to investigate the necessity of assumed component and interpolation, how computation error will change when we increase the mesh size ratio and how to determine the fine mesh region in order to improve the numerical accuracy. In this chapter, we will first examine the validness of assumed component and interpolation when using non-uniform mesh. Next, examination of dependence of calculation error on ratio of different mesh intervals is carried out of three antennas. In the forth part of this section, we will investigate computation error due to size of fine mesh region.

3.1 Reflection Error From Discontinue Junction

3.1.1 Linear Interpolation

The key issue in non-uniform mesh technique is the coupling of the fine and coarse meshes. (Away from the boundary between two mesh intervals, the standard FDTD update equations are used.) Reflection error occurs from the boundary because of the discontinuity. In Chapter 2, our solution by using an assumed component and linear interpolation in space to update the fields on the boundary between the fine and coarse grids has been introduced. Before apply the approach to antenna's simulation, we will examine the reflection error by using proposed approach in this section.

A one dimensional transmission line model(Fig. 3.1) is used to examine the reflection error from discontinuous boundary. Table 3.1 shows parameters be used in simulation. And the transmission line is terminated with Mur's 1st order approximate absorbing boundary condition. Two kinds of mesh interval are used in the computation region.

By change the ratio of coarse and fine mesh sizes, reflection error from the junction due to mesh size ratio can be obtained. Figure 3.2 and 3.3 show reflection error be observed at a point which have an interval of 0.025[m] away from incident point when ratio of mesh intervals are 3, 5, 24 and 40. We notice that a large reflection error can

be observed when using the non-uniform mesh technique without interpolation. The reflection error is increasing rapidly in proportion to a rise of mesh size ratio.

By using the proposed approach, the error can be reduced to a level of less than -40dB. And Fig. 3.4 shows the maximum value of reflection error versus ratio of different mesh sizes, we notice that reflection error has been cut down greatly at all cases. We can reduce the reflection error at a level of less than -40dB by using an arbitrary mesh ratio under the condition that the coarse mesh size is less than $\lambda_{min}/15$. As a result, the proposed approach is effectively for decrease the reflection error at the discontinuity.

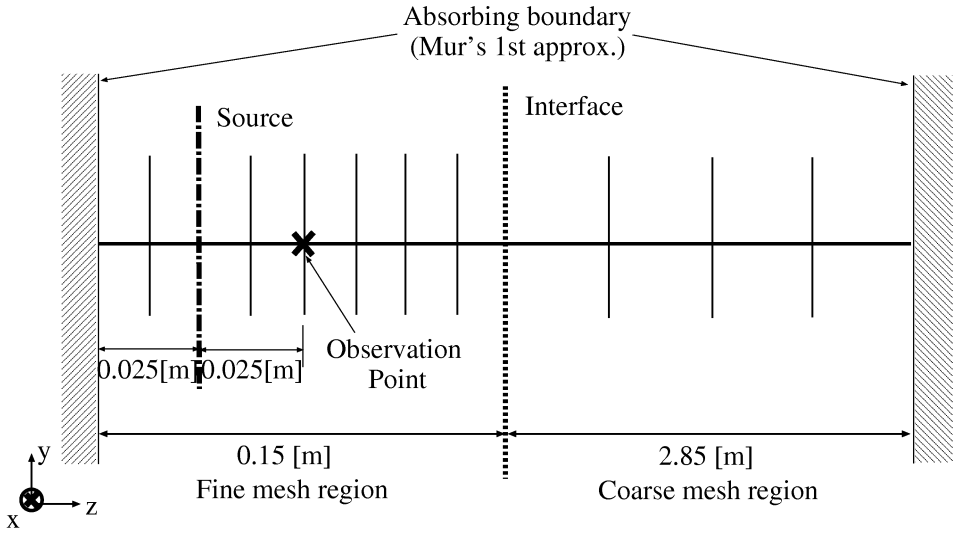

Figure 3.1: One dimensional transmission line model

Table 3.1: Computation parameter

Computation space	$L = 3[m]$
Cell size	$[I] \quad \Delta_{fine} = 0.00025[m]$ $[II] \quad \Delta_{coarse} = 0.00025 \times ratio[m]$
Iteration	40000
Incident wave	Gaussian pulse
Absorbing Boundary Condition	Mur's 1st approx.

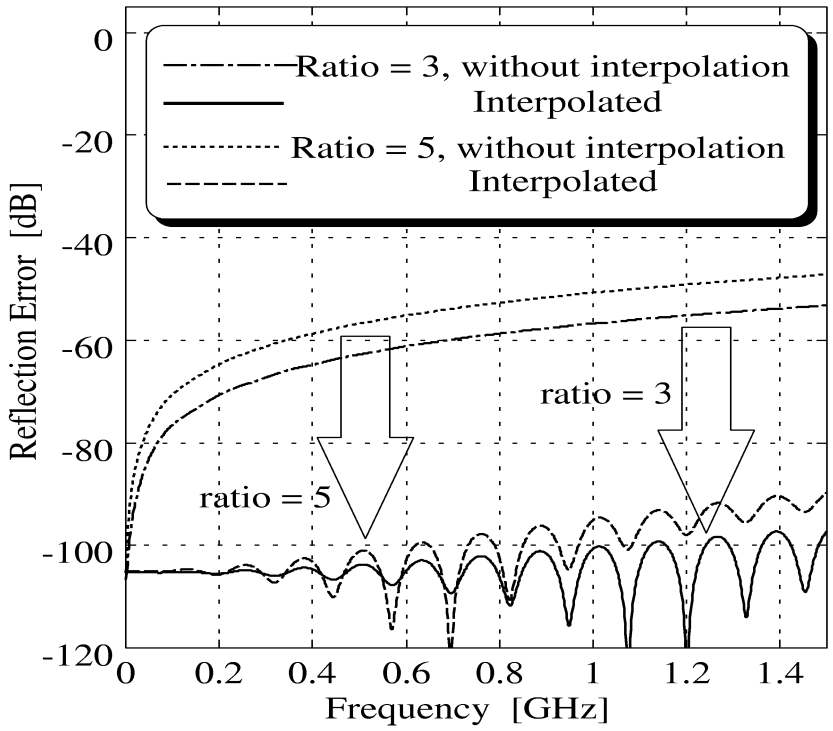

Figure 3.2: Reflection error from discontinued junction (Case of ratio = 3 and 5)

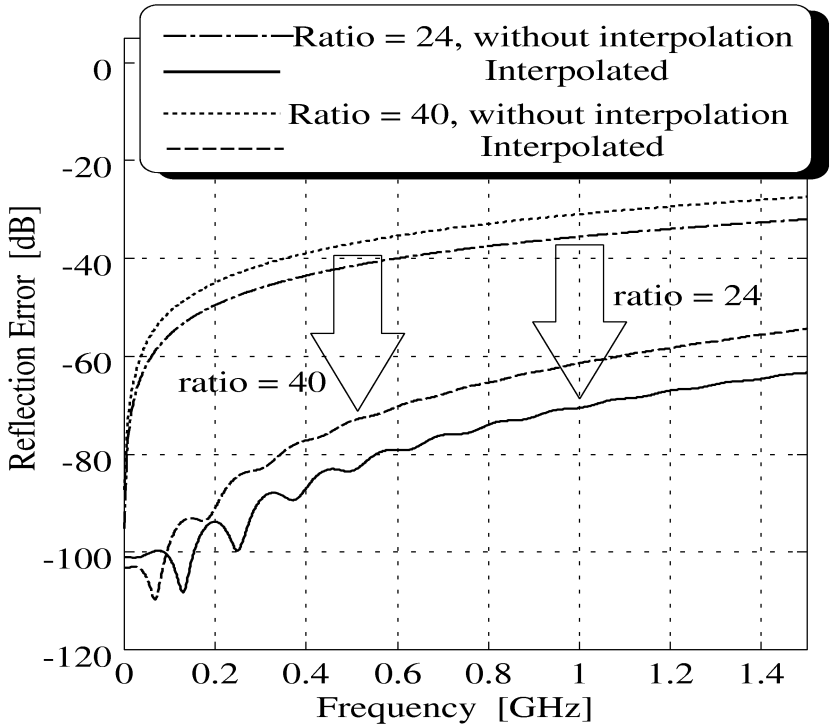

Figure 3.3: Reflection error from discontinued junction (Case of ratio = 24 and 40)

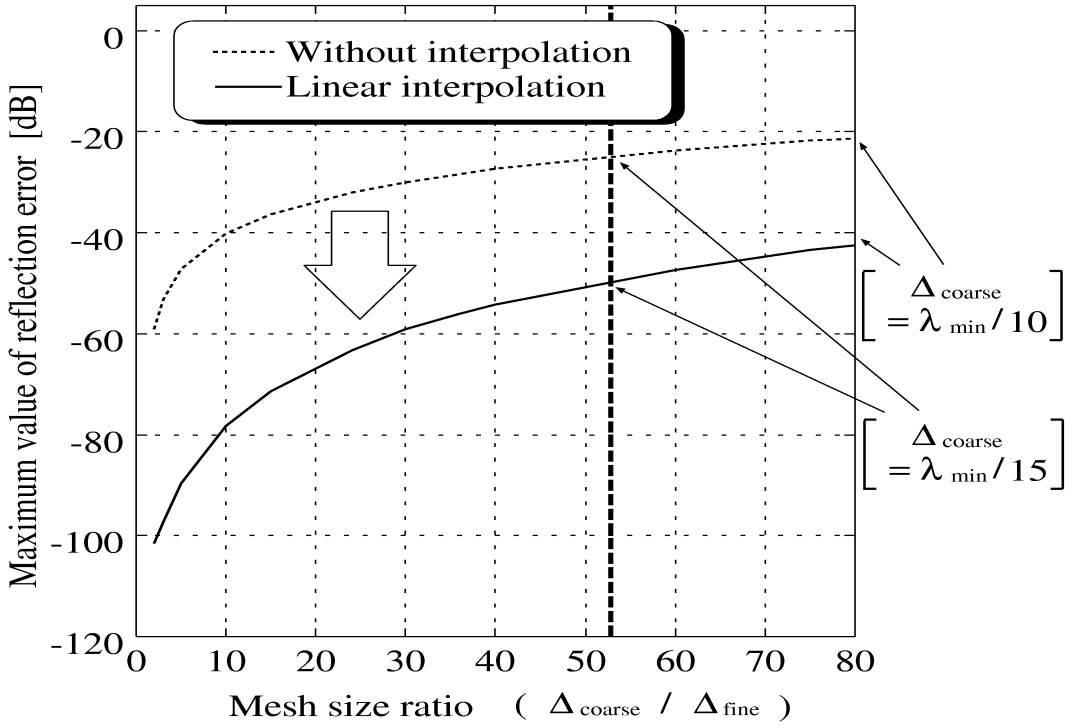

Figure 3.4: Reflection error from discontinued junction versus ratio of different mesh intervals

3.1.2 Quadratic Interpolation

In previous section, we investigate the reflection error due to mesh size ratio in case of using linear interpolation to obtain the assumed component value. And in this section, we will examine how reflection error will change when we use the quadratic interpolation instead of linear interpolation. To compare the computation result to the case of linear interpolation, same simulation model(Fig. 3.1) and parameters(Table 3.1) are used in the examination.

Figures 3.5 and 3.6 shown the comparison of reflection error of quadratic interpolation, linear interpolation and without interpolation when ratio of mesh sizes are 3 and 40. We notice that reflection error from discontinue junction hasn't change greatly in case of we use a small ratio. But in case of a high ratio is used in computation, reflection error become smaller if we use quadratic interpolation instead of linear interpolation.

Figure 3.7 shows the maximum value of reflection error from discontinue junction. Comparison of results of quadratic interpolation, linear interpolation and case of before interpolation are shown in the figure.

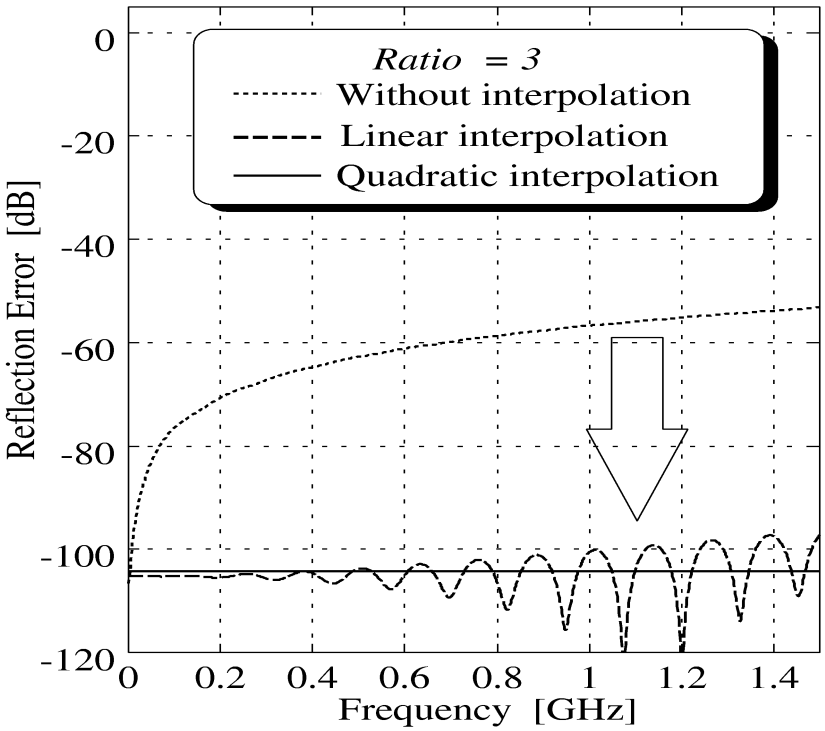

Figure 3.5: Reflection error from discontinue junction in case of ratio = 3

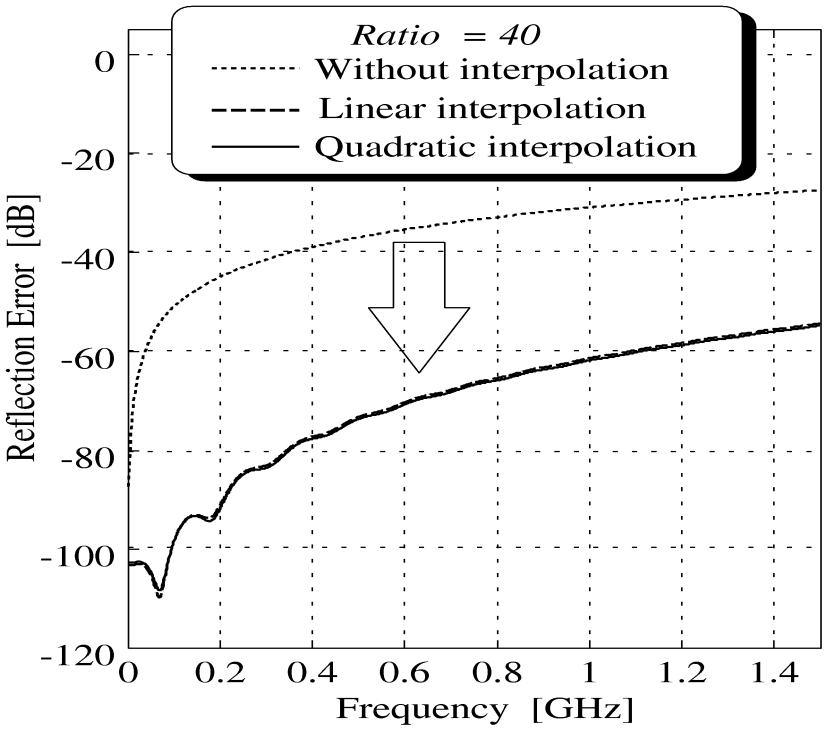

Figure 3.6: Reflection error from discontinue junction in case of ratio = 40

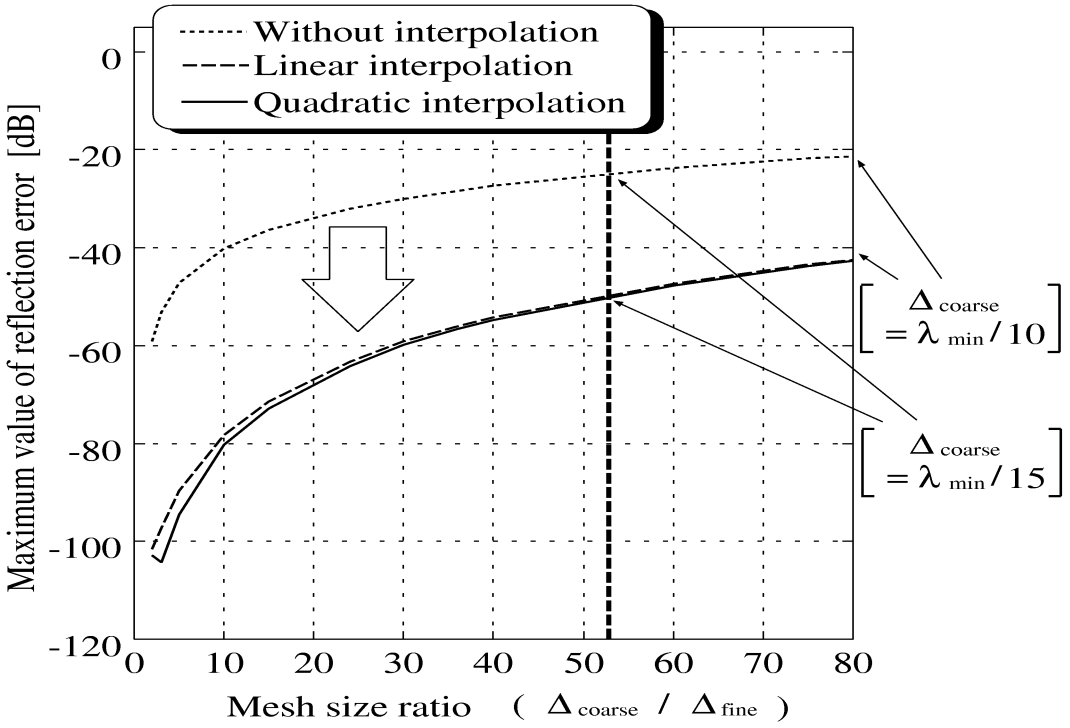

Figure 3.7: Maximum reflection error due to mesh size ratio

From results be shown above, we conclude this section as follows:

- Reflection error is in direct proportion to a rise in mesh size ratio, but by using the assume component and interpolation, reflection error from discontinue junction can be reduced greatly.
- Compare to the case of using linear interpolation, computation by using quadratic interpolation can improve the accuracy, especially in case of a small ratio is used in computation. And in case of a high ratio problem, although effectiveness is not as big as case of low ratio problem, it is possible for improve the accuracy by changing the differential formulation.
- It was reported that a dispersion problem occurred easily in case of a high order interpolation be used in FDTD analysis. But in our research, because an assumed component is used near the boundary of different meshes, a stable simulation can be achieved even when we use a very high ratio during the calculation.

3.1.3 Reflection Error in case of Multimesh Problem

In previous part of this paper, we examine the reflection error from discontinue junction in case of two kinds of mesh sizes is used. But in real simulation, very often we need

the third kind of mesh, a very fine mesh interval, to divide a part of antenna's structure. It is necessary to investigate how reflection error will change in case of multimesh problem. The examination is carried out as follows.

Figure 3.8 shows the simulation model, and Table 3.2 shown parameters be used in the calculation. In this model, three kinds of mesh, the finest mesh(Δ_{finest}), the fine mesh($\Delta_{fine} = \Delta_{finest} \times ratio1$) and the coarse mesh($\Delta_{coarse} = \Delta_{fine} \times ratio2$) is used in the simulation. By change the mesh size of fine mesh and coarse mesh, reflection error due to mesh size ratios are obtained by simulation.

Figure 3.9 shows the maximum value of reflection error from discontinue junction due to ratio of the coarse mesh and finest mesh. The computation result is compared to the case of two kinds of mesh intervals. From the figure, we can conclude that the reflection error from discontinue junction can be maintained a level of less than -15[dB] in case of the coarsest mesh size in the whole computation space is smaller than $\lambda/15$.

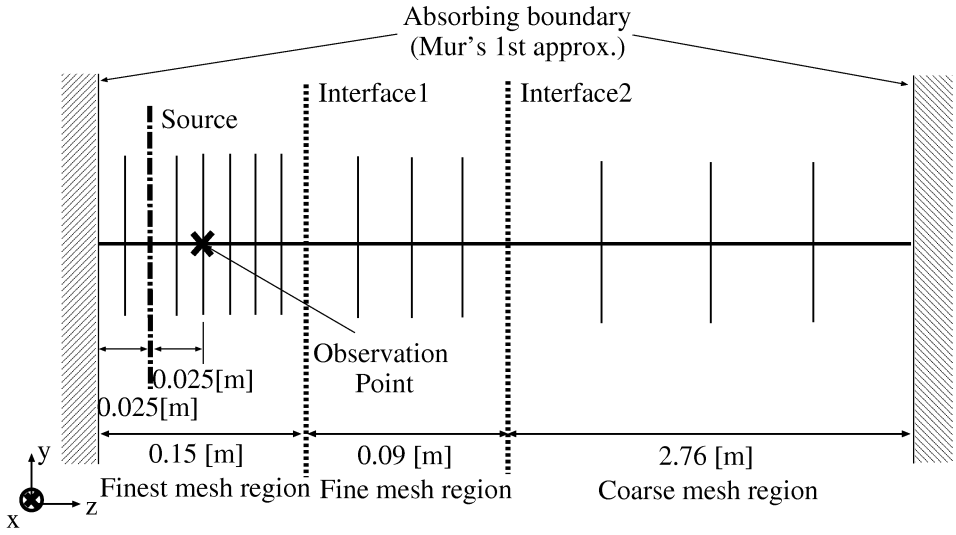

Figure 3.8: Computation model

Table 3.2: Computation parameter

Computation space	$L = 3[m]$
Cell size	$[I] \quad \Delta_{finest} = 0.00025[m]$ $[II] \quad \Delta_{fine} = 0.00025 \times ratio1[m]$ $[III] \quad \Delta_{coarse} = 0.00025 \times ratio2[m]$
Iteration	40000
Incident wave	Gaussian pulse
Absorbing Boundary Condition	Mur's 1st approx.

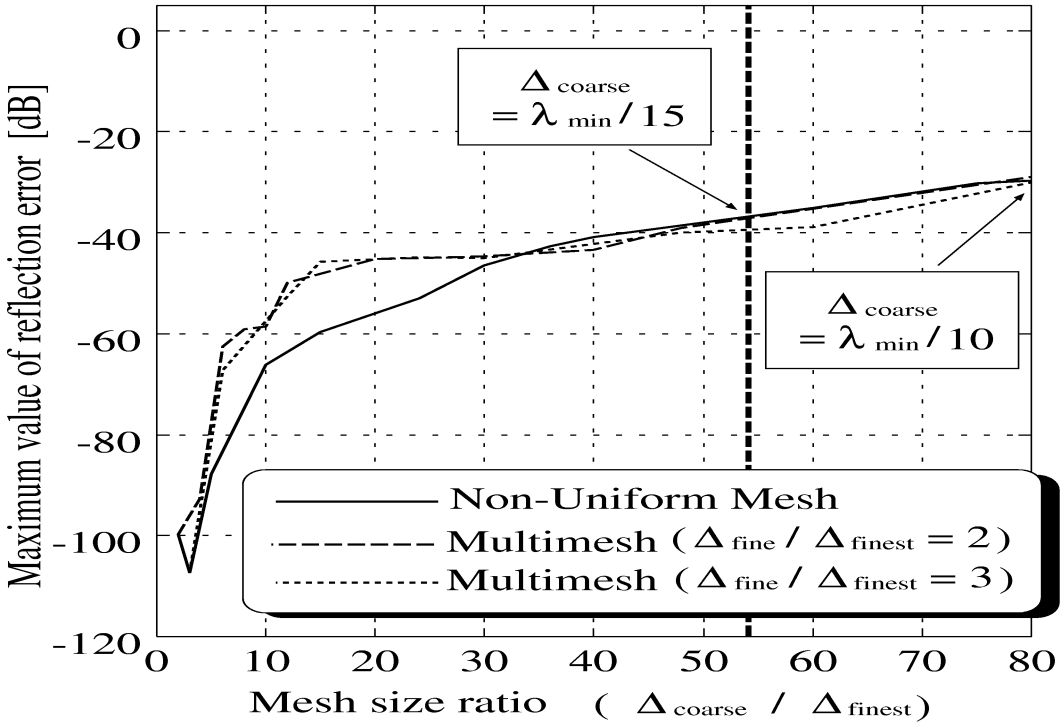

Figure 3.9: Maximum value of reflection error due to mesh sizes ratio

3.2 Effect of Interpolation

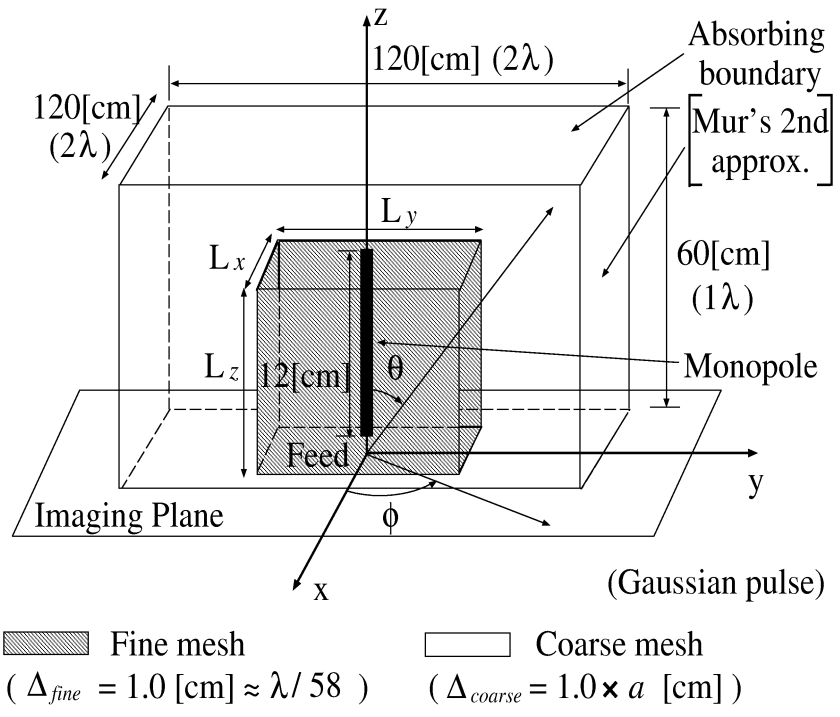

Figure 3.10: Simulation Model of Monopole Antenna

Table 3.3: Parameters of monopole's simulation

Size of object $[cm]$	L = 12
Computation space $[cm^3]$	$120 \times 120 \times 60$ $(\approx 2\lambda \times 2\lambda \times 1\lambda)$
Cell size $[cm]$ $(\Delta = \Delta x = \Delta y = \Delta z)$	$[I]$ $\Delta = 1.0 (\approx \lambda/58)$ $[II]$ $\Delta = 1.0 \times ratio$
Iteration	6000
Incident wave	Gaussian pulse
Absorbing boundary condition	Mur's 2nd approx.

First of all, an examination of proposed algorithm is carried out for monopole antenna(Fig. 3.10).

Figure 3.11 shows return loss characteristics by using non-uniform mesh (Case ratio = 2). By comparing with result of using uniform mesh and conventional non-uniform mesh method (without interpolation). We notice that difference of resonant frequency occurred by computation error in case of conventional method has disappeared by interpolation.

We got good agreement between using uniform mesh FDTD code and proposed method.

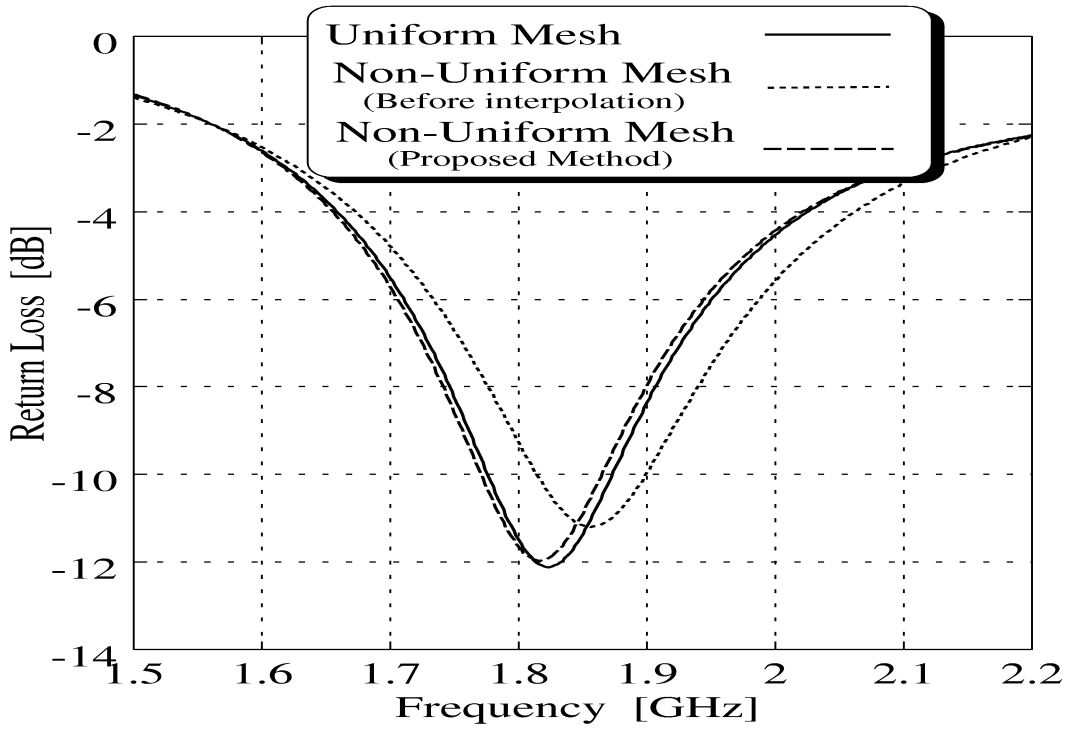

Figure 3.11: Return Loss Characteristics of Monopole Antenna

3.3 Calculation Results due to Ratio of Mesh Sizes

Before we use the non-uniform mesh, in order to confirm the availability of use large mesh ratio, it is necessary to investigate how computation error will change when we increase the mesh size ratio. The examination of computation error due to mesh size ratio is carried out in this section.

To examine the validity of proposed algorithm, we calculated a center-fed monopole antenna shown in Fig. 3.10 and patch antennas shown in Figs. 3.12 and 3.13. Table 3.3 shows detail parameters (computation space, cell size, etc.) of monopole's simulation. Two kinds of mesh interval were used in the computation. The fine mesh ([I] in Table 3.3) is used to model computation region include the object. And the coarse one ([II] in Table 3.3) is used to model computation region between object and absorbing boundary.

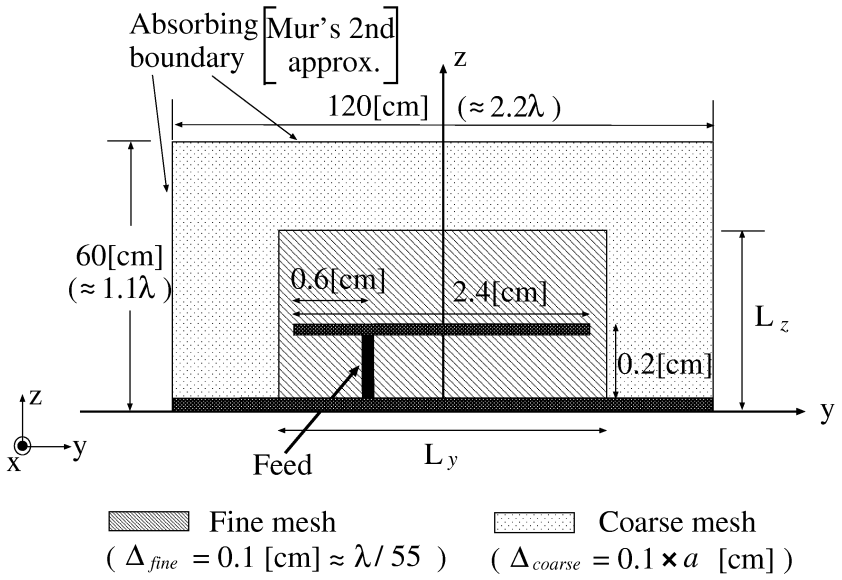

Figure 3.12: Simulation Model of Offset Fed Patch Antenna

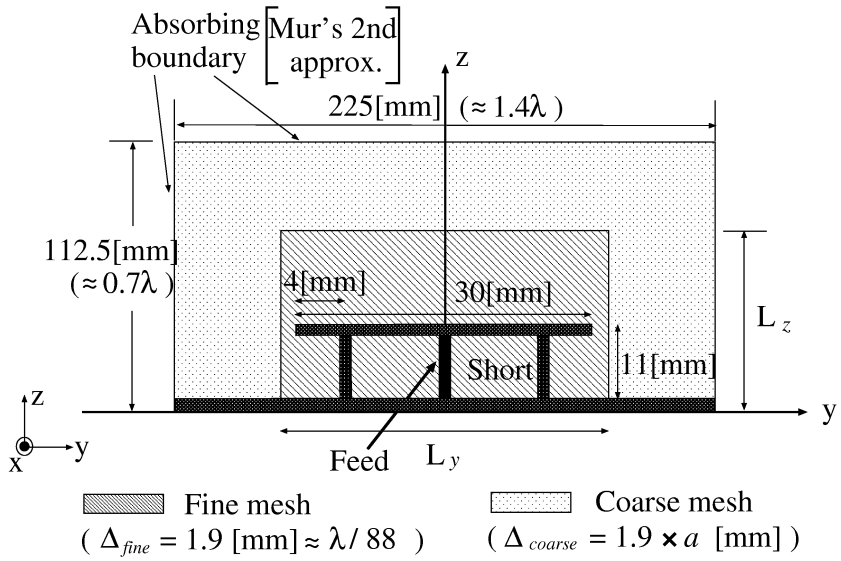

Figure 3.13: Simulation Model of Center Fed Top Loaded Monopole Antenna

At first, simulation of monopole antenna(Fig. 3.10) is carried out by using non-uniform mesh when the ratio of two kinds of mesh sizes changed from 2 to 5. To investigate the validly of non-uniform mesh, the computation results, resonant frequency, band width of return loss less than -10dB and input impedance Z_{in} (the radiation resistance at resonant frequency) are used to estimate the computation accuracy. And the memory space and CPU time in simulation is used to estimate the computation efficiency. All of them are normalized by the result using uniform mesh.

Table 3.4 shows relative value of computing resources and error, we note that memories and computation times are less than 12% for the computation in case ratio = 5, and error of resonant frequency, band width and input impedance are small enough in most cases.

Table 3.4: Relative Value of Computing Resources and Error of Result Normalized by the Uniform Mesh (Freq. = 517MHz, BW = 49MHz, $Z_{in} = 71.3\Omega$), Case of monopole antenna shown in Fig. 3.10, ($\Delta_{fine} \approx \lambda/58, \Delta_{coarse} = \Delta_{coarse} \times ratio, L_x = L_y = 28[cm], L_z = 14[cm]$)

Ratio	Resources		Computation error		
	Memory [%]	CPU time [%]	Resonate freq. [%]	Band width [%]	Input impedance [%]
Uniform	100	100	0	0	0
2	24.2	44.2	0.2	0.7	0.5
3	12.3	22.4	0.4	1.6	0.1
4	8.3	16.0	0.7	1.5	0.1
5	6.1	11.5	1.1	0.6	0.5

And then, same examination is carried out in the planer antennas be shown in Figs. 3.12 and 3.13. Same results are obtained in the simulation(Tables 3.5 and 3.6). Then we conclude that the FDTD code using non-uniform mesh is an effective tool to decrease the computing resources.

Table 3.5: Relative Value of Computing Resources and Error of Result Normalized by the Uniform Mesh (Freq. $= 5.4$GHz, BW $= 256$MHz, $Z_{in} = 73.4\Omega$), Case of offset fed patch antenna shown in Fig. 3.12, ($\Delta_{fine} \approx \lambda/55, \Delta_{coarse} = \Delta_{coarse} \times ratio, L_x = L_y = 28[mm], L_z = 14[mm]$)

Ratio	Resources		Computation Error		
	Memory [%]	CPU time [%]	Resonate freq. [%]	Band Width [%]	Input impedance [%]
Uniform	100	100	0	0	0
2	24.2	30.8	0.0	1.2	2.2
3	12.3	15.5	0.1	2.8	4.1
4	8.3	11.1	0.1	2.1	2.0

Table 3.6: Relative Value of Computing Resources and Error of Result Normalized by the Uniform Mesh (Freq. $= 1.8$GHz, BW $= 95$MHz), Case of top loaded low profile monopole antenna shown in Fig. 3.13, ($\Delta_{fine} \approx \lambda/88, \Delta_{coarse} = \Delta_{coarse} \times ratio, L_x = L_y = 34[mm], L_z = 17[mm]$)

Ratio	Resources		Computation Error		
	Memory [%]	CPU time [%]	Resonate freq. [%]	Band Width [%]	Input impedance [%]
Uniform	100	100	0	0	0
2	20.7	23.1	0.3	0.8	0.2
4	5.8	6.7	0.8	3.9	4.8
6	3.2	3.6	0.9	5.0	4.0
8	2.3	2.4	1.3	7.4	6.2

3.4 Calculation Results due to Space of Fine Region

During the simulation as previously mentioned, we determined the fine mesh region based on the electrical volume of antenna. In this case, boundary between different lattice regions is kept away from the feed point as same distance in x, y and z direction. And the distance is determined by the maximum size of object. However, the object, just like the monopole antenna, usually has one side much larger than other sides. To reduce the unnecessary fine division, improve the efficiency of calculation, it is necessary to

examine how to determine the fine mesh region. Simulation of monopole antenna (Fig. 3.10) and patch antenna (Fig. 3.12 and 3.13) are carried out next. Fine mesh region is adjusted by length of L_x, L_y *and* L_z.

3.4.1 Case of Monopole Antenna

Tables 3.7 and 3.8 show computation results by changing the size of fine mesh region. (The simulation is carried out without considering the radius of monopole).

Table 3.7: Relative Value of Computing Resources and Error of Result Normalized by the Uniform Mesh($ratio = 2, \Delta_{fine} \approx \lambda/58, \Delta_{coarse} \approx \lambda/29$), Case of monopole antenna shown in Fig. 3.10

$L_x \times L_y \times L_z$ $[cell^3]$	Resources		Computation Error		
	Mem. [%]	CPU time [%]	Resonate freq. [%]	Band width [%]	Input impedance [%]
Uniform	100	100	0	0	0
$2 \times 2 \times 14$	16.6	30.1	0.2	1.2	0.5
$4 \times 4 \times 14$	17.1	30.8	0.2	0.8	0.4
$8 \times 8 \times 14$	18.2	33.3	0.2	0.8	0.4
$28 \times 28 \times 14$	24.2	44.2	0.2	0.9	0.5
$32 \times 32 \times 16$	26.2	49.4	0.0	0.7	0.6

Table 3.8: Relative Value of Computing Resources and Error of Result Normalized by the Uniform Mesh($ratio = 4, \Delta_{fine} \approx \lambda/58, \Delta_{coarse} \approx \lambda/15$), Case of monopole antenna shown in Fig. 3.10

$L_x \times L_y \times L_z$ $[cell^3]$	Resources		Computation Error		
	Memory [%]	CPU time [%]	Resonate freq. [%]	Band width [%]	Input impedance [%]
Uniform	100	100	0	0	0
$2 \times 2 \times 14$	3.2	5.8	0.9	3.0	1.6
$4 \times 4 \times 14$	3.6	6.4	1.0	1.1	2.0
$8 \times 8 \times 14$	4.2	7.7	0.7	1.4	1.5
$28 \times 28 \times 14$	8.3	16.0	0.7	2.2	0.1
$32 \times 32 \times 16$	9.7	17.9	0.1	2.7	0.4

We note that computation error becomes small when we expand analysis region of fine division in most cases, but calculation time and memory increase. And when the

fine region is as big as the electrical size of object, $28 \times 28 \times 14$ (In this case, coarse-fine boundary is two cells away from antenna in z direction) in the Table, the numerical error will be smallest. On the other hand, as the result of reduction of fine region, calculation time and memory can be cutting down greatly, and error is limited in the permission region.

3.4.2 Case of Top Loaded Low Profile Monopole Antenna

Analysis of planer antenna is carried out in this section. At first, we calculated a center fed patch antenna shown in Fig. 3.13. From Tables 3.9 and 3.10, we note that same result as monopole antenna's is obtained. When the fine region is as big as the electrical size of object(case of $20 \times 20 \times 10$), the numerical error is the smallest.

Table 3.9: Relative Value of Computing Resources and Error of Result Normalized by the Uniform Mesh($ratio = 2, \Delta_{fine} \approx \lambda/88, \Delta_{coarse} \approx \lambda/44$), Case of top loaded low profile monopole antenna shown in Fig. 3.13

$L_x \times L_y \times L_z$ $[cell^3]$	Resources		Computation Error		
	Memory [%]	CPU time [%]	Resonate freq. [%]	Return loss [%]	Band width [%]
Uniform	100	100	0	0	0
$20 \times 20 \times 8$	20.1	22.9	0.4	0.2	0.6
$30 \times 30 \times 8$	23.1	25.7	0.4	1.2	1.9
$20 \times 20 \times 10$	20.7	23.1	0.3	0.2	0.8
$30 \times 30 \times 15$	23.7	26.2	0.4	1.3	2.3

Table 3.10: Relative Value of Computing Resources and Error of Result Normalized by the Uniform Mesh($ratio = 6, \Delta_{fine} \approx \lambda/88, \Delta_{coarse} \approx \lambda/15$), Case of top loaded low profile monopole antenna shown in Fig. 3.13

$L_x \times L_y \times L_z$ $[cell^3]$	Resources		Computation Error		
	Memory [%]	CPU time [%]	Resonate freq. [%]	Return loss [%]	Band width [%]
Uniform	100	100	0	0	0
$20 \times 20 \times 8$	3.0	3.3	1.5	8.9	7.6
$30 \times 30 \times 8$	4.4	5.2	1.7	7.1	6.6
$20 \times 20 \times 10$	3.2	3.6	0.9	4.0	5.0
$30 \times 30 \times 15$	4.6	5.5	1.1	2.2	3.4

3.4.3 Case of Offset Fed Patch Antenna

Next, in order to investigate whether same result also can be obtained when feed point is not in the center of antenna, simulation of an offset fed patch antenna shown in Fig. 3.12 is carried out. Tables 3.11 and 3.12 show computation results when fine mesh region is changed, and ratio of two kinds of mesh size is 2 and 4. We note that the computation error is smaller in most cases when fine mesh region is $28 \times 28 \times 14$(The case of coarse-fine boundary is two cells away from antenna in x & y direction). The reason is considered that the discrete wave most closely approximates the actual wave propagation, and grid dispersion errors are minimized in these two cases. So we conclude that small numerical error can be obtained when we determine the fine mesh region based on electrical volume of object, and the position of feed point will not influence the numerical accuracy.

Table 3.11: Relative Value of Computing Resources and Error of Result Normalized by the Uniform Mesh($ratio = 2, \Delta_{fine} \approx \lambda/55, \Delta_{coarse} \approx \lambda/27$), Case of offset fed patch antenna shown in Fig. 3.12

$L_x \times L_y \times L_z$ $[cell^3]$	Resources		Computation Error		
	Memory [%]	CPU time [%]	Resonate freq. [%]	Band width [%]	Input impedance [%]
Uniform	100	100	0	0	0
$28 \times 28 \times 4$	21.1	26.3	0.0	0.7	0.8
$28 \times 28 \times 14$	24.2	30.8	0.0	1.2	2.2
$32 \times 32 \times 16$	26.2	34.4	0.0	1.0	3.1

Table 3.12: Relative Value of Computing Resources and Error of Result Normalized by the Uniform Mesh($ratio = 4, \Delta_{fine} \approx \lambda/55, \Delta_{coarse} \approx \lambda/14$), Case of offset fed patch antenna shown in Fig. 3.12

$L_x \times L_y \times L_z$ $[cell^3]$	Resources		Computation Error		
	Memory [%]	CPU time [%]	Resonate freq. [%]	Band width [%]	Input impedance [%]
Uniform	100	100	0	0	0
$28 \times 28 \times 4$	5.9	7.7	0.1	1.2	1.0
$28 \times 28 \times 14$	8.3	11.1	0.1	2.1	2.0
$32 \times 32 \times 16$	9.7	12.3	0.2	2.8	8.8

3.5 Conclusions

In this chapter, we examed computation error due to mesh size ratio and fine mesh region. From computation result, we conclude that small numerical error can be obtained when we determine the fine mesh region based on electrical volume of object.

Chapter 4

Simulation of Antennas with Fine Structure Partly

At previous part of this paper, we discussed the computation accuracy of proposed approach and how to determine the fine mesh region for a smaller numerical error.

In this chapter, we apply this approach to antennas that are difficult to obtain accuracy result by conventional FDTD method. The first object is a typical wire antenna, monopole antenna. The second antenna is a notch antenna that loaded with high dielectric constant material. And in the third section, we explain a simulation for a top loaded low profile monopole antenna, because the matching structure is quite small compare to the wavelength, the multimesh is used in the simulation. In the last section of this chapter, we apply the non-uniform mesh FDTD method in optimization of low profile and small antenna.

4.1 Simulation of Monopole Antenna

First, a monopole antenna with 5[cm] in length is measured and simulated. By comparing return loss characteristic with calculation result of Induced Electromotive Force method(EMF), we got good agreement between experiment and EMF method. When compare these two results to computation result by conventional FDTD method, we note that resonant frequency shifted to the lower region of measurement and EMF method. The reason is considered as a gap excitation is used in FDTD analysis, the simulation model become larger than real antenna because of the gap. Computation accuracy depends on the cell size greatly, especially in wire antenna's simulation.

To reduce the influence of cell size, non-uniform mesh simulation is carried out. We use a very small cell size(less than $\lambda/420$ in this case) to model the object, and ratio of two kinds of mesh size is 10. The coarse mesh is used in space between antenna and absorbing boundary.

As results shown in Fig. 4.1, computation error due to gap excitation is decreased by using a very small cell size. The proposed technique is effective to increase the accuracy of computation.

Table 4.1: Parameters of Computation ($a = 10$)

Size of object $[cm]$	L = 5
Computation space $[cm^3]$	$30 \times 30 \times 30$ $(\approx 1.4\lambda \times 1.4\lambda \times 1.4\lambda)$
Cell size $[mm]$ $(\Delta = \Delta x = \Delta y = \Delta z)$	$[I]$ $\Delta = 0.5$ $(\approx \lambda/420)$ $[II]$ $\Delta = 0.5 \times ratio$
Iteration	6000
Incident wave	Gaussian pulse
Absorbing boundary condition	Mur's 2nd approx.

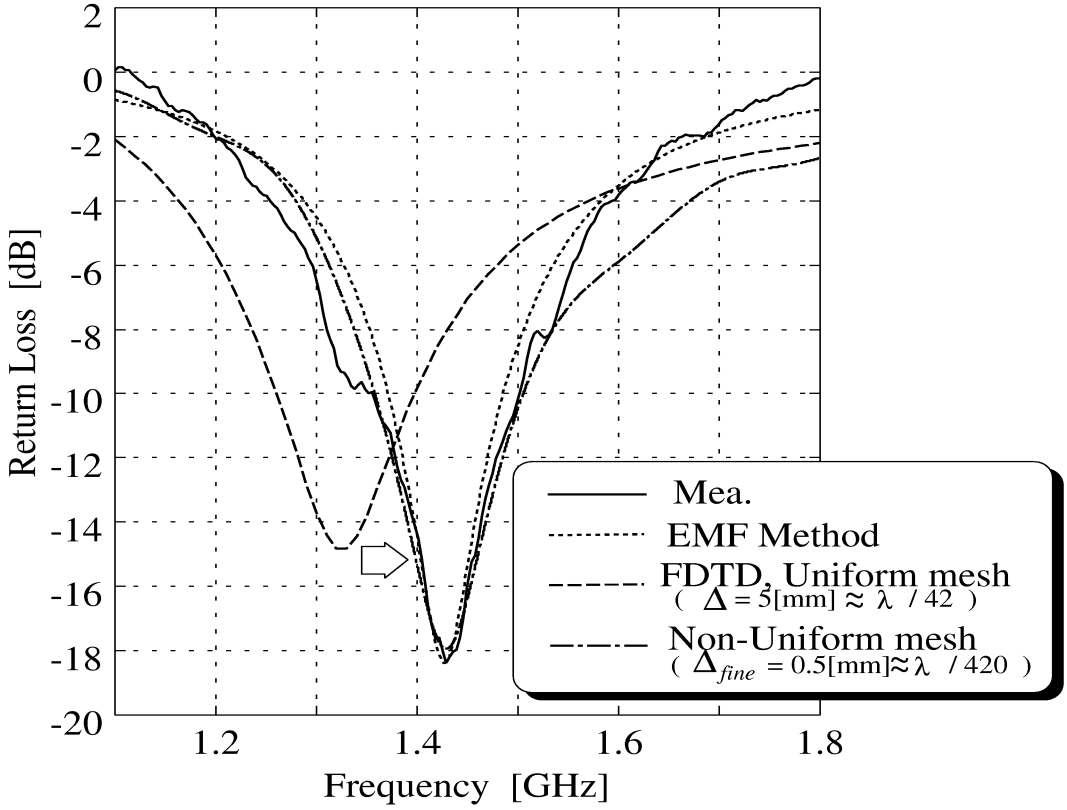

Figure 4.1: Return Loss Characteristics

4.2 Notch Antenna Loaded Dielectric Material

Next, a notch antenna shown in Fig.4.2 is calculated by using proposed method. Table 4.2 shows the detail parameters be used in simulation.

Two dielectric material blocks with high dielectric constant ($\epsilon_r = 11$) is loaded in the antenna. And the object has very complicated structure that required using smaller cell size.

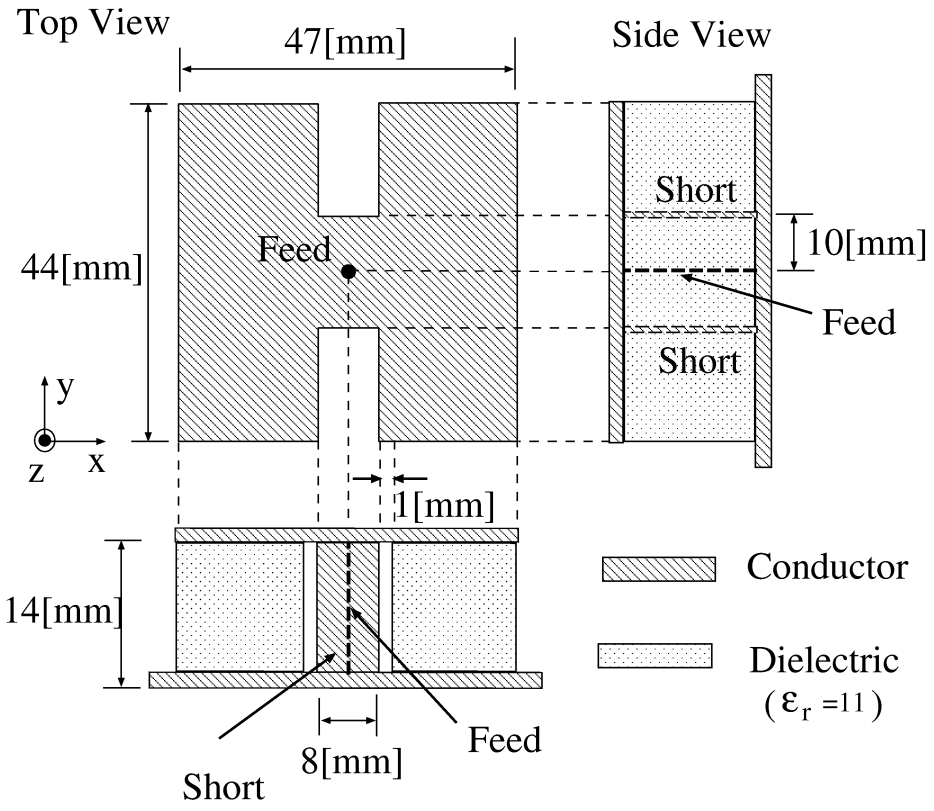

Figure 4.2: Notch antenna with dielectric material

Table 4.2: Parameters of Computation ($ratio = 16$)

Size of object $[mm]$	$44 \times 47 \times 14$
Computation space $[mm^3]$	$480 \times 480 \times 240$ $(\approx 1.3\lambda \times 1.3\lambda \times 0.7\lambda)$
Cell size $[mm]$ $(\Delta = \Delta x = \Delta y = \Delta z)$	$[I]$ $\Delta = 1.0$ $(\approx \lambda/366)$ $[II]$ $\Delta = 16.0$ $(\approx \lambda/23)$
Iteration	100000
Incident wave	Gaussian pulse
Absorbing boundary condition	Mur's 2nd approx.

As computation results shown in Fig.4.3, resonant frequency shifted in case of uniform mesh. The reason is that the computation resource limited us to use smaller cell enough to model the target accuracy.

By using the non-uniform mesh, smaller cells with less than $\lambda/366$ in size can be used to model the complicated structure of antenna. As the result, we got good agreement

with measurement and simulation result of proposed approach. We also noticed the different of bandwidth between them. The reason is considered that because the dielectric block has a layer structure, error can be decreased if we count the loss constant in simulation.

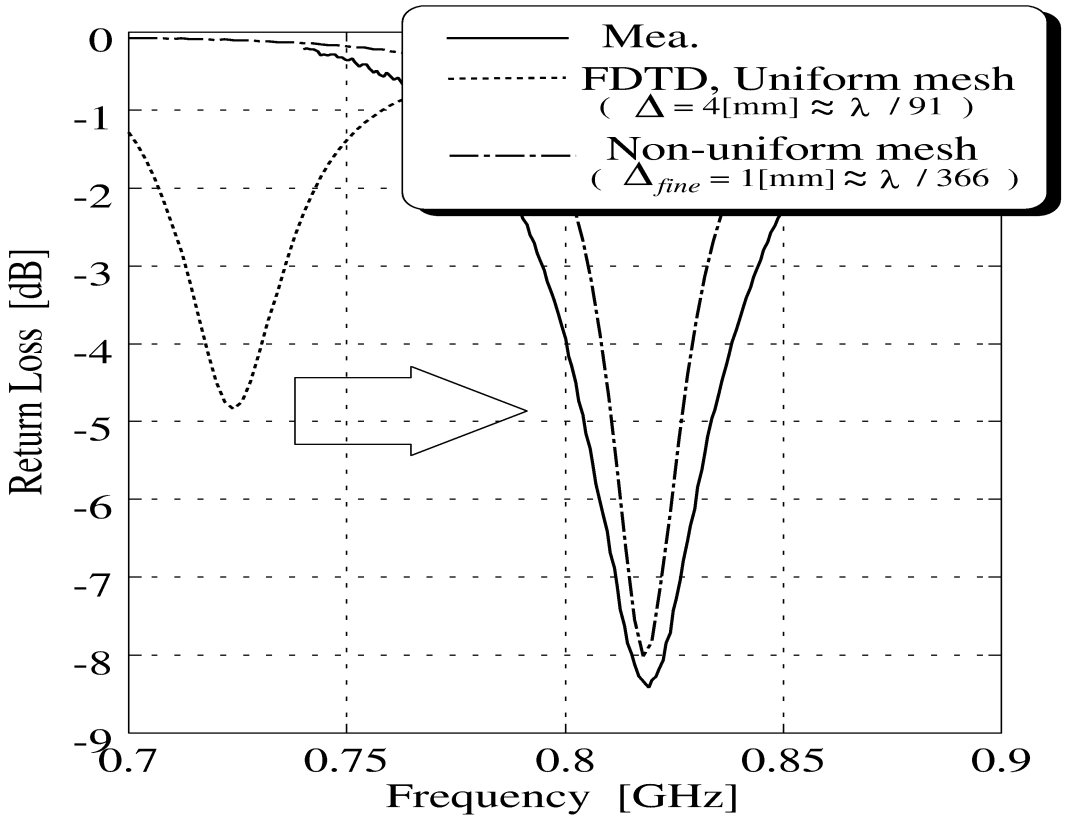

Figure 4.3: Return Loss Characteristics

4.3 Miniaturization of Top Loaded Low-Profile Monopole Antenna(TLMA)

In this section, we study a low profile top loaded monopole antenna . By changing the number, thickness, position and shape of post(s), the input and radiation characteristic due to parameters of matching post(s) are investigated. The low profile top loaded monopole antenna(TLMA) is known as a suitable way for antenna's miniaturization. But it is also reported that the parameters of matching post influence the input and radiation characteristic greatly. The FDTD method[2] is well suit for use in analyzing both the plate and wire structure. And to improve the calculation effect efficiency, the non-uniform mesh FDTD algorithm is used. From the measurement and simulation results, we propose the most suitable parameters of matching structure for low profile top loaded monopole antenna.

4.3.1 Introduction

In recent years, the need for smaller antennas has become increasingly important because the effect of large-scale integration of electronic components generally isolates the antenna as the most bulky, heavy and obtrusive part of the equipment. But it is an accepted fact that electrically smaller antennas have narrower bandwidths and poorer efficiencies than their larger counterparts. This would incur significant power losses and reduce the efficiency of the receiver as well as increasing equipment costs.

The inverted-L antenna is a low-profile structure, because the height of the vertical element is usually constrained to a fraction of the wavelength. Since the antenna is essentially a vertical short monopole loaded with a long horizontal wire at the end of monopole, the input impedance is nearly equal to that of the short monopole plus the reactance of the horizontal wire closely placed to the ground plane.

To increase the radiation resistance, another small inverted L shaped element is attached at the end of the vertical element, which is famous known as inverted-F antenna. The input impedance can be arranged to have an appropriate value to match the load impedance, without using any additional circuit between the antenna and the load.

On the other hand, a modification can be made by replacing the wire element with a plate(Disk Loaded Antenna, DLA)[12][13]. Matching posts are installed around the feed pin to increase the radiation resistance. By changing the position and thickness of short pins around feed point, the input impedance can be arranged to have an appropriate value to match the load impedance. Sekine introduced a wide band Disk-Loaded Folded Monopole Antenna[14]. By install a capacitive matching plate between Disc and ground plane, and an inductive matching post close to the feed pin, the fractional bandwidth is broaden.

However, this study is proceeded by experimentally way mainly till now[12]. In design of small antennas, optimization of parameters by using numerical simulation is necessary. In early works, numerical simulation by using wire-mesh method[15] and diakoptic theory[16] have been reported. In Moment method analysis, a special treatment is necessary for the joint part between plate segment and wire segment[18]. And in DK theory, it was reported that it was difficult to deal with the plate structure and wire element simultaneously. The FDTD method[2] is well suit for use in analyzing both the plate and wire structure. FDTD method is good at deal with antenna's complicated structures. Yang[19] introduced a FDTD simulation of a low profile multiplates antenna. FDTD analysis is considered suitable for deal with the plate and wire element simultaneously.

If the object under consideration has a structure that matching posts are very close to feed pin, it is very difficult to be simulated by FDTD analysis except we use an extremely small cell to model the gap between posts and feed pin. Because it will lead a remarkable increase of CPU time and memory be required in simulation. In addition,

the numerical analysis of matching technique by using same analysis method hasn't been reported yet.

In this section, we calculate four kinds of top loaded low profile monopole antennas that have different matching elements by using FDTD method. By changing the structure of matching element, examination of matching technique of low profile antenna is carried out in this paper. To improve the computation efficiency, the FDTD analysis by using non-uniform mesh is used during the simulation.

4.3.2 Simulation Models and Parameter

Figures 4.4 and 4.5 show two kinds of top loaded monopole antenna(TLMA). Model I in Fig. 4.4 is the antenna which have one short pin on side of feed pin. And in Model II, matching posts are installed on both sides of feed pin. And parameters used in the simulation is shown in Table. 4.3. The detail algorithm of FDTD analysis by using non-uniform mesh is described in previous chapter. In brief, we use two kinds of mesh sizes in the whole computation region, the fine mesh ([I] in Table 4.3) to model antenna structure precisely, and the coarse mesh ([II] in Table 4.3) is used in computation region between target and absorbing boundary. And ratio of two kinds of mesh sizes be used in simulation is 10. By using the non-uniform mesh, precise modeling is achieved by less computation resources and CPU time.

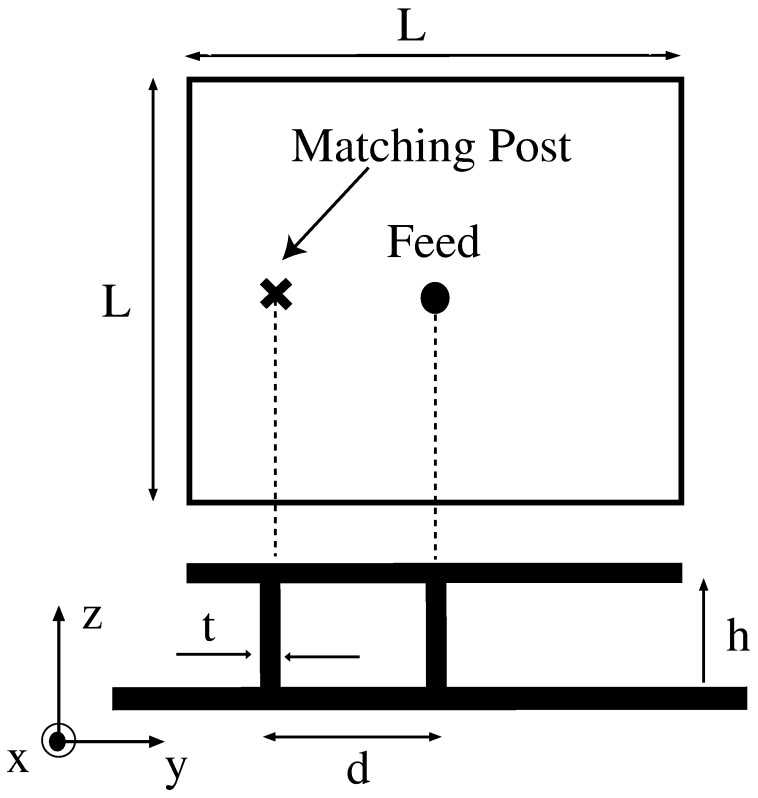

Figure 4.4: Simulation Model(Model I)

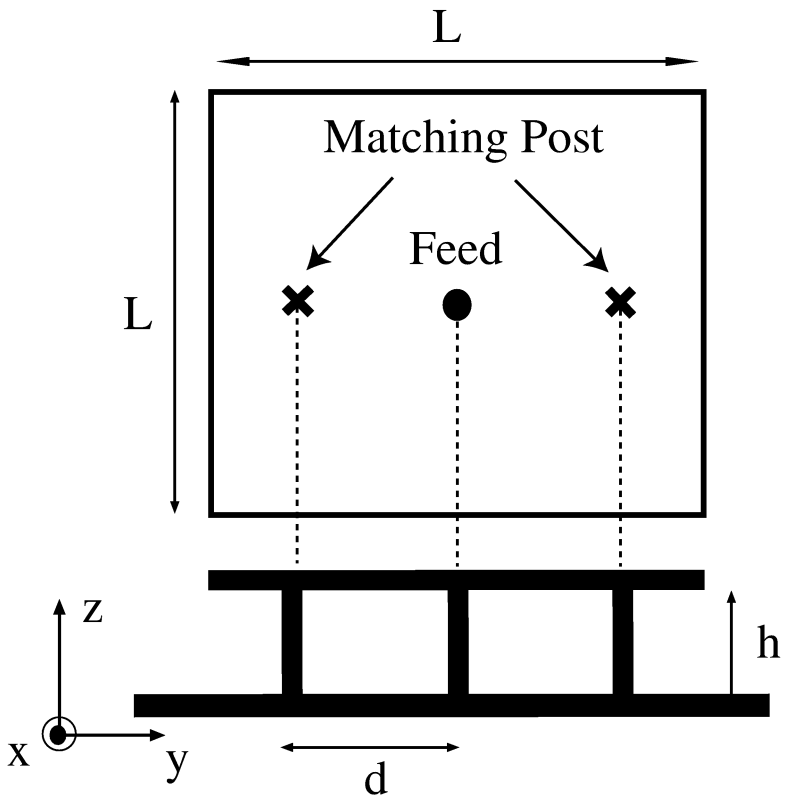

Figure 4.5: Simulation Model(Model II)

Table 4.3: Parameters be used in Simulation

Computation space	$300 \times 300 \times 150[mm^3]$ $(\approx 1.5\lambda \times 1.5\lambda \times 0.75\lambda)$
Size of object	$30 \times 30 \times 10[mm^3]$
Cell size [mm]	$[I]\ \Delta_{fine} = 1.0\ (\approx \lambda/200)$ $[II]\ \Delta_{coarse} = 10.0\ (\approx \lambda/20)$
Iteration	20000
Incident wave	Gaussian pulse
A. B. C.	Mur's 2nd approx.

4.3.3 Input and Radiation Characteristics of Model I and Model II

As previously mentioned, It is well known that the position, thickness and number of posts will influence the input impedance greatly. First of all, it is necessary to investigate how input characteristics will change due to the number of matching post.

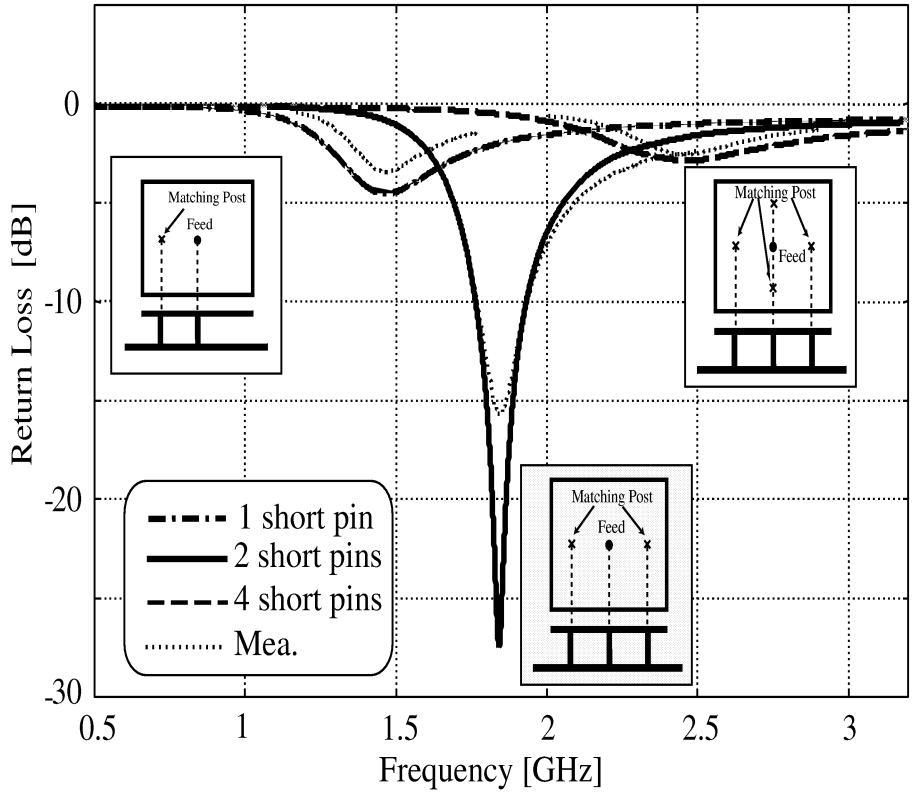

Figure 4.6: Return Loss Characteristic due to Number of Posts (d = $1.5h$, L = $3h$, $h = 10$[mm]), dotted lines show measurement results on each case

Figure 4.6 shows the return loss characteristic when number of matching post is 1, 2 and 4. To examine the effective of simulation method and model, measurement of same models are carried out. Dotted lines show measurement results on each case. We got good agreement between simulation and measurement. The validity of simulation model is verified. Curves on Fig. 4.6 show that although the resonant frequency shift to higher region compare to case of one post, the input impedance matches easier compare to the former. Next, we investigate the input impedance and radiation pattern of two models separately due to distance d and the effect of matching post's thickness.

TLMA with One Matching Post(Model I)

In this subsection, we investigate the dependence of input characteristics on distance d. Figure 4.8 shows the input characteristics when we move the post from a position which is very close to feed pin toward the edge of patch element. Next, in order to investigate them quantitatively, eigenvalue k_0h and fractional bandwidth when $VSWR <= 2.0$ are calculated. Figure 4.12 shows eigenvalue k_0h and fractional bandwidth due to d. Horizontal axis is the ratio of distance d to half width of plate(L/2). Vertical axis are eigenvalue k_0h and bandwidth ratio at $VSWR <= 2.0$, respectively. $k_0 = 2\pi/\lambda_0 = 2\pi f/C$ is wavenumber, where h is the height of top loaded monopole antenna(Model

I). Thus eigenvalue k_0h, which is proportional to resonant frequency, is one measure of antenna's miniaturization.

With the distance d increases, resonant frequency shift to the higher region. Bandwidth ratio reaches to a peak level of 2.2% when d/h is around 0.9, and then decreases with d increases. A most suitable value of d that impedance matching can be achieved easily is exist.

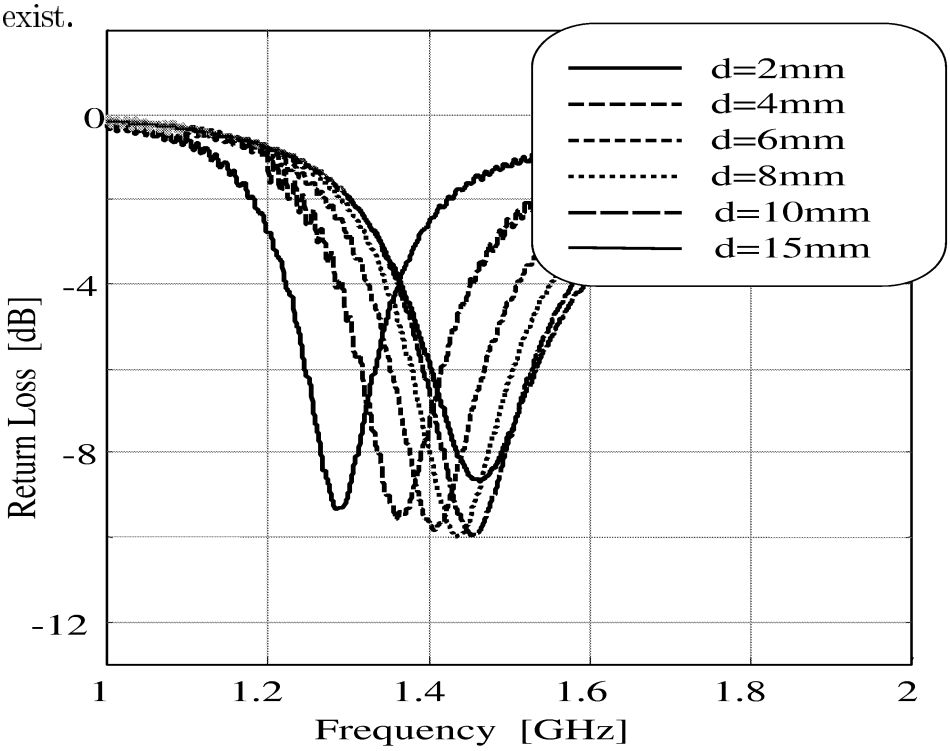

Figure 4.7: Return Loss Characteristic due to d (Model I)

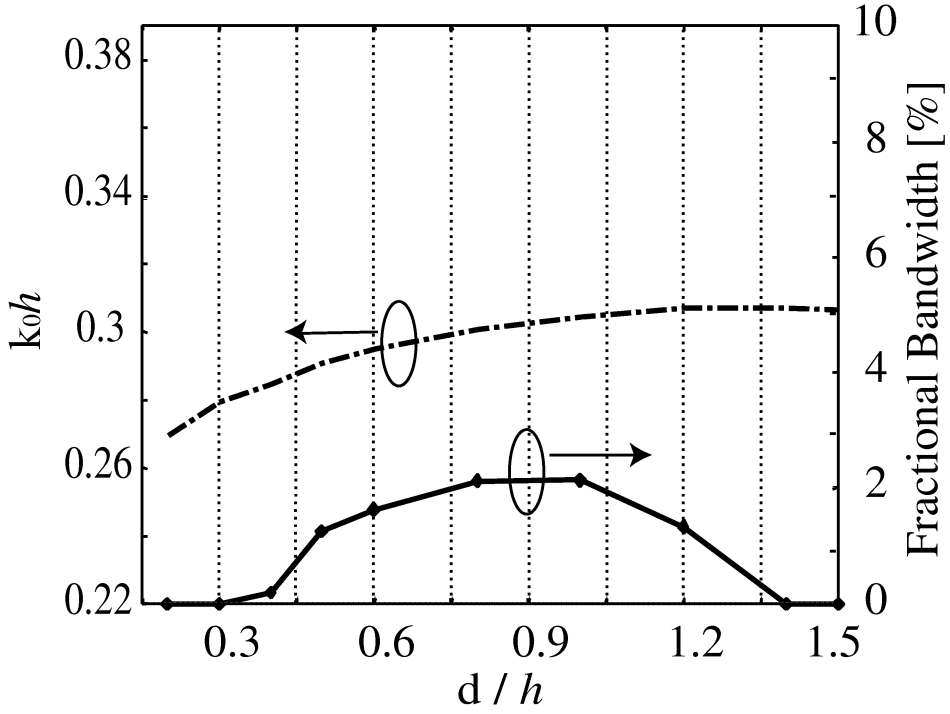

Figure 4.8: Eigenvalue k_0h due to d (Model I, L = $3h$, h = 10[mm], $VSWR <= 2.0$)

And then, radiation pattern when we install the post in the edge of patch element and the post being very close to the feed pin are calculated. Figures 4.9 and 4.10 show the radiation pattern in case of d are 2[mm](d=0.2h) and 15[mm](d=1.5h). We notice that an excitation of the cross polarization because of the horizontal element occurred in Z-X plane. And the crossing polarization increases when we move the post element toward the edge of patch element. The resonance of Model I is considered as same resonance as inversed-F antenna.

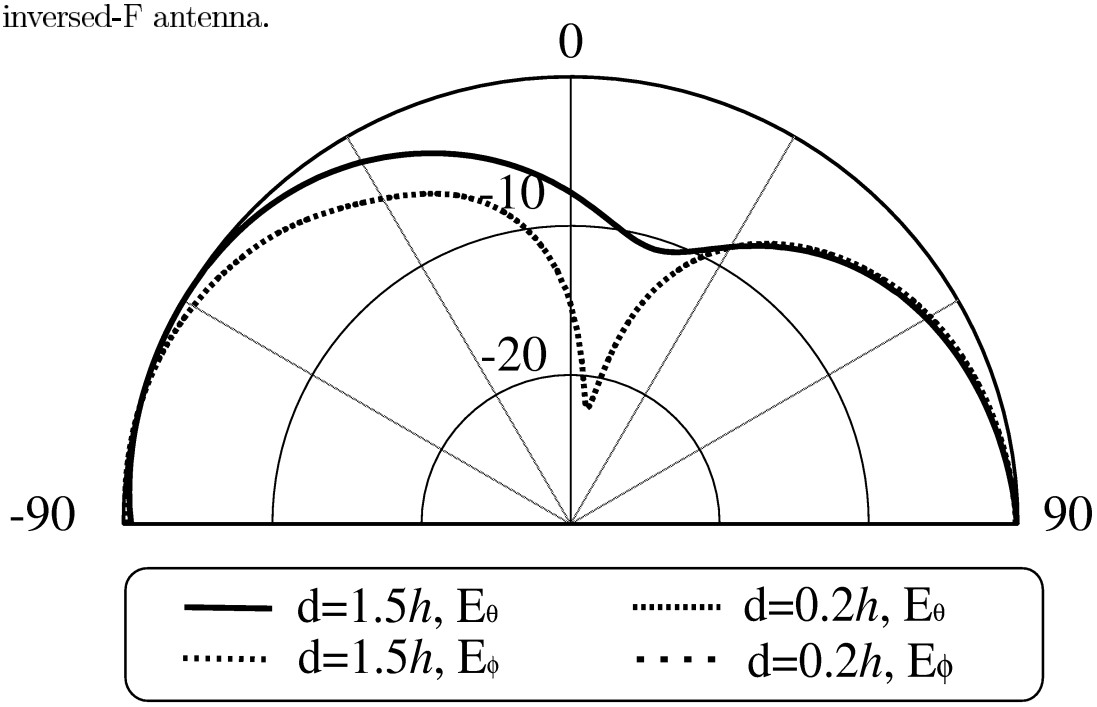

Figure 4.9: Radiation Pattern in yz Plane (Model I, L = 3h, h = 10[mm])

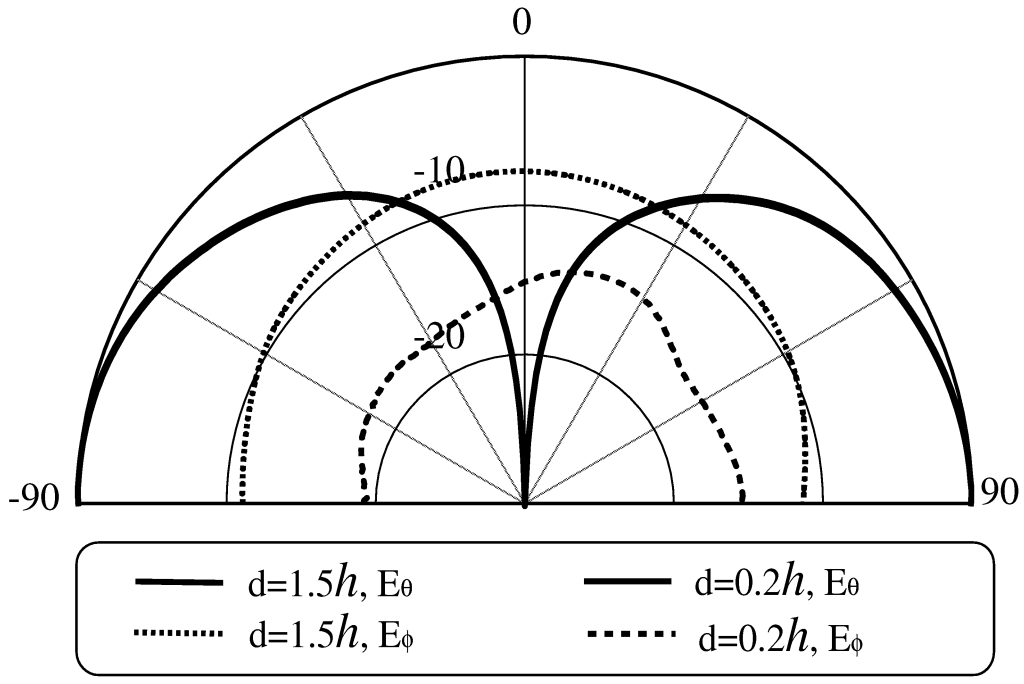

Figure 4.10: Radiation Pattern in zx Plane (Model I, L = 3h, h = 10[mm])

TLMA with Two Short Pins (Model II)

Using parameters be previously mentioned, we calculate the top loaded low profile monopole antenna with two short pins. By changing the distance (d) between matching posts and feed pin, resonant characteristic due to d is investigated. Figure 4.11 shows return loss characteristic due to d. Return loss characteristic change greatly depends on distance d. Impedance matching can be achieved when we install two posts at the edge of patch. Next, in order to investigate them quantitatively, eigenvalue k_0h and bandwidth ratio of $VSWR <= 2.0$ are calculated. Figure 4.12 shows eigenvalue k_0h and bandwidth ratio due to d/h. When we move matching posts away from feed pin, eigenvalue k_0h and bandwidth ratio increases. And bandwidth ratio reaches to a level of 9.6% when we install two matching posts at the edge of patch (d=1.5h).

And then, the radiation pattern of TLMA with two posts at the edge of patch is calculated. We got a symmetrical pattern in xy, zx and yz plane. Radiation pattern in zx and yz plane are as same as monopole antenna. But in xy plane, radiation on y direction are 2dB less than x direction(Fig. 4.13).

This resonance is considered as same as the resonance of loop antenna that is composed by feed pin and short pins when an image by ground plane is under consideration. And when post pins are moved toward the feed pin, resonant frequency become shift to the lower region. The antenna become electrically smaller, but impedance matching become more difficult with the decrease of d, the total efficiency decrease due to the additional losses in the matching unit.

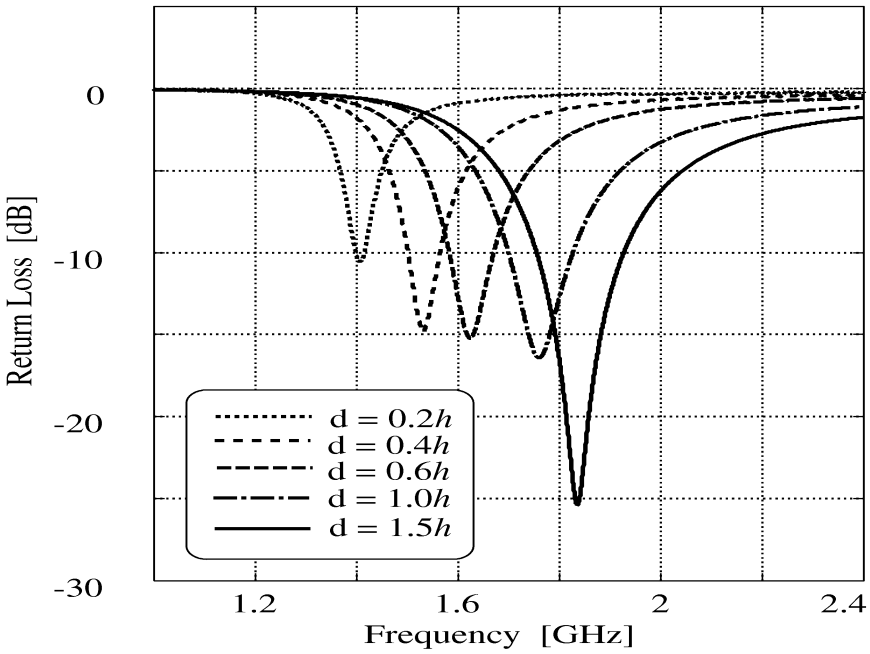

Figure 4.11: Return Loss Characteristic due to Distance between Post Pins and Feed Pin d (Model II, L = 3h, h = 10[mm])

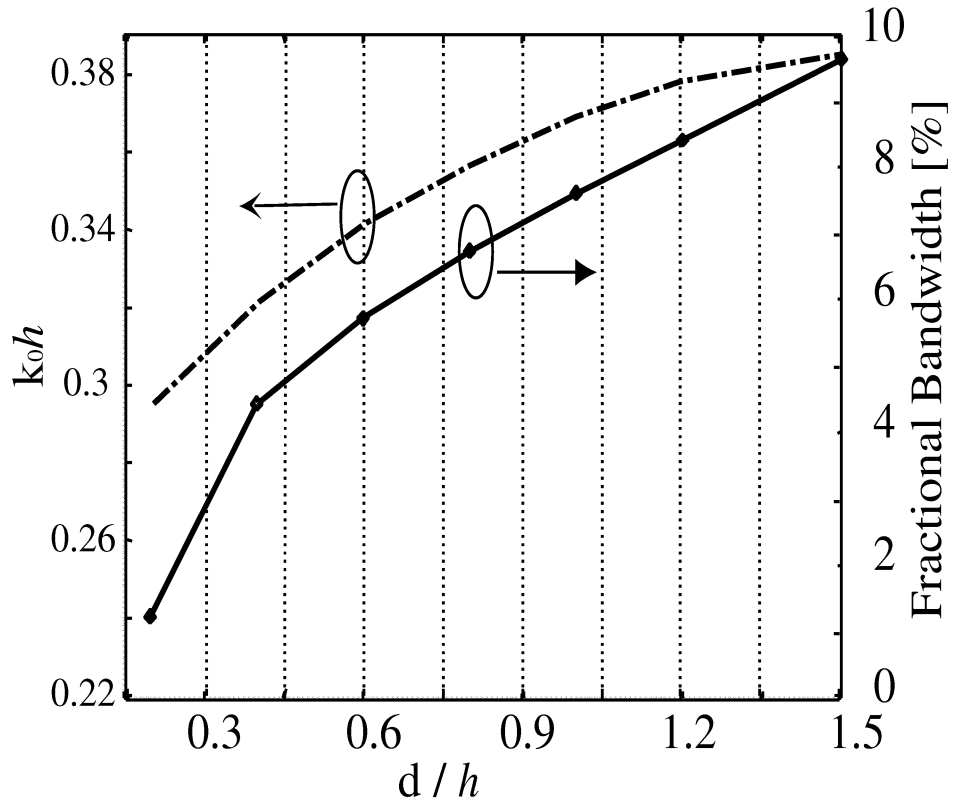

Figure 4.12: Eigenvalue k_0h and Bandwidth Ratio due to Distance d (Model II, L = $3h$, $h = 10$[mm], $VSWR <= 2.0$)

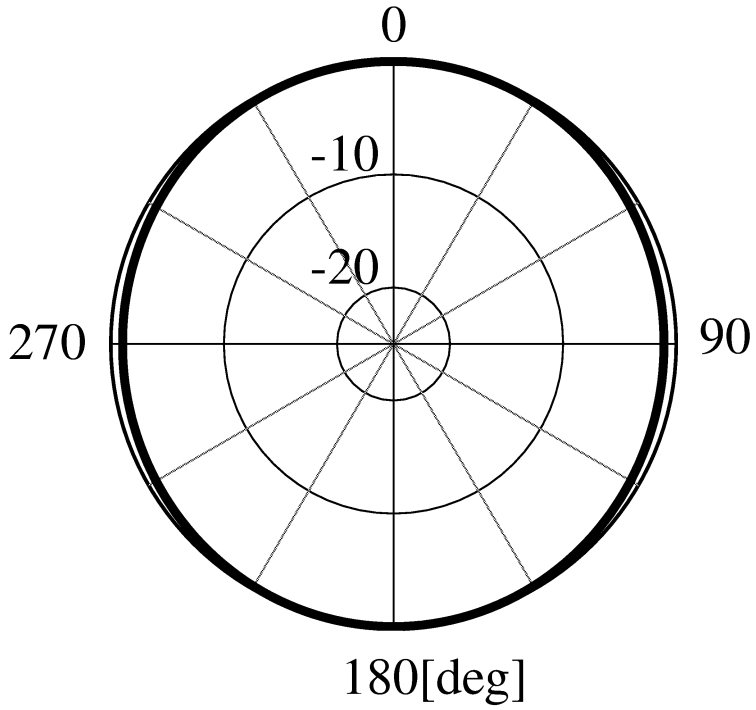

Figure 4.13: Radiation Pattern in X-Y plane (Model II, d = $1.5h$, L = $3h$, $h = 10$[mm])

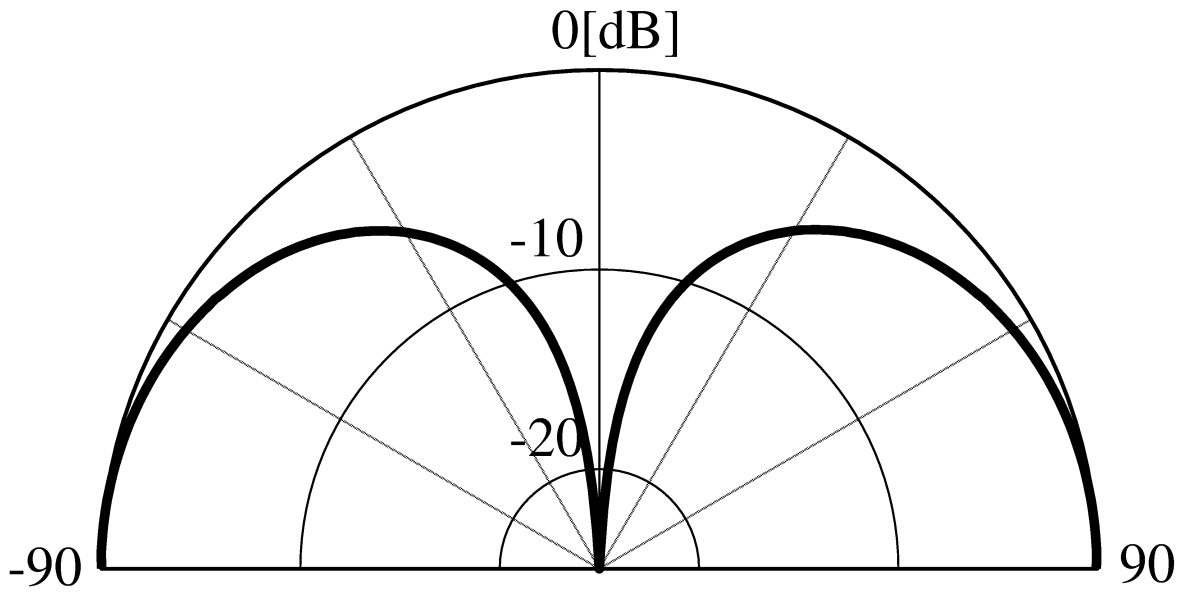

Figure 4.14: Radiation Pattern in Y-Z plane (Model II, d = 1.5h, L = 3h, h = 10[mm])

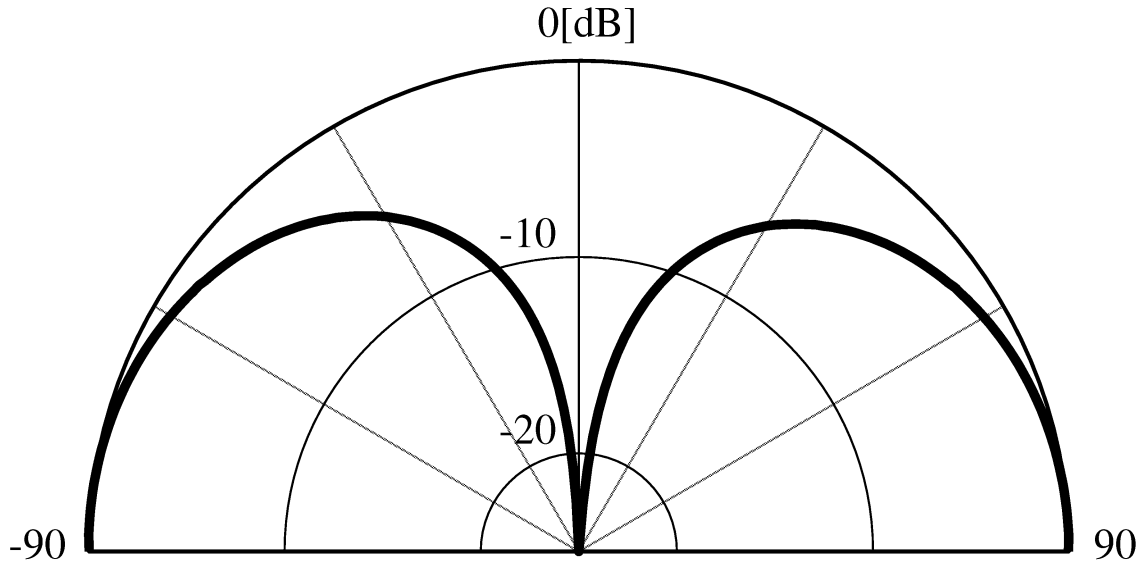

Figure 4.15: Radiation Pattern in Z-X plane (Model II, d = 1.5h, L = 3h, h = 10[mm])

Input Characteristic due to Thickness of short pin (Model I)

To simplify the problem, in previous simulation we model the matching post as a wire with no thickness($t = 0[mm]$ in Fig. 4.4). But the thickness of matching post is considered will influence the input impedance greatly. It is necessary to investigate how input characteristic will change when we consider the thickness of matching post. The simulation model is shown in Fig. 4.4.

Using the parameters be previously mentioned, we calculate the input characteristic when we change the thickness(diameter) of matching post from $0.2h$ to $0.4h$.

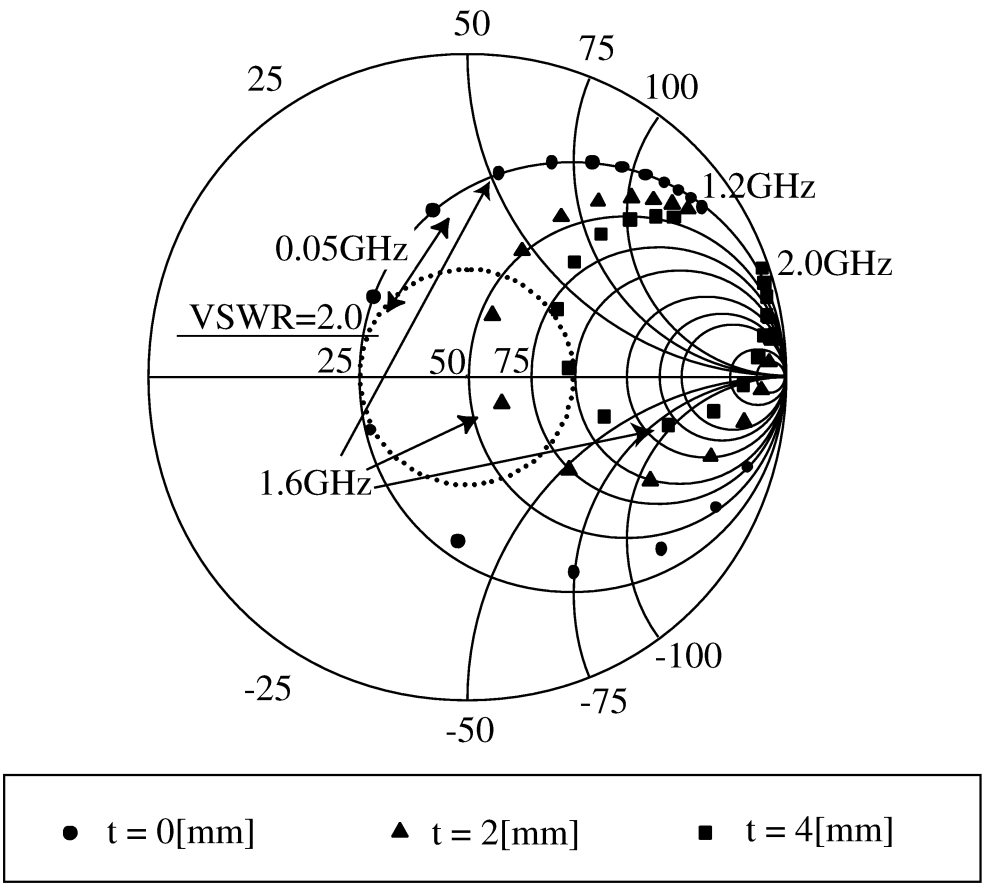

Figure 4.16: Input Characteristic due to Thickness of Shortpin t (Model II, d = $1.2h$, L = $3h$, $h = 10$[mm])

Figure 4.16 shows the input impedance in case of d is $1.2h$. Loci of input impedance when t are 0[mm], 2[mm]($0.2h$) and 4[mm]($0.4h$) are shown in the figure. Resonant frequency shift to the higher region when we increase the thickness of matching post.

And input impedance can be arranged to 50[Ω] when diameter of matching post is around 2[mm] in this case.

We also calculate input impedance due to t when distance d are changed from $0.4h$ to $1.3h$. Impedance matching can be achieved by using appropriate thickness of matching post for each d.

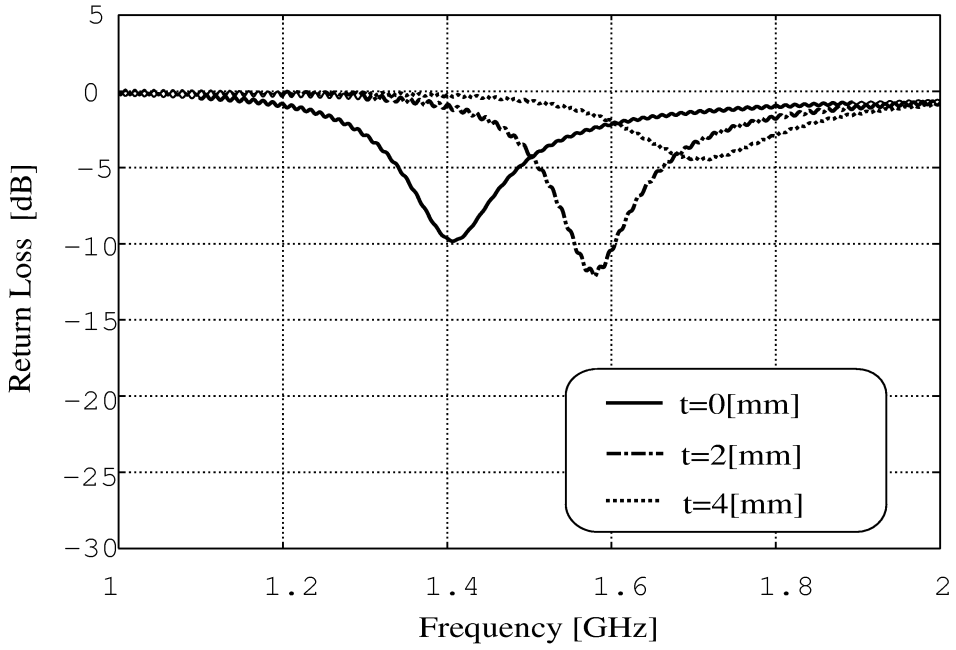

Figure 4.17: Return Loss Characteristic due to thickness of shortpin t (Model II, d = $0.4h$, L = $3h$, h = 10[mm])

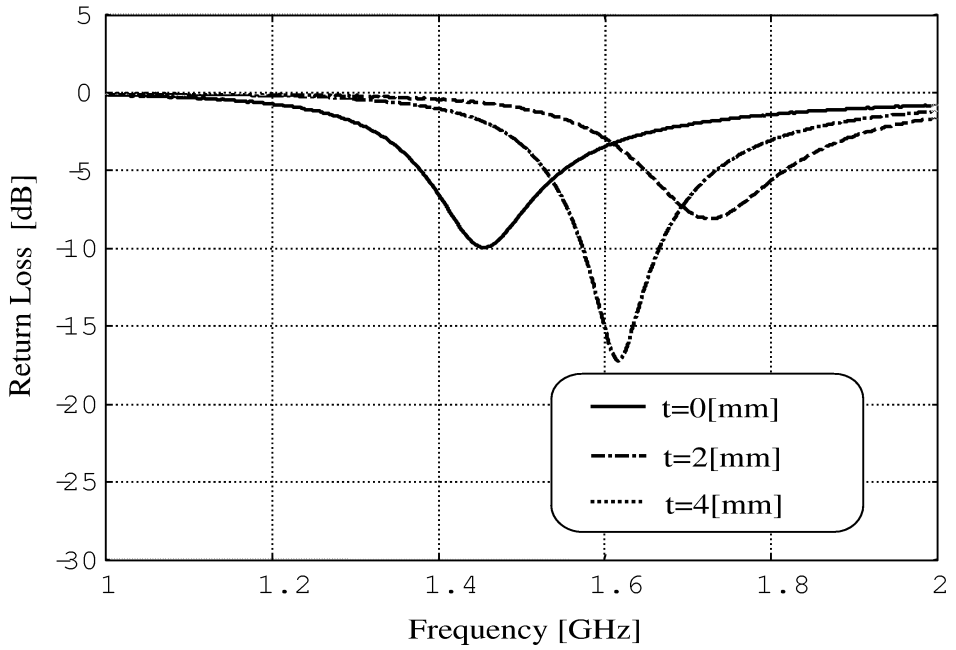

Figure 4.18: Return Loss Characteristic due to Thickness of Short Pin t (Model II, d = $1.0h$, L = $3h$, h = 10[mm])

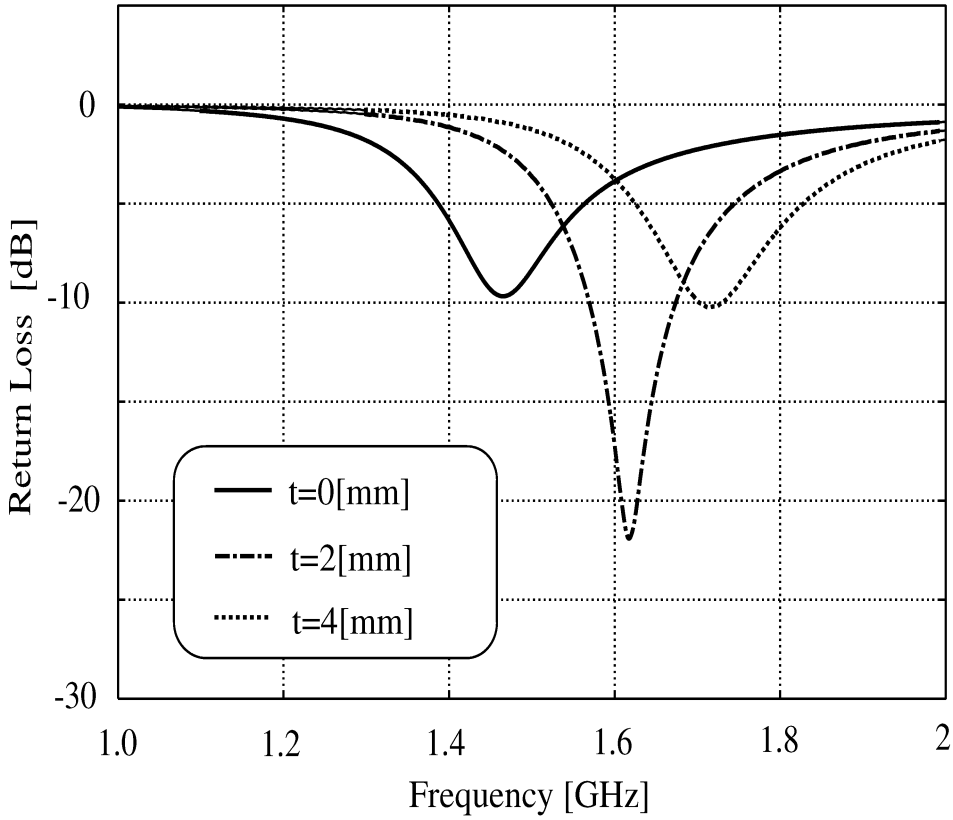

Figure 4.19: Return Loss Characteristic due to Thickness of Short Pin t (Model II, d = $1.2h$, L = $3h$, $h = 10$[mm])

In conclusion, the increase of matching post's thickness can be considered as the same effect with increase number of matching post. Change thickness and number of matching post(s) can arrange a suitable input impedance to match the load. This is considered an efficient matching technique. This result is also reported by simulation using DK method[16].

4.3.4 TLMA with bent matching structure

In previous section, we calculate the TLMA with one and two matching post(s) (Model I & Model II). As the result, the miniaturization can be achieved when we install matching posts close to the feed pin, but impedance matching become difficult in this case. It is necessary to investigate the suitable matching element for this kind of antenna.

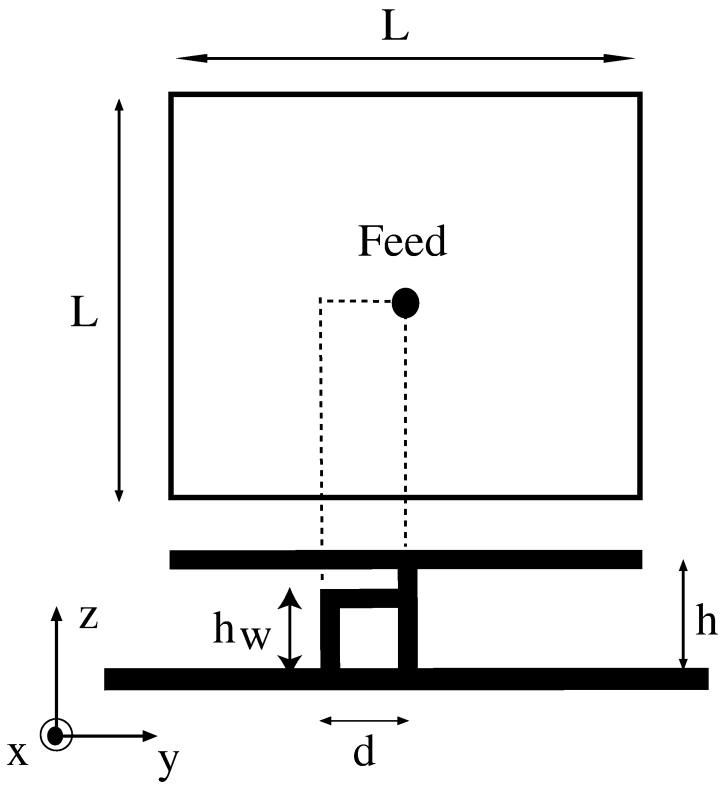

Figure 4.20: Simulation Model(Model III)

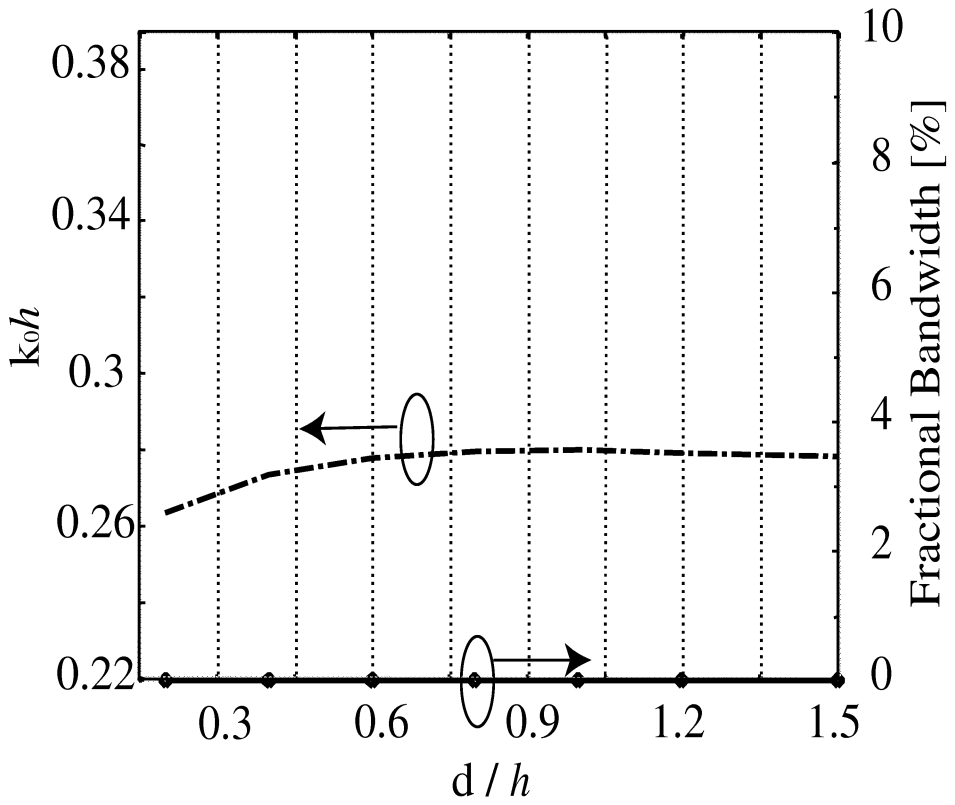

Figure 4.21: Eigenvalue k_0h and Bandwidth Ratio due to Distance d (Model III, L = $3h$, $h = 10$[mm], $VSWR <= 2.0$)

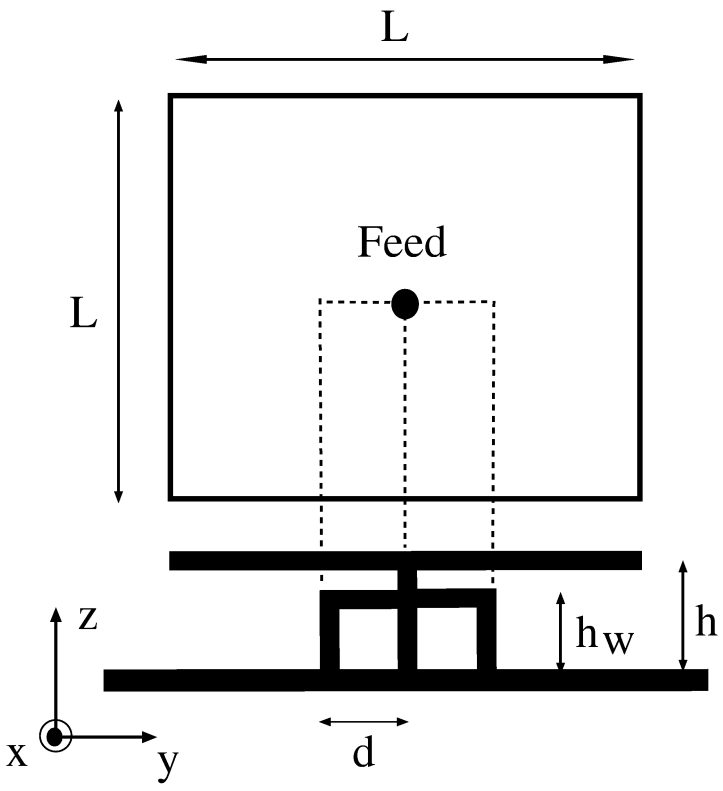

Figure 4.22: Simulation Model(Model IV)

For an inverted F antenna, a bent element is effective in impedance matching. Here, when we bend the matching element to feed pin(structure as Model III shown in Fig. 4.20), the central frequency is arranged to a lower level compare to short pin case(Fig. 4.21). But the impedance matching become worse because of the large absolute value of input impedance.

Next, another bent matching element is installed on the other side of feed pin, as Model IV be shown in Fig. 4.22.

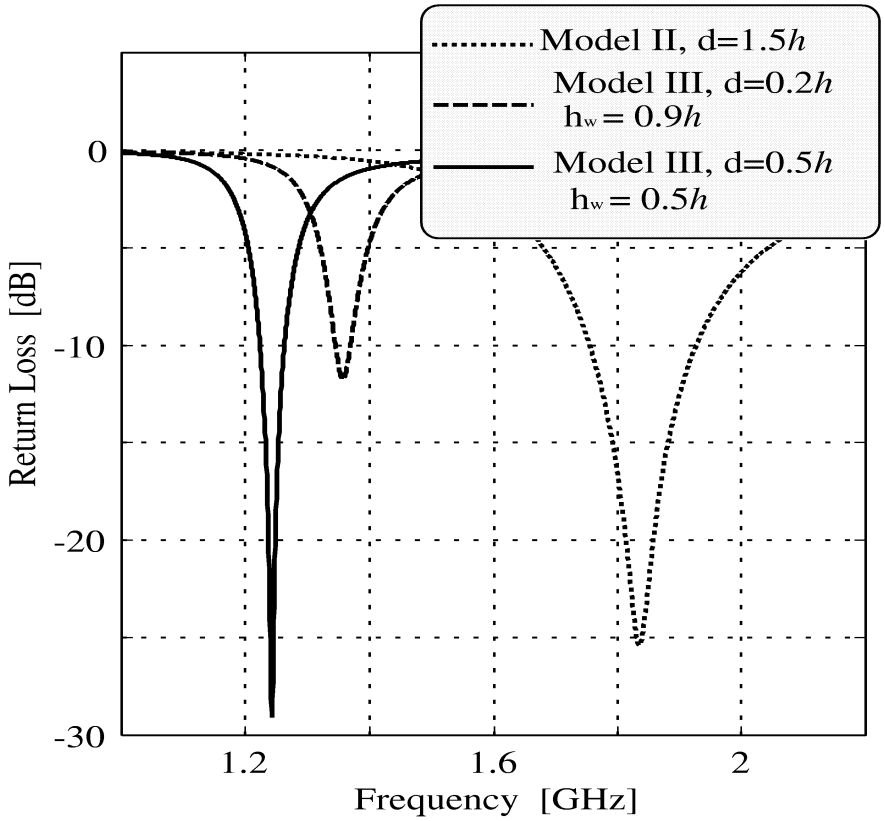

Figure 4.23: Comparison of Return Loss Characteristic (L = $3h$, h = 10[mm])

Simulation of input characteristic due to distance between feed pin and matching element d and height of matching element h_w is carried out. Because the upper part of matching element will close to patch element very much when h_w are 8[mm](0.8h) and 9[mm](0.9h), accurate modeling is considered difficult if we use a 1[mm] mesh. In these two cases, a very fine mesh($\Delta_{fine} = 0.5[mm] \approx \lambda/400$ in Table 4.3) is used in simulation. The result is compared to case of TLMA with two short pins(Fig. 4.23). The resonant frequency become shift to lower region, and the matching is also better than Model II.

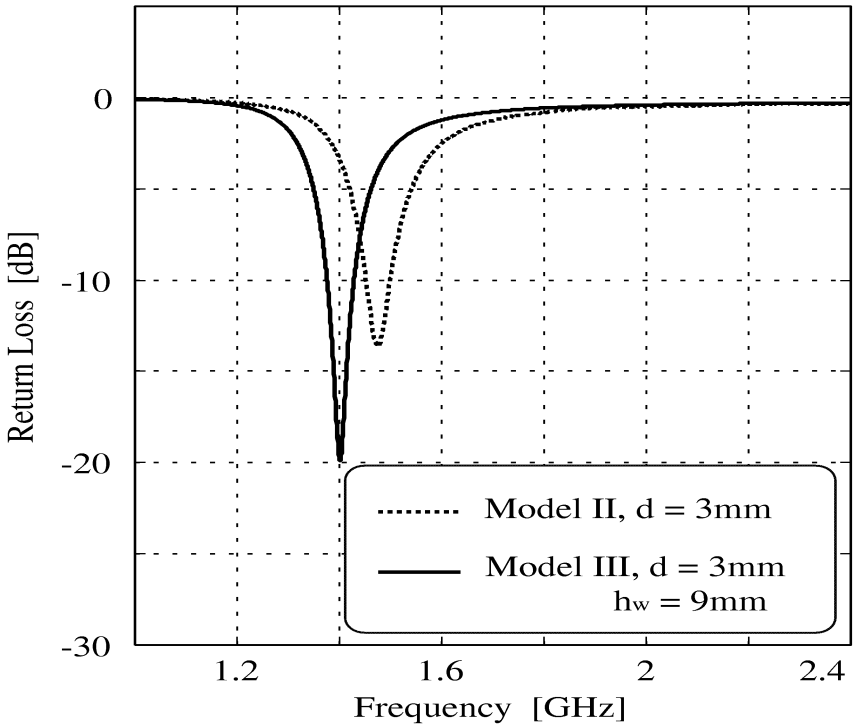

Figure 4.24: Comparison of Return Loss Characteristic (L = $3h$, h = 10[mm])

To investigate the most suitable parameters of matching element, examination of input characteristic due to h_w(Height of matching element) and d(Distance between matching element and feed pin) is carried out.

Height of matching element(h_w)

Using parameters be previously mentioned, input characteristic due to h_w is simulated. To evaluate the most suitable value of h_w, eigenvalue k_0h and bandwidth ratio $Bandwidth/f_0$ are calculated.

Figures 4.25 and 4.26 show h_w/h versus bandwidth ratio when d is change from 2[mm] to 11[mm]. The higher h_w is, the easier impedance matching can be achieved.

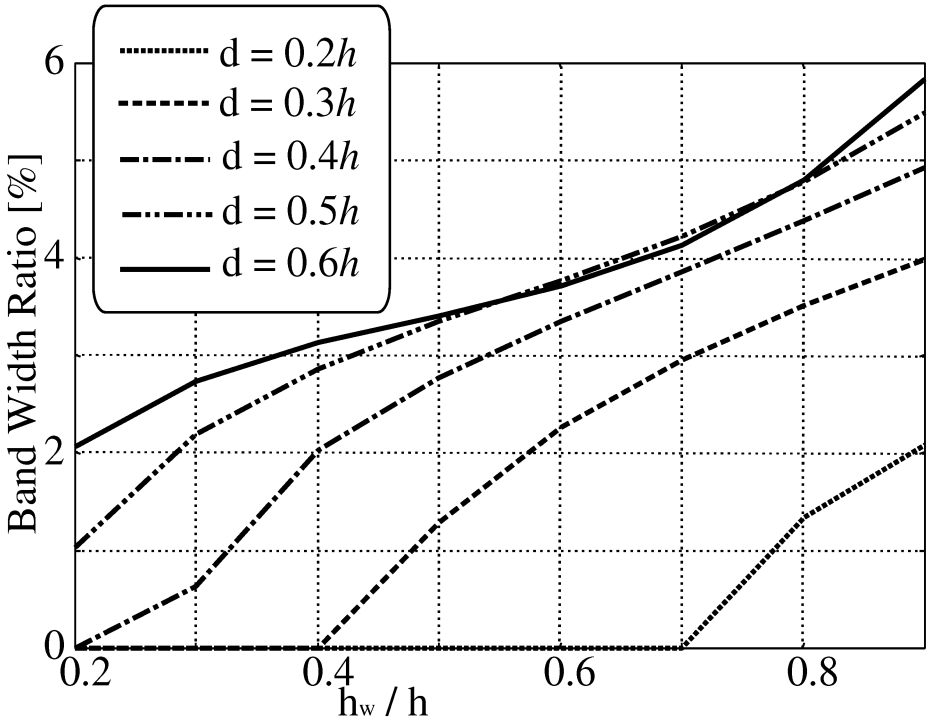

Figure 4.25: Bandwidth Ratio due to h_w(2-1)(Model IV, L = $3h$, h = 10[mm], $VSWR <= 2.0$)

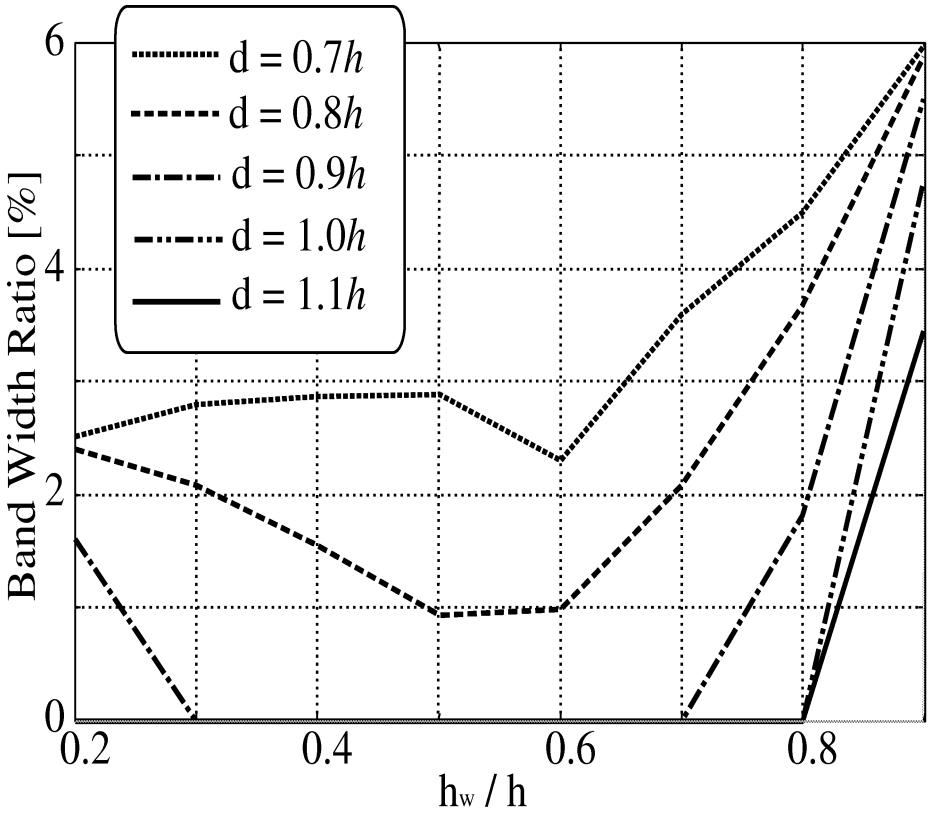

Figure 4.26: Bandwidth Ratio due to h_w(2-2)(Model IV, L = $3h$, h = 10[mm], $VSWR <= 2.0$)

Distance between Matching Element and Feed Pin(d)

In above results, it is clear that there is a most suitable value for d existed. Investigation of bandwidth ratio characteristic due to d is carried out. Figure 4.27 shows d/h versus bandwidth ratio. For comparison, curves of h_w changes from $0.2h$ to $0.9h$ are shown in the graph. Each curve shows an optimum value of d from $0.5h$ to $0.7h$, depends on h_w. At the same time, maximum value of bandwidth ratio changes greatly due to h_w. When $d \approx 0.7h$, and $h_w = 0.9h$, the bandwidth ratio reaches to a level of 6%.

Figure 4.28 shows d/h versus eigenvalue k_0h and bandwidth ratio when h_w is $0.9h$. When peak level of bandwidth ratio shown at $d \approx 0.7h$, eigenvalue is around 0.31. Height of antenna is less than $\lambda/20$ in this case. Compare to the result of TLMA with two short pins(Fig. 4.12), eigenvalue is smaller than Model II case on purpose to obtain same bandwidth ratio.

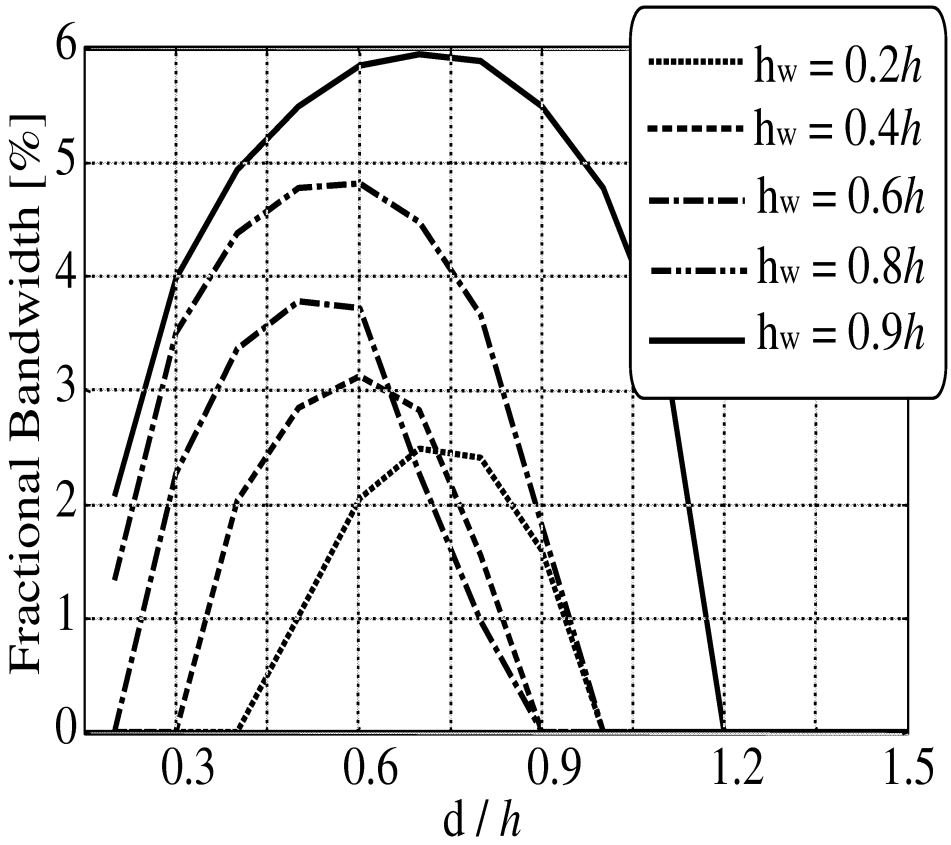

Figure 4.27: Bandwidth Ratio due to Distance d(Model IV, L = $3h$, h = 10[mm], $VSWR <= 2.0$)

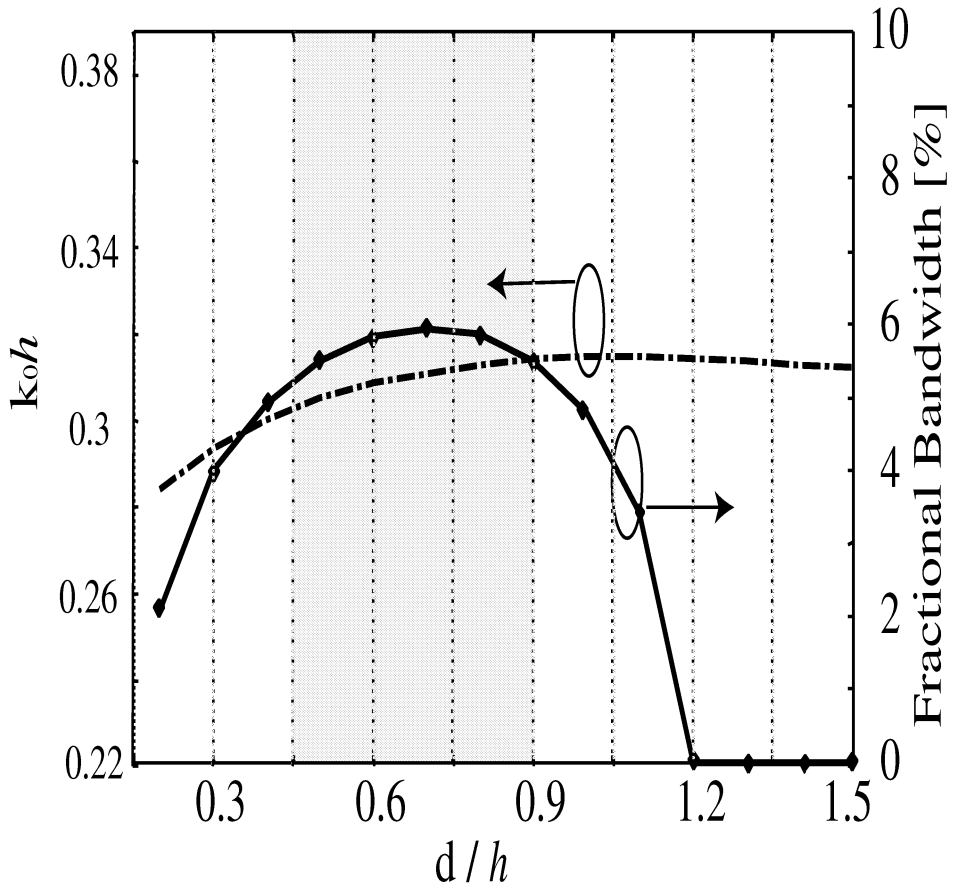

Figure 4.28: Eigenvalue k_0h and Bandwidth Ratio due to Distance d (Model IV, L = $3h$, $h_w = 0.9h$, $h = 10$[mm], $VSWR <= 2.0$)

Height and length of patch element (h/L)

In previous subsections, we fix patch element's height as high as $3h$. It is necessary to investigate the optimum value of height and length of patch element (h/L). Figures 4.29 and 4.30 show fractional bandwidth and eigenvalue k_0h due to ratio of height and length of patch element(h/L). For comparison, curves of TLMA with two short pins(Model II in Fig. 4.5) are shown on same figures. Although fractional bandwidth of Model II reaches higher level compare to Model IV(Fig. 4.30), eigenvalue k_0h is also higher than Model IV case(Fig. 4.29). For miniaturization purpose, Model IV is considered more suitable.

When h/L is around $0.3 \sim 0.35$, antenna's height is less than $\lambda/20$, and impedance matching also can be achieved easily.

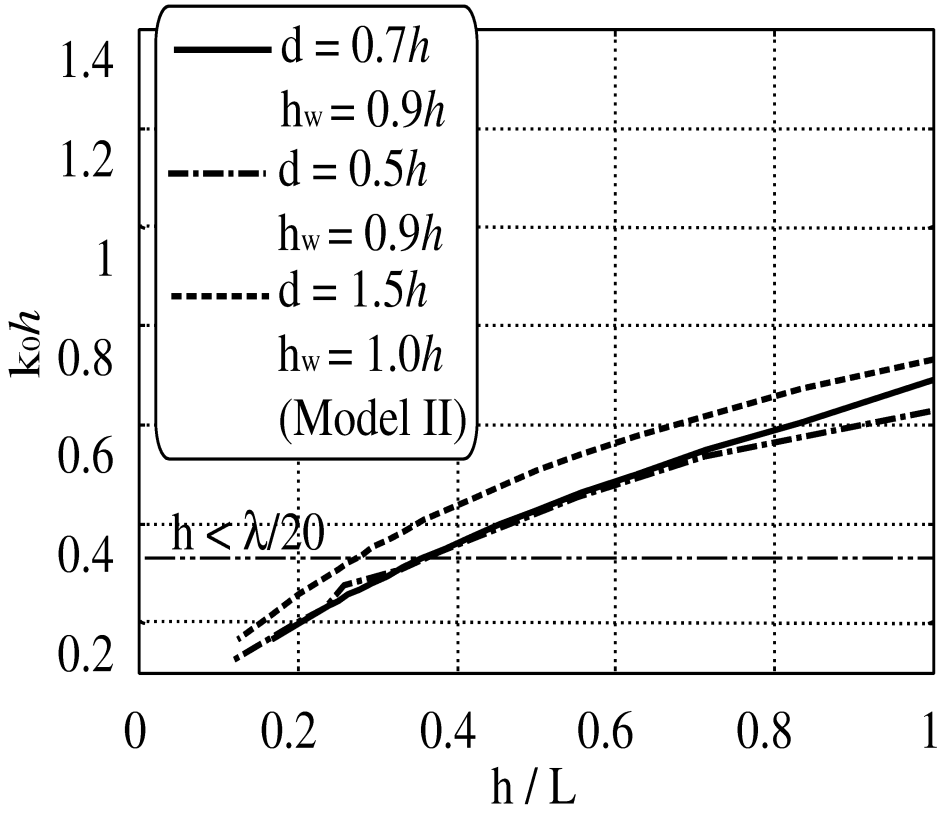

Figure 4.29: Eigenvalue k_0h due to h/L(Model IV, $h = 10$[mm])

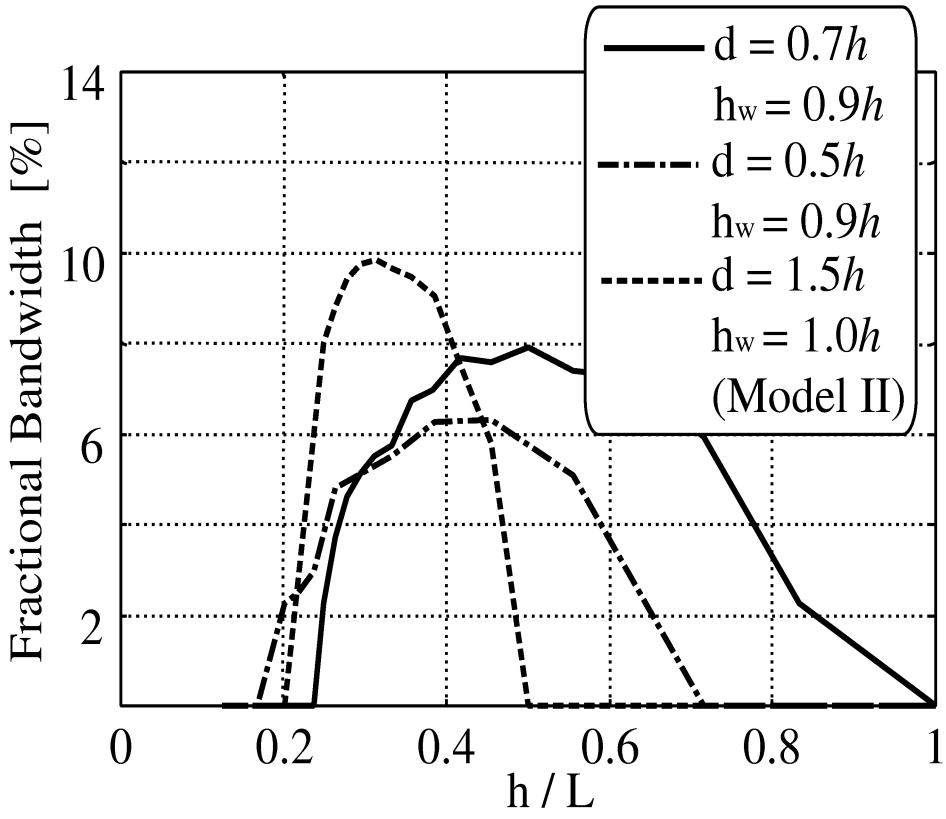

Figure 4.30: Fractional Bandwidth due to h/L(Model IV, $h = 10$[mm])

Radiation Pattern

Radiation pattern of Model IV (L = $3h$, d = $0.5h$, $h_w = 0.9h$, $h = 10$[mm])) is investigated. We get same radiation characteristic as monopole antenna. The resonance of Model IV is considered as same resonance as loaded folded monopole antenna. TLMA which have bent matching element(s) is considered more efficiency on miniaturization purpose.

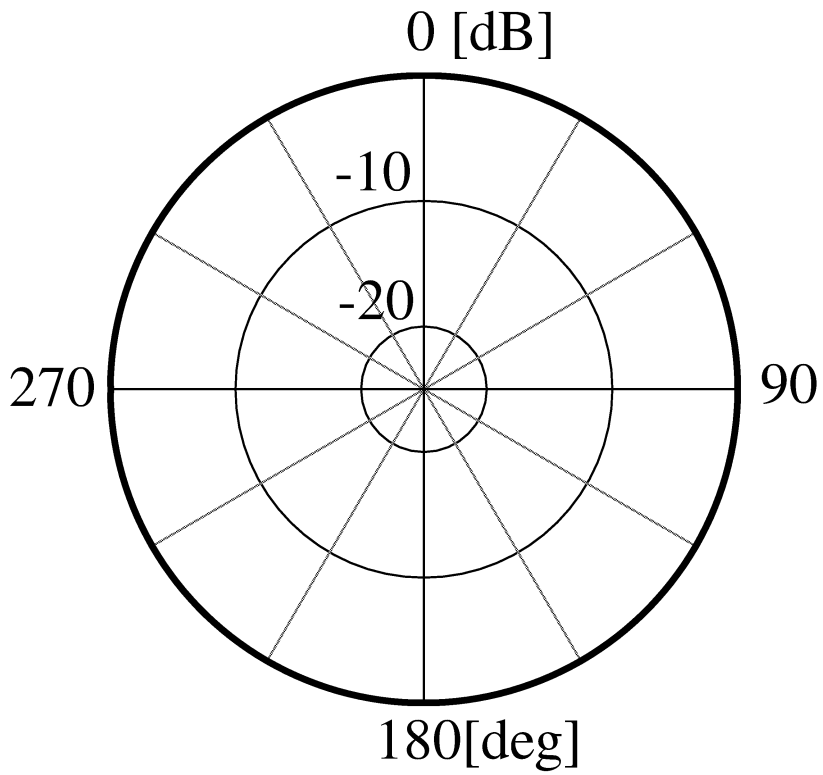

Figure 4.31: Radiation Pattern in X-Y plane (Model IV, L = $3h$, d = $0.5h$, $h_w = 0.9h$, $h = 10$[mm])

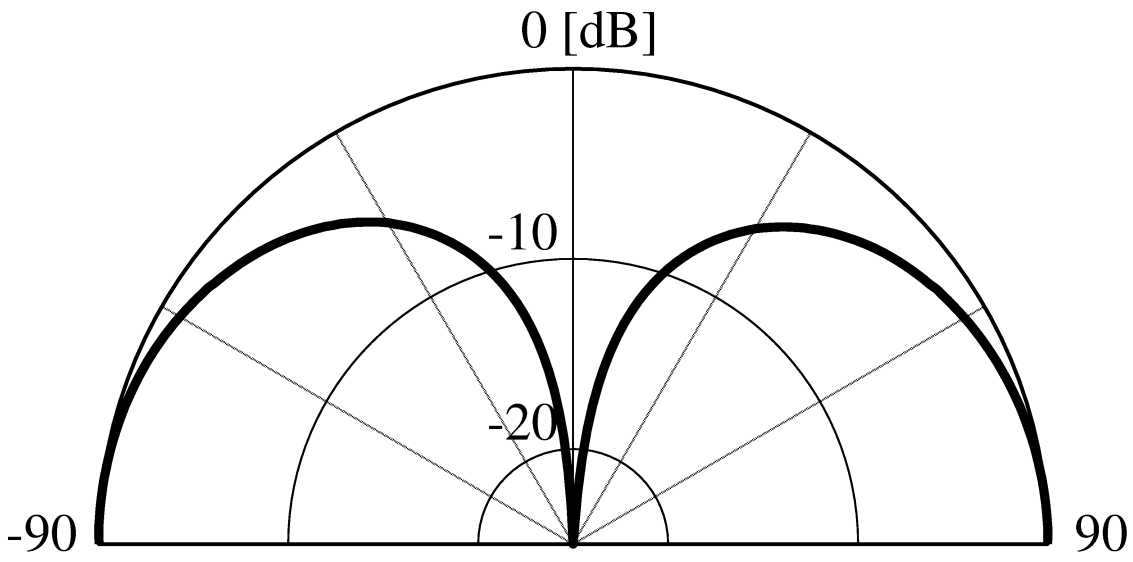

Figure 4.32: Radiation Pattern in Y-Z plane (Model IV, L = $3h$, d = $0.5h$, $h_w = 0.9h$, $h = 10$[mm])

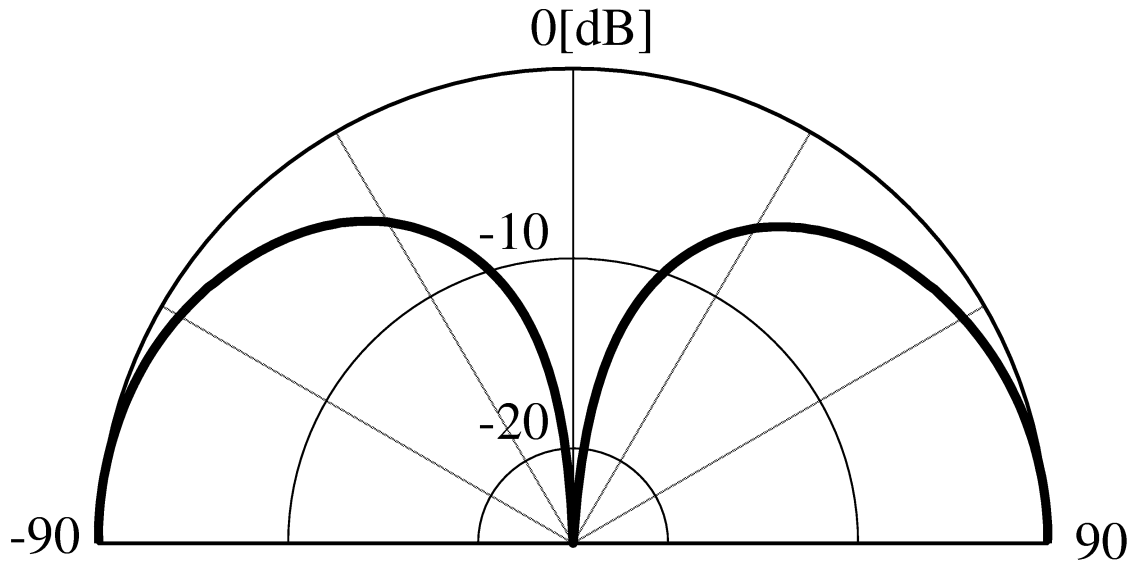

Figure 4.33: Radiation Pattern in Z-X plane (Model IV, L = $3h$, d = $0.5h$, $h_w = 0.9h$, $h = 10$[mm])

4.3.5 Conclusions

Using the Non-Uniform Mesh FDTD analysis, we investigate matching technique of top loaded low profile monopole antenna due to parameters of matching element(s). By changing the number, thickness, position and structure of matching elements, we conclude that different of resonance occurred due to these parameters of matching elements. And on purpose to achieve the miniaturization, the matching element with bent structure (Model IV) is considered efficiently. And optimum value of antenna's height(h), matching element's d and h_w are exist.

4.4 Small Pager's Base Station Antenna

In this section, a simulation for a pager's base station antenna is carried out. The resonate frequency is near 280MHz. For a miniaturization purpose, the antenna is constructed with a top loaded low-profile monopole antenna and two dielectric blocks ($\epsilon_r = 2.4$). The wire structure is used for matching purpose. To modeling the antenna precisely, the thickness of wire(about 2[mm]) is need to be counted. This requires a very small cell size(less than 1.0[mm], about $\lambda/1064$) compare to the main body of antenna be used in the simulation.

Moreover, because the ground plane is quite small compare to the wavelength, the return loss characteristic and radiation pattern will change if we count the ABS cover of antenna in computation. So it is also necessary to model the cover which has a thickness of 3[mm]. All of them require a smaller cell size, but the computation resources limited the smallest cell size even when we use the non-uniform mesh FDTD analysis which used two kinds of mesh intervals.

In this section, we model the antenna precisely by using three kinds of mesh sizes. And optimization of matching structure is also carried out.

First, Fig. 4.34 shown the simulation model of top loaded low profile monopole antenna. The whole computation space is divided by three kinds of meshes as follows:

1) Finest mesh: The finest mesh($1[mm] \times 1[mm] \times 1[mm]$) which are used mainly in modeling of space around matching(wire) structure.
2) Fine mesh: Meshes which are bigger than the finest mesh($3[mm] \times 3[mm] \times 1[mm]$) which are used mainly in modeling of space around object except the finest mesh region.
3) Coarse mesh: The coarse mesh ($75[mm] \times 75[mm] \times 25[mm]$) which are used in space between object and absorbing boundary.

Table 4.4 shown the detail parameters be used in simulation, for example, computation space, cell size, etc.

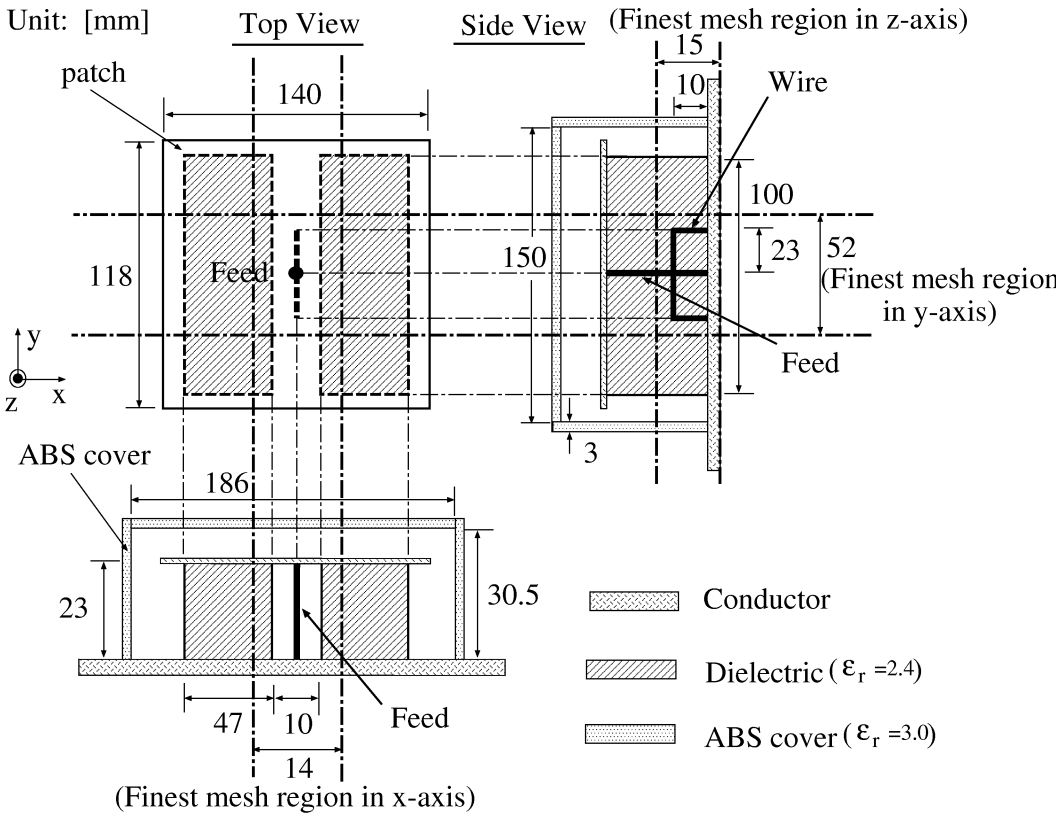

Figure 4.34: Top Loaded Low Profile Monopole Antenna

Table 4.4: Simulation Parameters

Size of object [m]		$0.192 \times 0.156 \times 0.0335$
Computation space $[m^3]$		$2.4 \times 2.4 \times 1.1$ ($\approx 2.3\lambda \times 2.3\lambda \times 1.1\lambda$)
Cell size $[m]$	Δ_{finest}	$0.001 \times 0.001 \times 0.001$ ($\approx \lambda/1064 \times \lambda/1064 \times \lambda/1064$)
$[m]$	Δ_{fine}	$0.003 \times 0.003 \times 0.001$ ($\approx \lambda/355 \times \lambda/355 \times \lambda/1064$)
	Δ_{coarse}	$0.075 \times 0.075 \times 0.025$ ($\approx \lambda/14 \times \lambda/14 \times \lambda/42$)
Iteration		200000
Feed model		Delta gap excitation
Incident wave		Gaussian pulse
Absorbing Boundary Condition		Mur's 2nd approx.

Figure 4.35 shows the return loss characteristic of the simulation model. From the figure, we notice that the return loss around 280[MHz] is more than -3[dB]. The total efficiency decreased due to the additional losses in the matching unit. Next, simulation

of changing parameters of matching structure was carried out. Figures 4.36 and 4.37 show the return loss characteristic when we change the structure of wire. From these figures, we conclude that an optimization for the matching structure is possible.

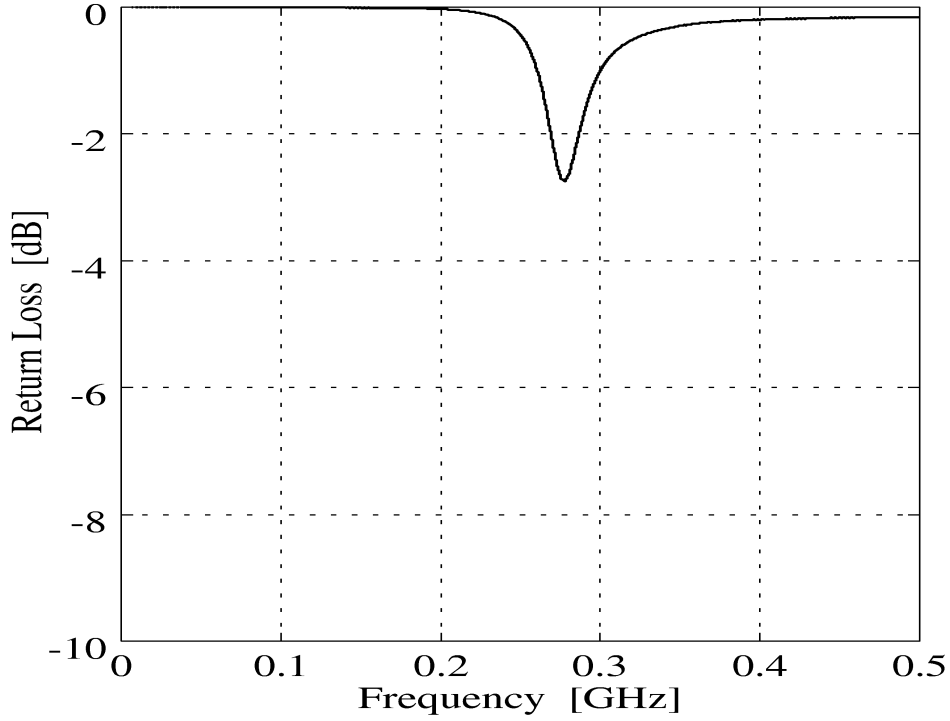

Figure 4.35: Return Loss Characteristic

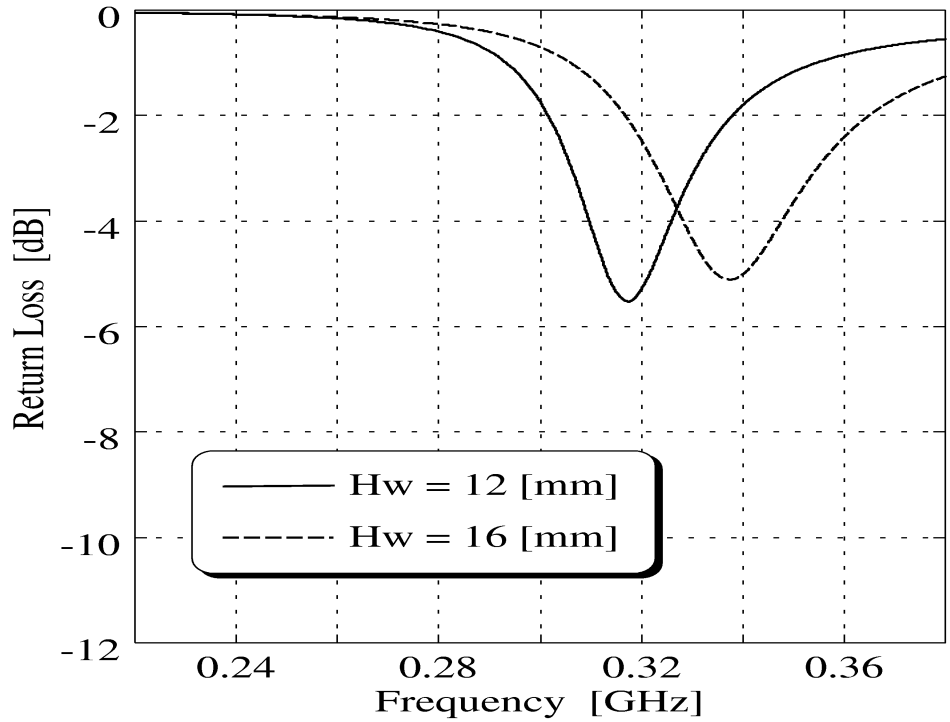

Figure 4.36: Return Loss Characteristic due to Height of Wire Structure $H_w(H_p = 24[mm], L_w = 24[mm])$

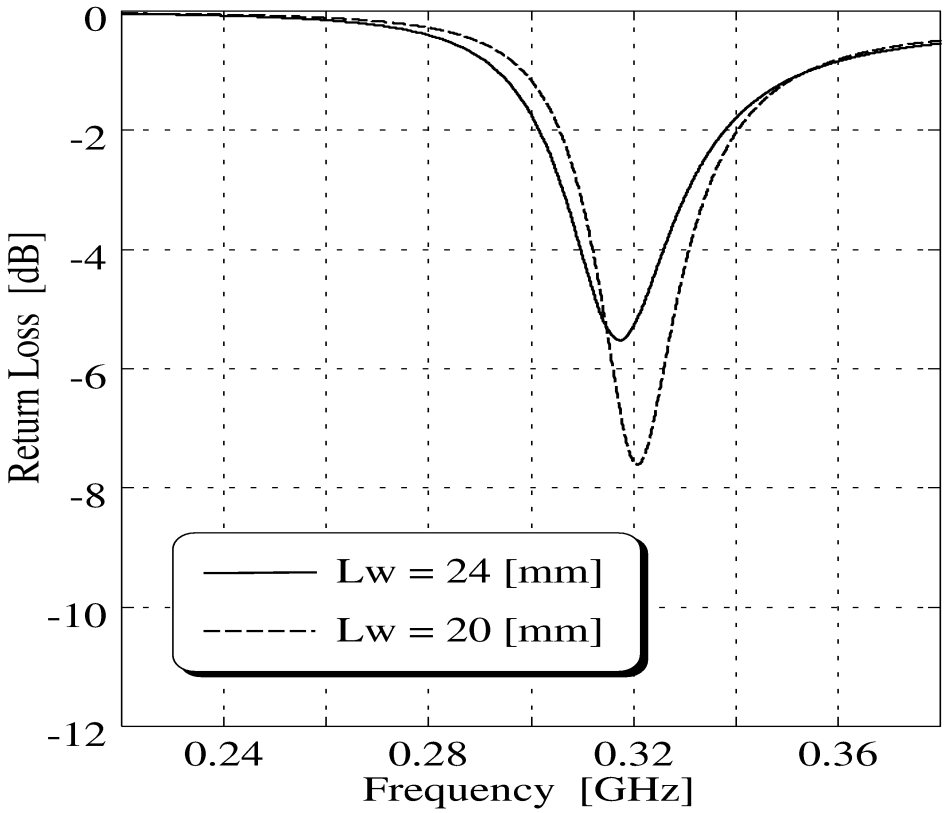

Figure 4.37: Return Loss Characteristic due to Length of Wire Structure $L_w(H_p = 24[mm], H_w = 12[mm])$

4.5 Optimization of Circular Polarized Patch Antenna with Cross-shaped Slit

In recently, GPS(Global Position System) has come into wide use in Japan. A high performance and low cost, small GPS antenna is required. In this paper, a small circular polarized patch antenna for GPS satellite's receiver is investigated.

Patch antenna's miniaturization can be achieved by add slit or slot on patch element of antenna. Current path on patch element increases, and resonant frequency drops by adding slit on patch element.

It is introduced an experiment of circular patch antenna with deep notches[20]. But investigation of antenna's miniaturization due to notch's parameter has not be carried out in detail.

In this section, we first investigate the case of square patch antenna with 4 slits from both sides of patch. By changing parameter of slit structure, an optimum slit parameter for antenna's miniaturization is proposed. Then, in order to achieve more miniaturization, a patch antenna with cross-shaped slit is simulated. Parameter's optimization is carried out. Finally, antenna's axial ratio is investigated, and an optimum small circular

polarized antenna is proposed.

To clarify the input and radiation characteristics due to antenna's parameter, FDTD Simulation is considered as the most suitable. It becomes a large analysis problem if we handle such an antenna that have fine structure partly by using FDTD method. The high performance three-dimensional FDTD algorithm by using non-uniform mesh that allows flexible cell size to improve the accuracy of modeling and reduce the computation resource is adopted in this study.

4.5.1 Patch Antenna with 4 Slits

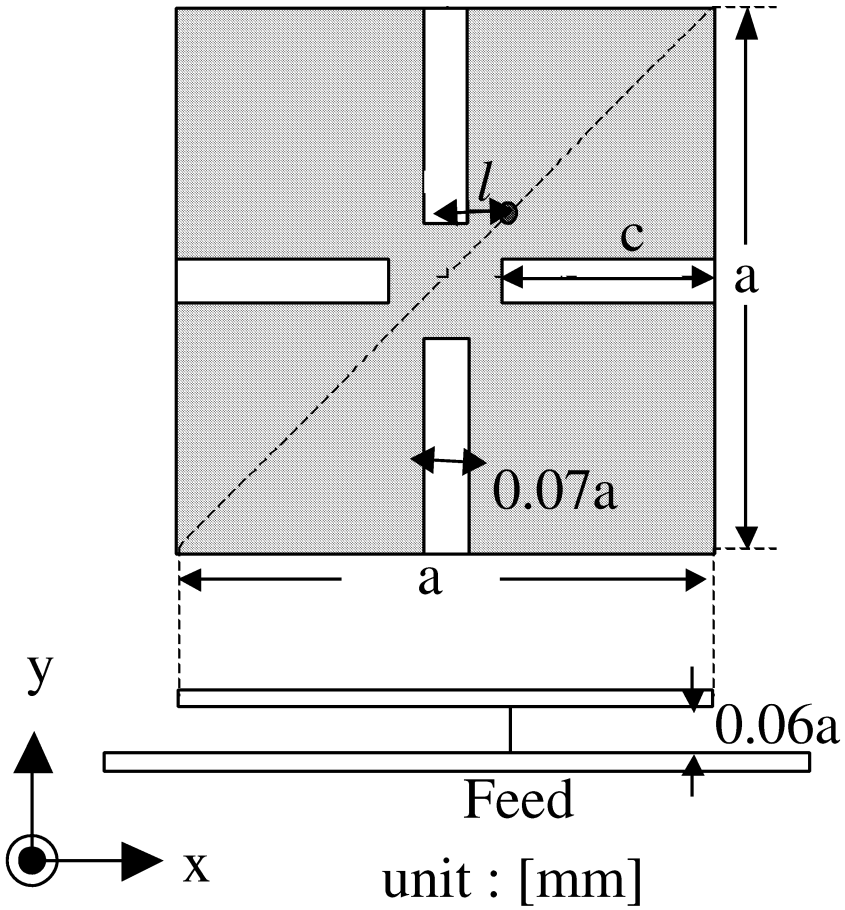

Figure 4.38: Computation Model I

Figure 4.38 shows simulation model in this study. Figure 4.38 is a patch antenna that have 4 slits from both sides of patch. FDTD calculation by changing length of slit(c) is carried out to examine impedance characteristic due to c.

To verify the antenna's miniaturization due to c, eigenvalue $k_0 a$ is adopted, where a is the length of patch, k_0 is wave number. Therefore $k_0 a$ is in proportion to resonant frequency, a decrease in eigenvalue indicates antenna's miniaturization.

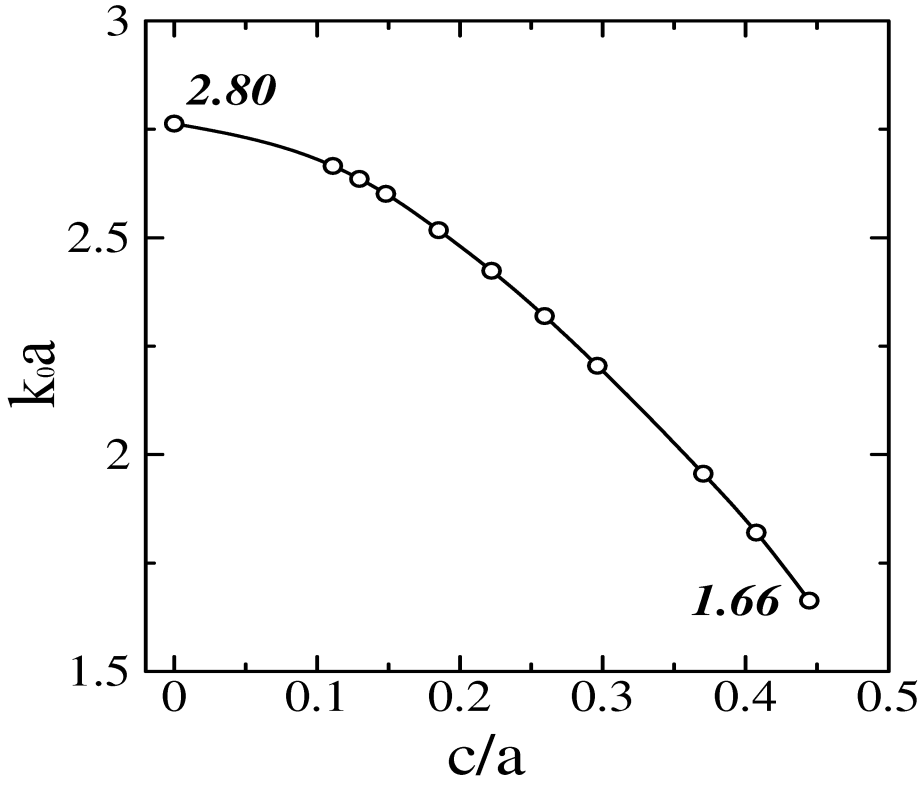

Figure 4.39: k_0a due to c(Model I)

Figure 4.39 shows the eigenvalue characteristic k_0a due to c. Eigenvalue k_0a decreased as c increased. The reason is considered that current path increased in proportion to c.

Compare to the result of patch antenna without slit($c/a = 0$ in Fig. 4.39), eigenvalue k_0a of Model I in Fig. 4.39 is dropped from 2.80 to 1.66.

4.5.2 Patch Antenna with 4 Cross-shaped Slits

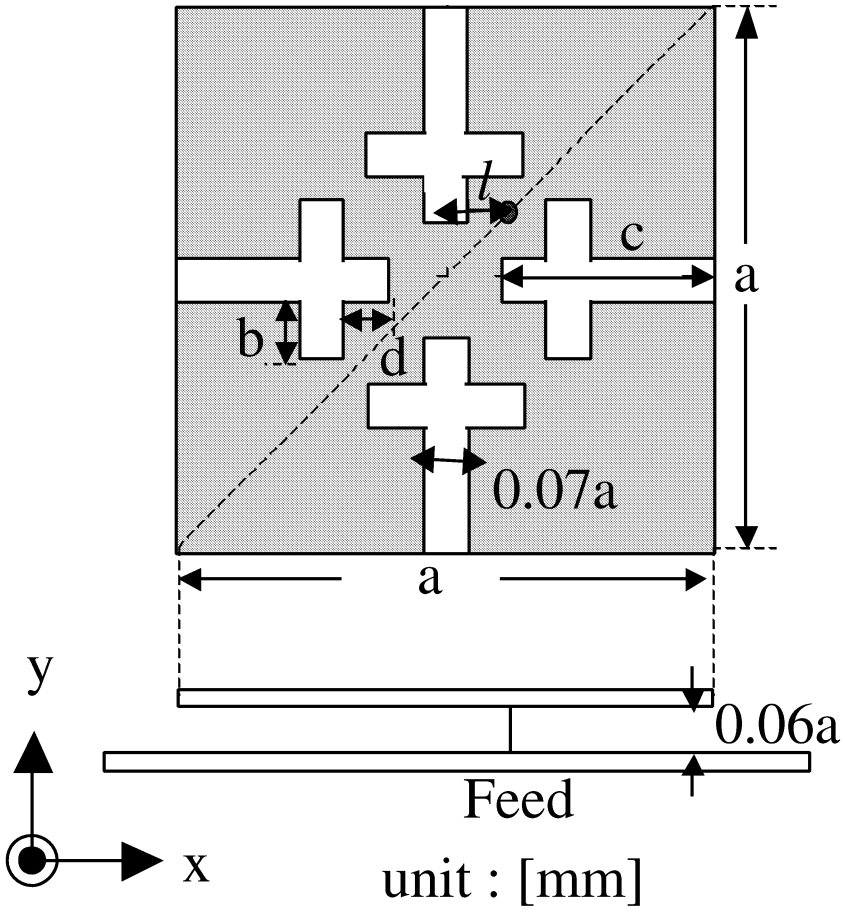

Figure 4.40: Computation Model II

Computation Space [mm]	$65 \times 65 \times 20$ $(\approx 1.08\lambda_0 \times 1.08\lambda_0 \times 0.33\lambda_0)$
Cell Size [mm]	$\Delta x_{fine} = \Delta y_{fine} = 0.5$ $\Delta z_{fine} = 0.4$ $\Delta x_{coarse} = \Delta y_{coarse} = 2.0$ $\Delta z_{coarse} = 1.6$
A. B. C.	Mur2nd

Table 4.5: Computation Parameters $< f_0 = 5.0[GHz] >$

In order to achieve more miniaturization at the same outer size, simulation of Model II(Fig. 4.40) is carried out. Four cross-shaped slits is adopted instead of slits in Model I. FDTD calculation of input characteristics is carried out by changing parameter b and d. Table 4.5 shows computation parameters of FDTD simulation.

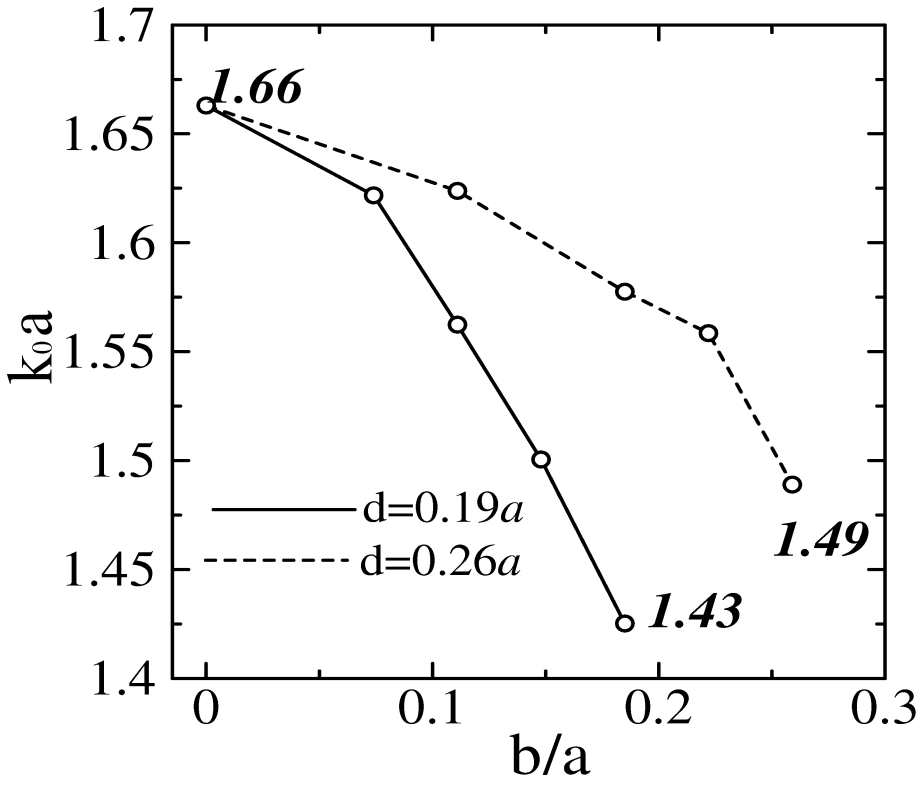

Figure 4.41: k_0a due to b and d (Model II)

Figure 4.41 shows the eigenvalue characteristic due to b and d. Current path increased in proportion to b, and eigenvalue is reduced by increase of b. On the other hand, eigenvalue is in proportion to d, the reason is that when d decreased, current density around center of patch increased, which can be considered as same effect as add inductance circuits. Reactance shows inductive, and leads a decrease of resonant frequency.

Compare to the result of patch antenna with 4 slits($b/a = 0$ in Fig. 4.41), eigenvalue k_0a of Model II in Fig. 4.41 is dropped from 1.66 to 1.43.

4.5.3 Circular Polarization

In this subsection, we investigate antenna's circular polarization. Degeneracy separation method is considered an effective way to achieve circular polarization. Add degeneracy on Model II's small antenna, optimization for circular polarization is carried out.

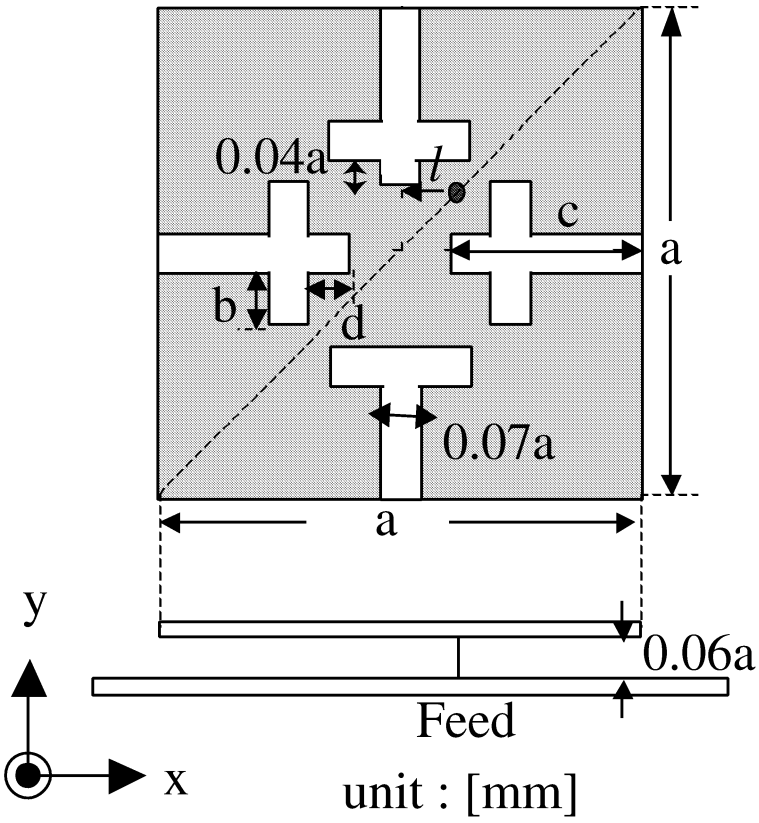

Figure 4.42: Computation Model III

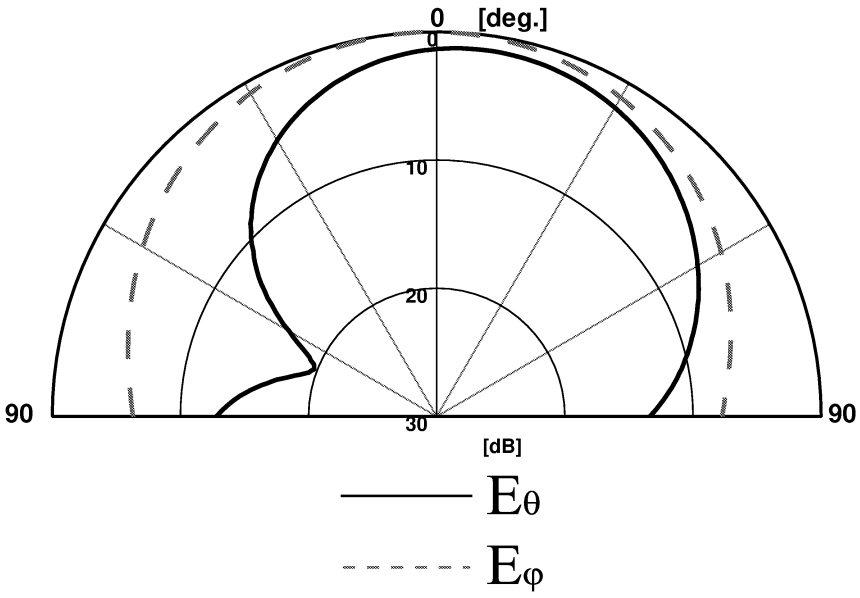

Figure 4.43: Radiation Pattern of zx plane < f=3.96[GHz] >

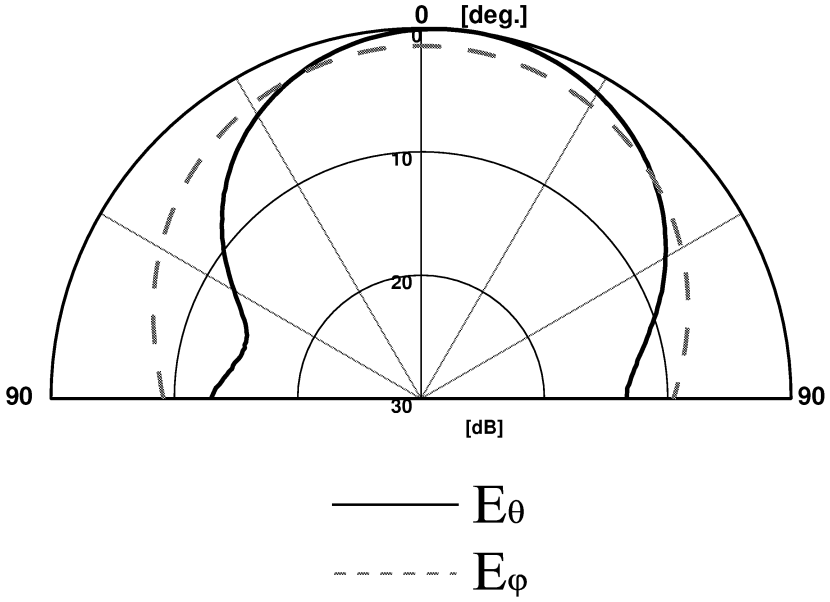

Figure 4.44: Radiation Pattern of yz plane < f=3.96[GHz] >

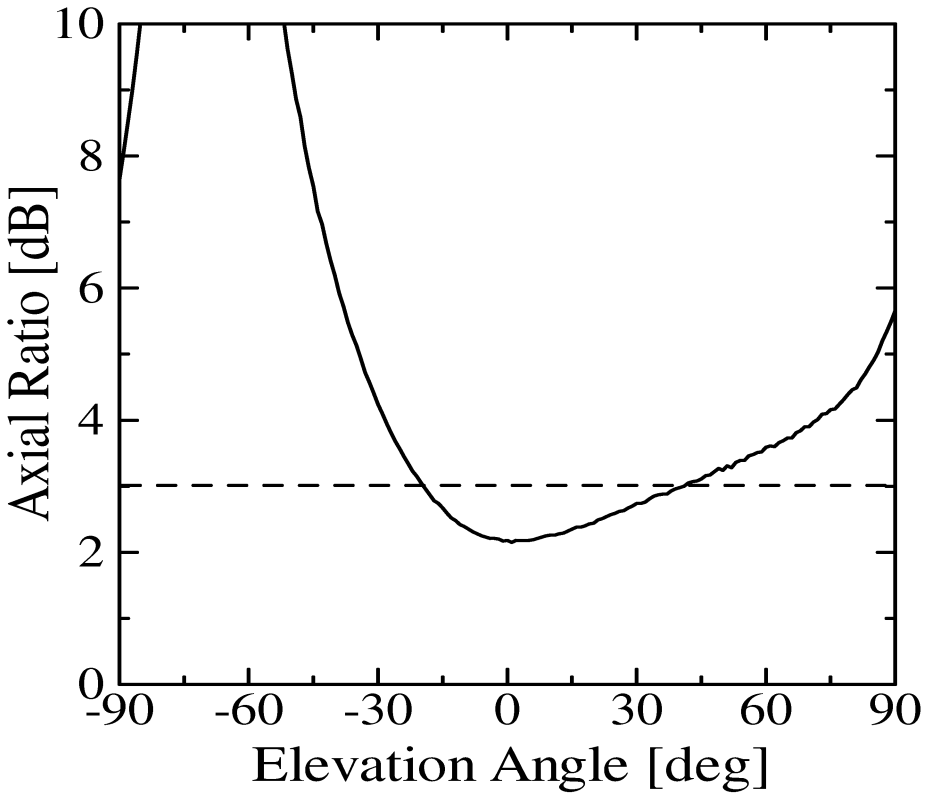

Figure 4.45: Axial Ratio Characteristic ($\phi = 0^o, f = 3.96[GHz]$)

Figure 4.42 shows the simulation model(Model III) with 4 cross-shaped slits. Radiation pattern of Model III is calculated.

Figures 4.43 and 4.44 show radiation pattern at $f_0 = 3.96[GHz]$. And Fig. 4.45 shows axial ratio characteristic at $\phi = 0^o$.

Axial ratio is less than -3[dB] from $\theta = -20^o$ to 40^o in zx plane. Circular polarization is achieved in this case.

4.5.4 Conclusions

In this section, we investigated antenna's miniaturization by adding 4 slits on a square patch antenna. Increase the length of slit leads an obvious decrease of eigenvalue $k_0 a$, which indicate antenna's miniaturization. Compare to the patch that without any slit, Model I's eigenvalue is reduced 40.7%. And the input impedance can be arranged to have an appropriate value to match the load impedance if we change position of feed point.

Further miniaturization is investigated by using a cross-shaped slit instead of slit in Model I. The eigenvalue $k_0 a$ is reduced 48.9%(f_0 =2.52[GHz]). Using degeneracy separation method, a circular polarization is achieved.

4.6 Conclusions

In this chapter, we calculated several kinds of antenna that have fine structure compare to main part of antenna by using Non-Uniform Mesh FDTD.

- Monopole antenna;
- Notch antenna loaded dielectric material;
- Top loaded low-profile monopole antenna(TLMA)'s miniaturization;
- Small pager's base station antenna;
- Circular polarized patch antenna with cross-shaped slit's optimization;

A key conclusion is that, by applying smaller mesh size on fine structure, precise simulation is carried out by less computation resource.

Non-uniform mesh FDTD algorithm has a powerful ability to provide accuracy simulation of small antenna.

Chapter 5

Investigation of Antenna-Radome Interaction

In this chapter, we study a 2GHz omni antenna that is covered with a circular cylindrical dielectric radome. By changing the thickness, radius, permittivity constant of dielectric radome and resonant frequency of radiation element, the influence of dielectric cylindrical radome on antenna's resonant frequency, bandwidth ratio are investigated.

The interaction between radiation element and dielectric radome is known as a long-standing complicated problem. With the increase of high frequency band for mobile communication systems, the influence of dielectric radome become a factor that can't be ignored in design of base station antenna.

The FDTD method is well suit for use in analyzing both the antenna and the surrounding radome in the same computational model, thereby capturing the electromagnetic wave physics of the antenna-radome interaction.

To improve the calculation effect efficiency, the non-uniform mesh FDTD algorithm is used during the study. From the measurement and simulation results, we propose to count the radome's influence in antenna design's early stage.

5.1 Introduction

In recent years, the requirement of mobile communication has become greatly increased. For base station antennas, it is required to have an appropriate electrical characteristics as an antenna. But for base station antennas that are installed at the outdoor environment, it is also required to have suitable characteristics on corrosion resistance, loading because of wind pressure, etc. Because cylindrical's loading due to wind pressure is smallest, base station antennas are usually installed inside a cylindrical radome. The frequency band of mobile communication system till now is not so high to consider the influence of dielectric radome. Traditionally, the radome and its internal

antenna are designed separately and there interaction is ignored. There doesn't exist any big problem in antenna's design and development. But in the next generation system, which is famous known as IMT-2000, the frequency band is around 2GHz. It is expected that higher frequency band will be adopted in further mobile communication systems. The interaction between radiation element and dielectric radome must become increasingly a factor that can't be ignored. And the far field radiation pattern of antenna with dielectric radome also will change from the case of element only. It is necessary to count the influence of radome in antenna's design. Investigation of the change of antenna's input characteristics and radiation pattern due to cylindrical radome is required.

To investigate the interaction between radiation element and dielectric radome, Rengarajan presented a detailed analysis of assumptions and limitations of physical optics and stationary phase techniques for radomes [21]. Orta introduced a method based on the reciprocity theorem and identify the asymptotic expression of the radome [22]. Allen calculated the complex electromagnetic wave interactions between the missile's antenna and radome by FDTD method [3].

As far as our knowledge, there is no published work on the interaction between radiation element and radome for mobile communication system's base station antenna. The purpose of this study is to investigate input and radiation characteristics of antenna due to parameters of dielectric cylindrical radome.

First of all, in order to estimate the basic characteristics due to cylindrical radome, we examined the input characteristics of omni antenna due to parameters(radius, thickness, permittivity constant) of dielectric cylindrical radome. To clarify the mechanism of radome effect, FDTD Simulation [2] is considered as the most suitable. It becomes a large analysis problem if we handle the radiation element and dielectric radome simultaneously by FDTD method. The high performance three-dimensional FDTD algorithm by using non-uniform mesh that allows flexible cell size to improve the accuracy of modeling and reduce the computation resource is adopted in this study.

5.2 2GHz Band Omni Antenna

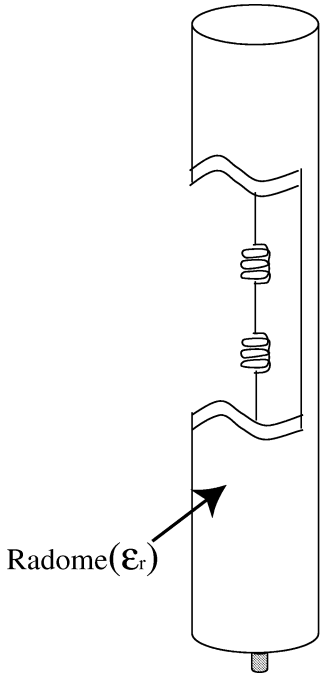

Figure 5.1: Base Station Antenna

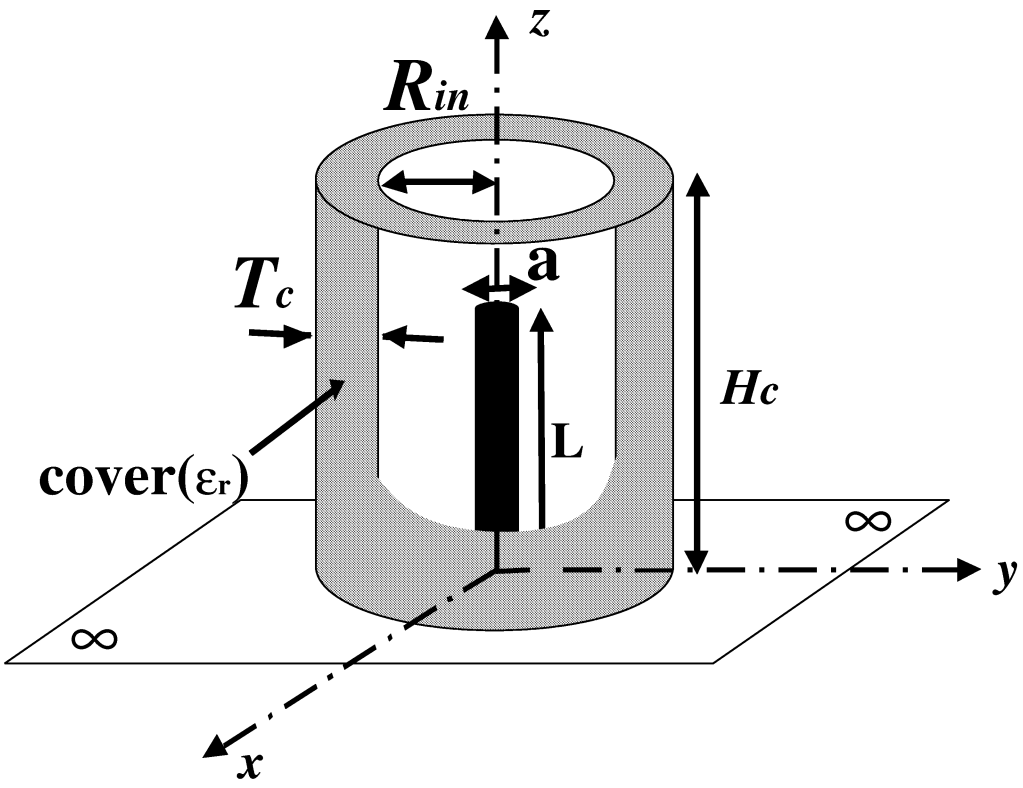

Figure 5.2: Simulation and Measurement Model

5.2.1 Comparison between Measurement and Calculation Results

In this subsection, we introduce the measurement and calculation model in this study. Figure 5.1 shows the model of base station antenna for mobile communication system. As the figure shows, base station antenna is usually constructed by several radiation elements arrayed in series in the dielectric radome. Each component works at different frequency band, or different polarization. In this paper, we will investigate the case of vertical polarization.

Figure 5.2 shows the measurement and simulation model in this study. Radiation element is installed in the middle of radome. In simulation, the imaging plane that has infinite size is used to reduce the computation volume. And in measurement, the conducting plane that enough larger than radome is used. Changing the length of element can allow us obtain the measurement and simulation results from 800[MHz] to 2.4[GHz]. By changing parameters of radius, thickness and permittivity constant of radome, input impedance due to radome parameters can be given.

In order to verify the influence of dielectric radome, measurement is carried out. Table 5.1 shows parameters of measurement. And in measurement, the monopole antenna is installed on a $65 \times 65[mm^2]$ rectangular perfect conducting plane.

Table 5.1: Parameters of Measurement

Length of monopole (L)	28 — 88 [mm]
Resonant freq. (f_r) [GHz]	0.8, 1.1, 1.6, 1.9, 2.3
Thickness of monopole (a)	5 [mm]
Height of cover (H_c)	100 [mm]
Radius of cover (R_{in})	12.5, 25, 37.5[mm]
Thickness of cover (T_c)	12.5, 25[mm]
Permitivity of cover (ϵ_r)	1.0(Free space), 2.0, 3.0

As previously mentioned, measurement by using parameters shown in Table 5.1 is carried out. Changing the length of radiation element, the antenna is matched at frequency band near 0.8[GHz], 1.1[GHz], 1.6[GHz], 1.9[GHz] and 2.3[GHz], respectively. Figure 5.3 shows the return loss characteristics of radiation element only(without radome) in each frequency band.

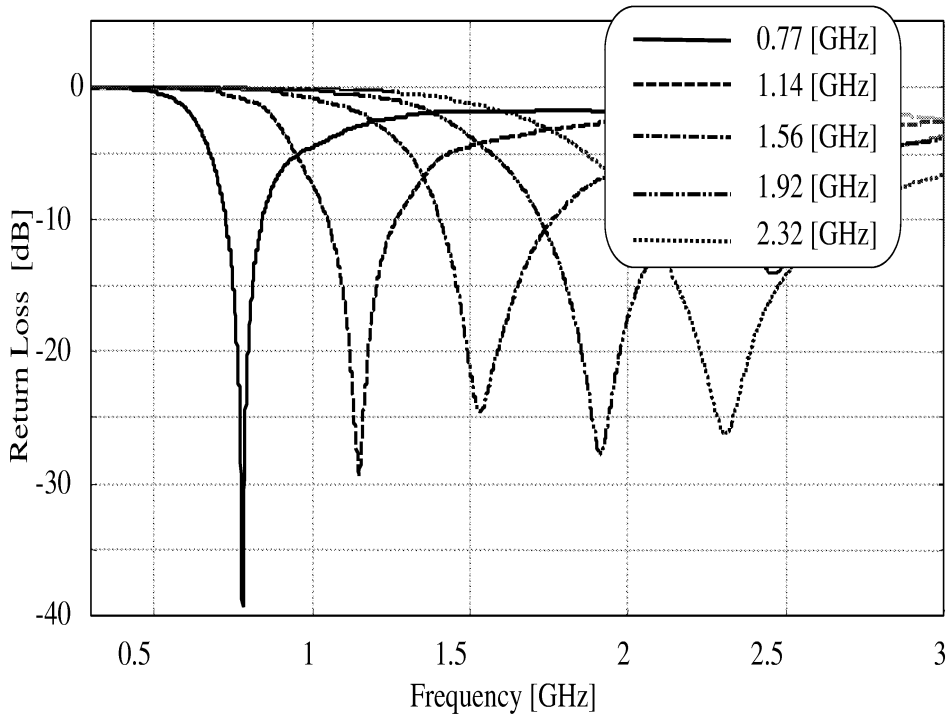

Figure 5.3: Return Loss of Radiation Element

In order to examine the change of input characteristics (central frequency, bandwidth, etc.) due to parameters of cylindrical radome, we select the central frequency and bandwidth ratio of element only(without radome) f_0 and BW_0 as the reference. The ratio f_c/f_0 shows the central frequency f_c normalized by reference value f_0. And ratio BW_c/BW_0 shows the bandwidth ratio BW_c normalized by reference value BW_0. Bandwidth ratio of VSWR < 1.5 and VSWR < 2.0 are observed.

As our knowledge, influence due to dielectric material depends on the resonant frequency band greatly. To examine the change of input impedance at different frequency band, measurement is carried out. Same cylindrical radome($R_{in} = 25[mm], T_c = 25[mm], \epsilon_r = 2.0$) is used during measurement. By changing the resonant element(resonates at 0.8GHz, 1.1GHz, 1.6GHz, 1.9GHz, 2.3GHz respectively), change of input characteristics at different frequency band can be obtained.

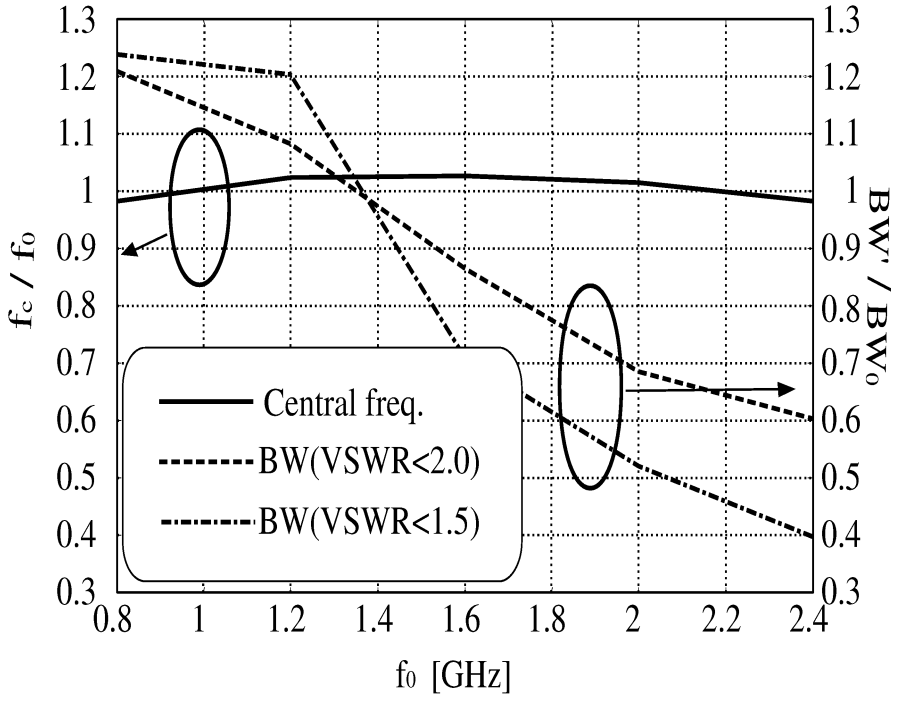

Figure 5.4: Measurement result of Input Characteristic due to Frequency($\epsilon_r = 2.0, R_{in} = 25[mm], T_c = 25[mm]$)

Figure 5.4 shows input characteristics of central frequency and bandwidth ratio (VSWR < 1.5 and VSWR < 2.0) at different frequency band. From the curve of central frequency shown in figure, we notice that the central frequency shows different tendency in each frequency band. And in most bands, central frequency is higher than case of without dielectric radome($f_c/f_0 > 1.0$). About the bandwidth ratio, BW_c/BW_0 changes from 0.4 to 1.25, and bandwidth which is wider than without radome case($BW_c/BW_0 > 1.0$) is also appeared. As our knowledge, as the frequency band increases, bandwidth become wider. But from the curve, we notice that the bandwidth ratio decreased as frequency band increased. The reason is considered as the reflection from dielectric radome. Same results are obtained at radome which have other R_{in}, T_c and ϵ_r. This testified the complexity of interaction between radiation element and dielectric radome. It is necessary to clarify the mechanism of this interaction by simulation solution.

First of all, it is important to estimate the accuracy of simulation model and method. Measurement and calculation for estimation are carried out. The simulation method we used in this study is FDTD method by using Non-Uniform Mesh. We have described the detail algorithm of FDTD analysis by using non-uniform mesh in previous chapter. In brief, we use two kinds of mesh size in the whole computation region, the fine mesh ([I] in Table 5.2) to model antenna structure(include cylindrical radome) precisely, and

the coarse mesh ([II] in Table 5.2) is used in computation region between radome and absorbing boundary. And the thickness of radiation element is under consideration (Fig. 5.5). By using the non-uniform mesh, precise modeling is achieved by less computation resources and CPU time. Table 5.2 shows the simulation parameters are used in FDTD simulation.

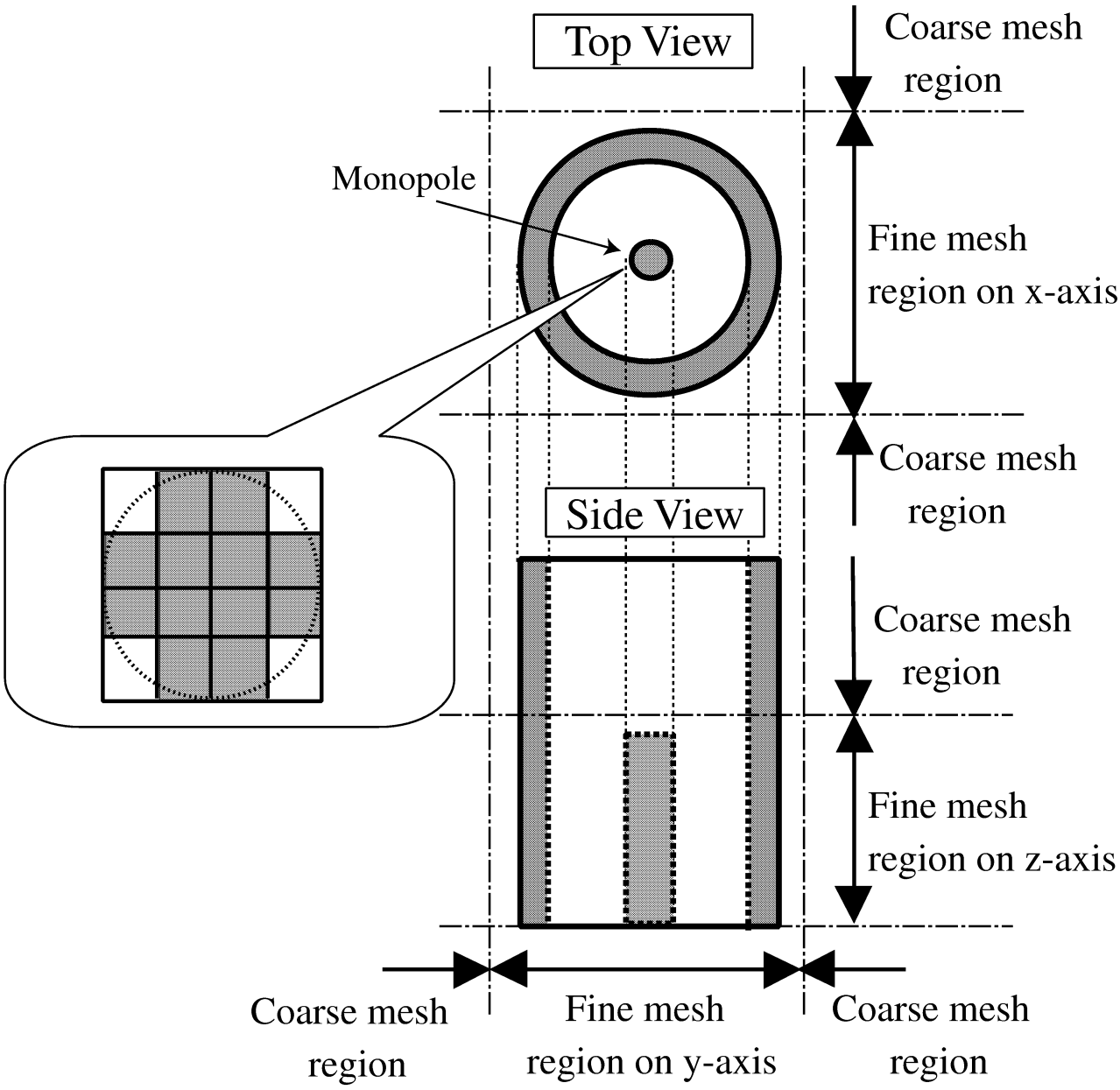

Figure 5.5: FDTD Simulation Model

Using parameters be previously mentioned, measurement and simulation of same model are carried out. Figure 5.6 shows the return loss characteristics of same model's measurement and simulation. We got good agreement between calculation and measure-

Table 5.2: Parameters for FDTD analysis (Case of $f_r = 1.92$[GHz])

Length of monopole (L)	34 [mm]
Thickness of monopole (a)	5 [mm]
Height of cover (H_c)	100 [mm]
Radius of cover (R_{in})	10 — 90[mm] ($\approx 0.05\lambda_0$ — $0.56\lambda_0$)
Thickness of cover (T_c)	2.5 — 12.5[mm] ($\approx 0.016\lambda_0$ — $0.08\lambda_0$)
Permitivity of cover (ϵ_r)	1.0(Free space), 2.0 — 4.0
Compu. space	$0.8[m] \times 0.8[m] \times 0.4[m]$ ($\approx 5\lambda_0 \times 5\lambda_0 \times 2.5\lambda_0$)
Cell size	$[I]$ $\Delta_{fine} = 1.25[mm]$ ($\approx \lambda_0/125$) $[II]$ $\Delta_{coarse} = 11.25[mm]$ ($\approx \lambda_0/14$)
Iteration	6000
Incident wave	Gaussian pulse
A. B. C.	Mur's 2nd approx.

ment results. Same estimation is carried out in other radome parameter and frequency bands. Good agreement between measurement and simulation is obtained, too. The accuracy of simulation method and model is verified.

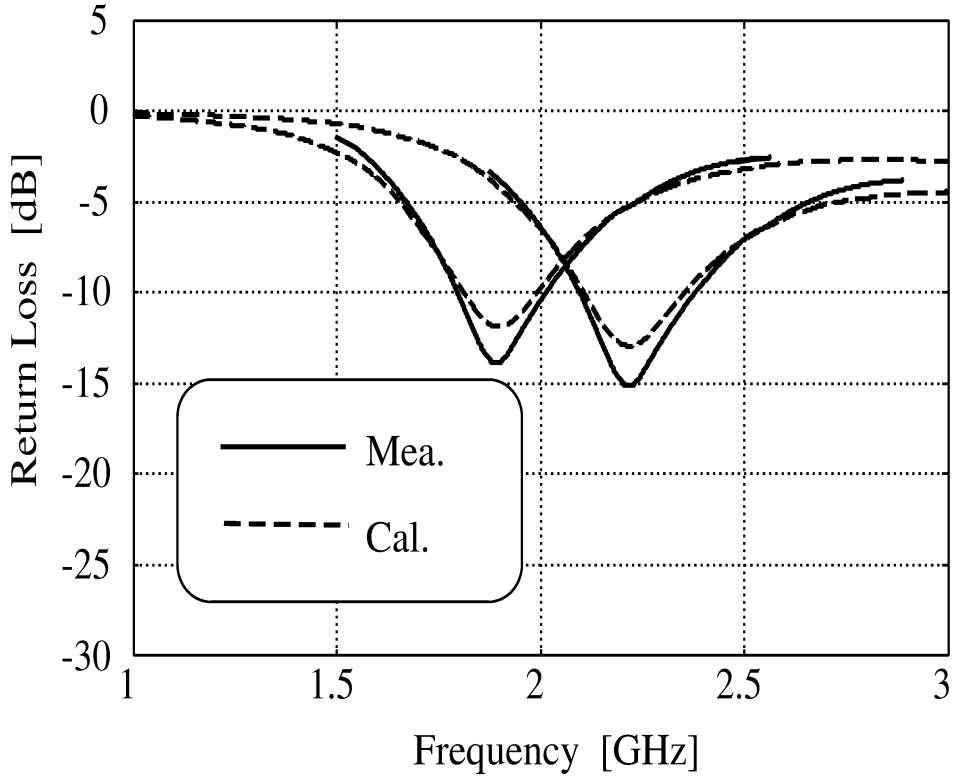

Figure 5.6: Comparison between Simulation and Measurement result($\epsilon_r = 2.96, R_{in} = 25mm, T_c = 25[mm]$)

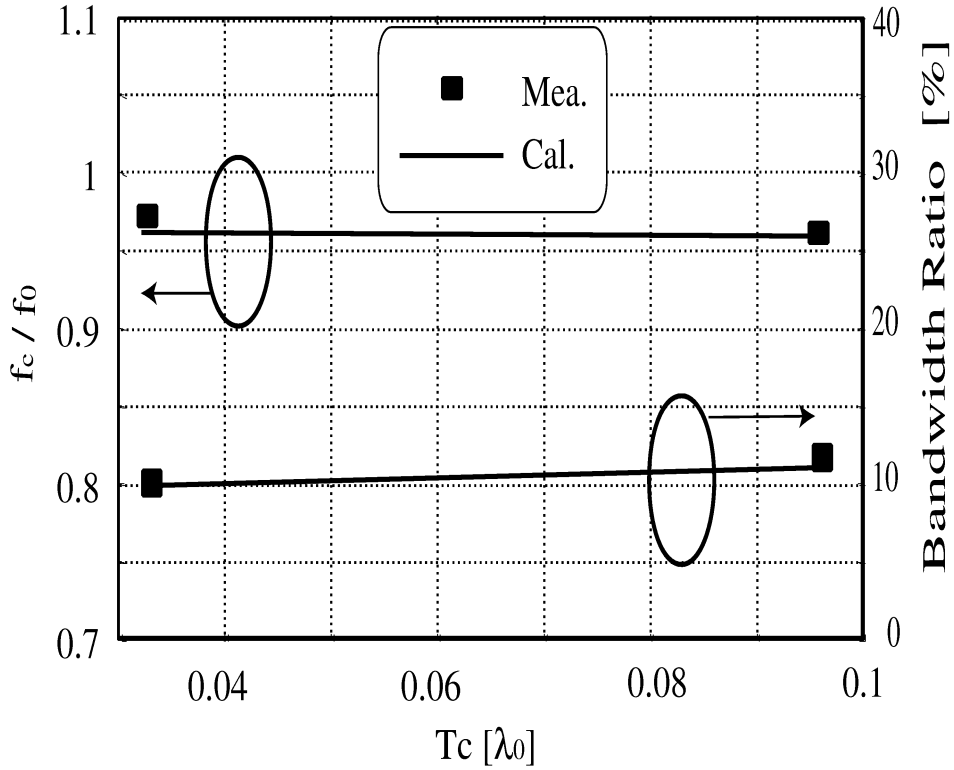

Figure 5.7: Comparison between Simulation and Measurement result($f_0 = 0.77[GHz], \epsilon_r = 2.0, R_{in} = 12.5mm(0.032\lambda_0), VSWR <= 1.5$)

5.2.2 Radius of radome(R_{in})

First, we calculated the input characteristics due to radius of cylindrical radome(R_{in}). In order to examine the change of central frequency due to R_{in}, we select the central frequency of element only (without radome) f_0 as the reference. Figure 5.8 shows central frequency f_c normalized by reference level, characteristics of f_c/f_0 due to radius of radome(R_{in}). And Fig. 5.9 shows bandwidth ratio of VSWR < 2.0 due to R_{in}. Dash line shows at level of 26% is bandwidth ratio of without radome case. Thickness of radome is 2.5mm($0.016\lambda_0$), 3.75mm($0.024\lambda_0$), 5mm($0.032\lambda_0$) and 6.25mm($0.04\lambda_0$), respectively.

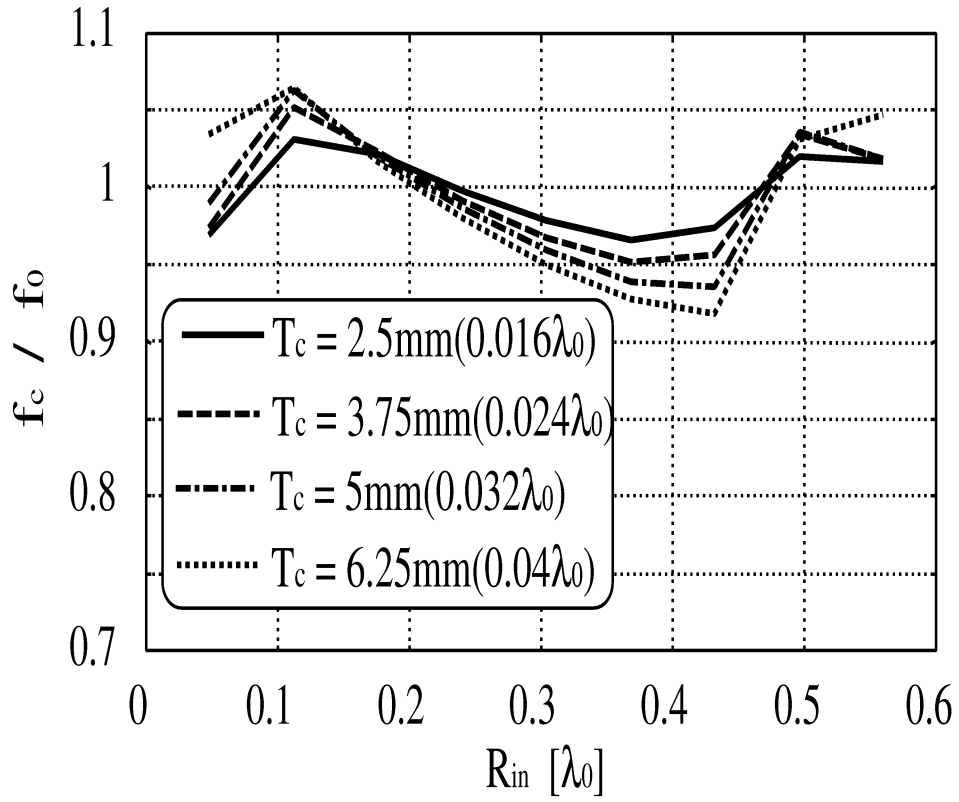

Figure 5.8: Central Frequency due to Radius of Cylindrical Radome($f_0 = 1.92[GHz], \epsilon_r = 4.0$)

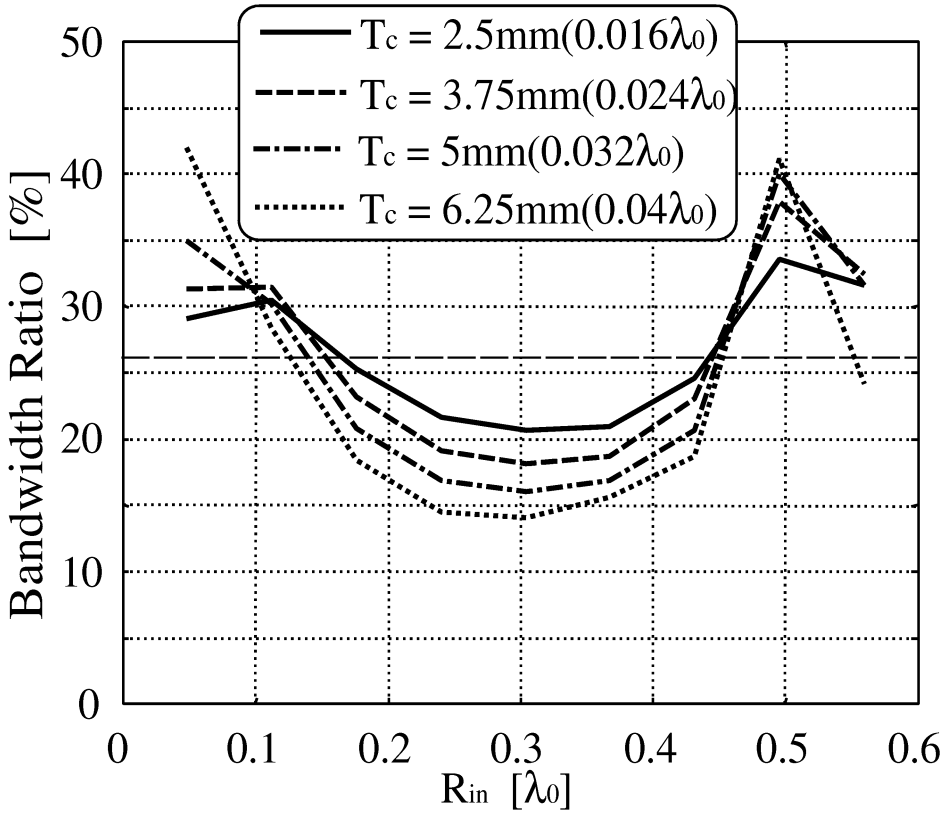

Figure 5.9: Bandwidth Ratio due to Radius of Cylindrical Radome($f_0 = 1.92[GHz], \epsilon_r = 4.0, VSWR <= 2.0$)

From these figures, we notice that there are two peaks that change the slope of curve in each case. As the thickness T_c thicker, the peak level becomes higher in each case. First, when we focus curves of central frequency (Fig. 5.8), as the radius of cylindrical radome increased, central frequency shifts to the high region temporarily, then decreases gradually after peak. About the bandwidth ratio (Fig. 5.9), with the increase of cylindrical radome's radius, bandwidth ratio increases temporarily before peak, then goes down gradually. And when the R_{in} is close to $0.5\lambda_0$, the second peak appears on each curves.

We would like to focus attention on the level of these peak points, the maximum central frequency and bandwidth ratio reach to level of 1.06 and 1.6 times larger than without radome case. Thin cylindrical radome resonates with element easily. When R_{in} is thick enough(depends on thickness of radome), central frequency decreases, and bandwidth ratio goes down gradually with the increase of radius.

To our knowledge, because the wavelength propagated in dielectric material is shorter than in the free space, it is well know that dielectric material will cause a lower frequency and narrower bandwidth compare to without radome case. But from results be shown in Figs. 5.8 - 5.9, higher central frequency and wider bandwidth ratio obtained in case of thin radome ($R_{in} < 0.15\lambda_0$).

In order to investigate the mechanism of this phenomenon, observation of electric distribution is carried out. Figure 5.10 shows the magnitude of E_z component when R_{in} is 0(Free space), $0.07\lambda_0$, $0.13\lambda_0$ and $0.32\lambda_0$, respectively. From these figures, we notice that the radome is working as an electric wall ($E_z = 0$) in each cases. This is considered as the reason of high central frequency and wide bandwidth ratio.

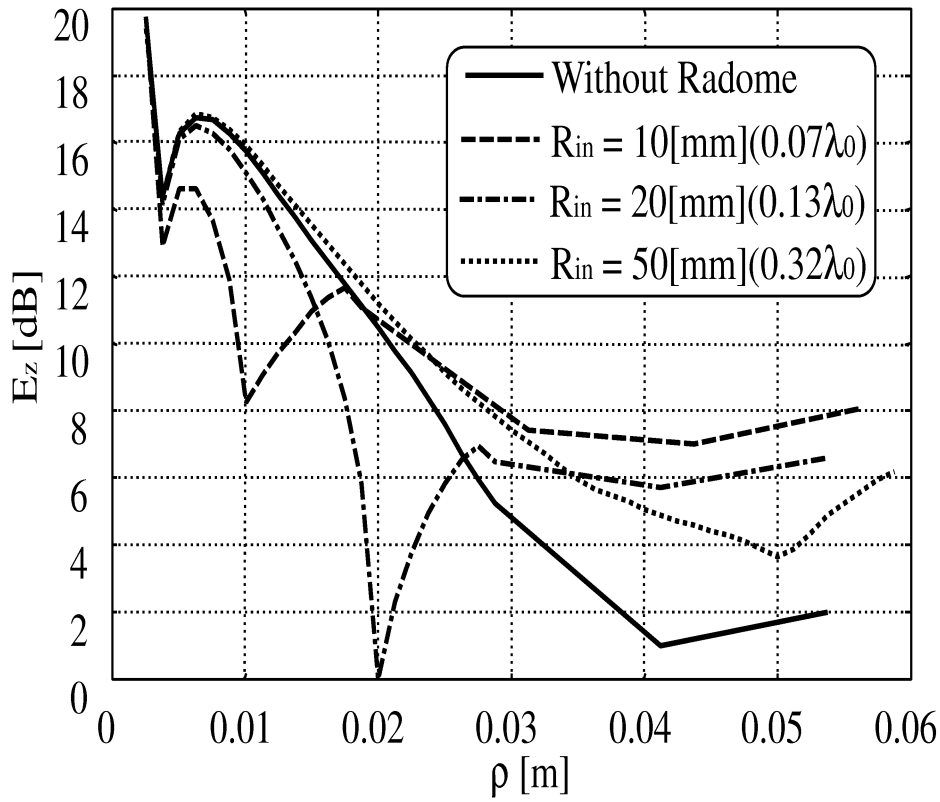

Figure 5.10: Magnitude of Ez Component due to Distance to Origin(ρ) ($f_0 = 1.92[GHz], Tc = 6.25[mm](0.04\lambda_0), \epsilon_r = 4.0$)

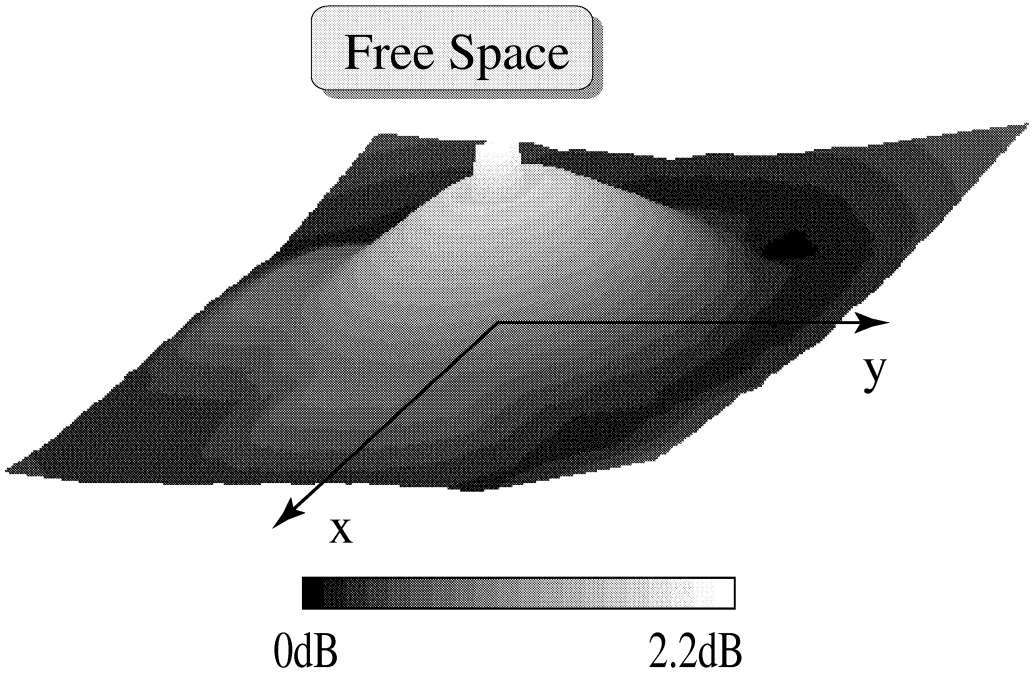

Figure 5.11: Electric Distribution(Ez)($f_0 = 1.92[GHz]$)

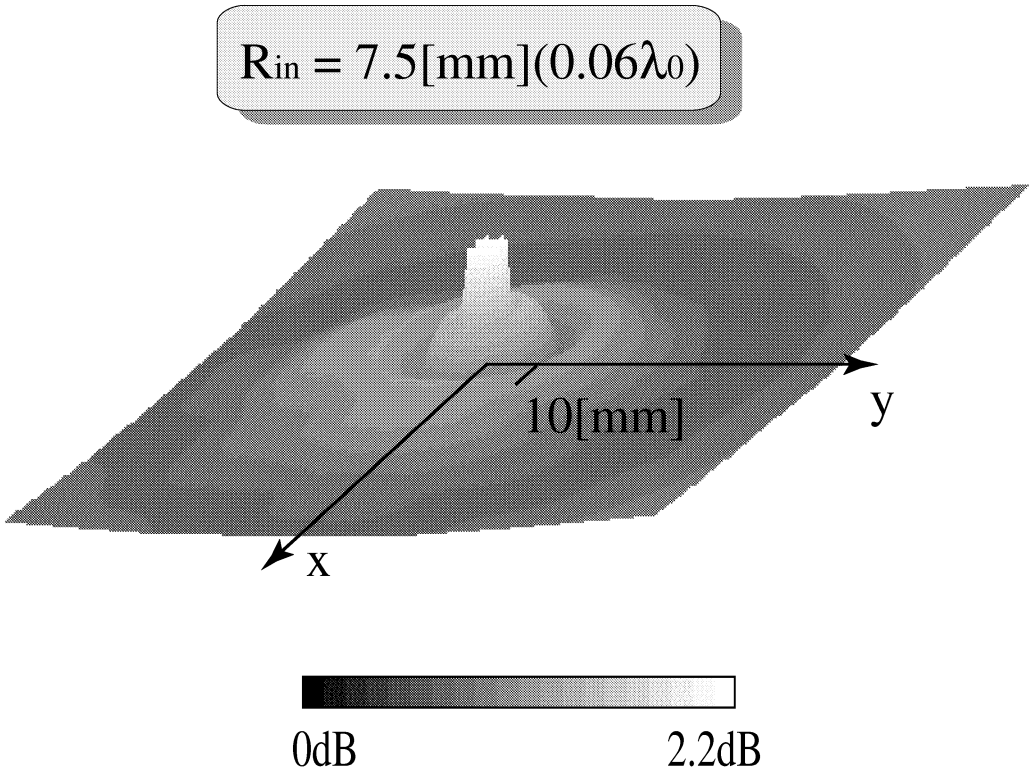

Figure 5.12: Electric Distribution(Ez)($f_0 = 1.92[GHz], R_{in} = 10[mm](0.06\lambda_0), Tc = 6.25[mm](0.04\lambda_0), \epsilon_r = 4.0$)

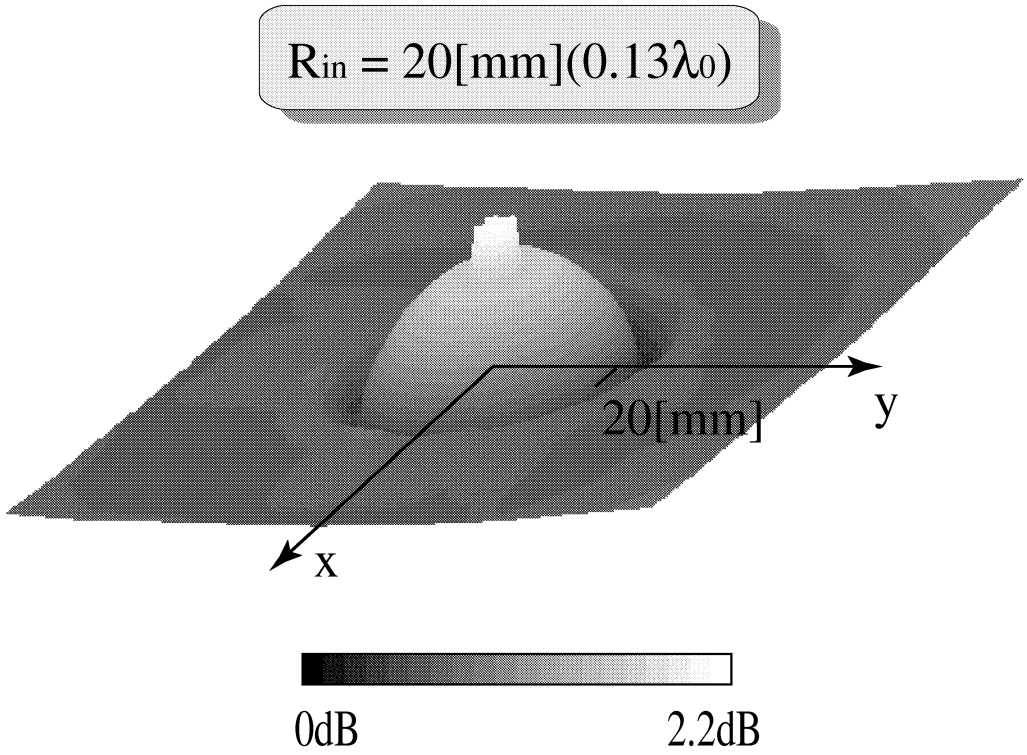

Figure 5.13: Electric Distribution(Ez)($f_0 = 1.92[GHz], R_{in} = 20[mm](0.13\lambda_0), Tc = 6.25[mm](0.04\lambda_0), \epsilon_r = 4.0$)

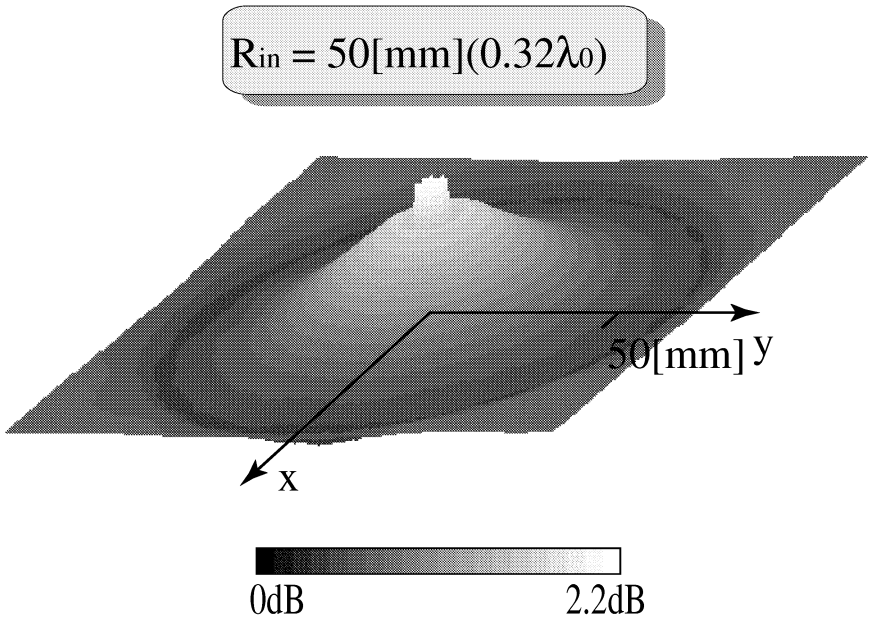

Figure 5.14: Electric Distribution(Ez)($f_0 = 1.92[GHz], R_{in} = 50[mm](0.32\lambda_0), Tc = 6.25[mm](0.04\lambda_0), \epsilon_r = 4.0$)

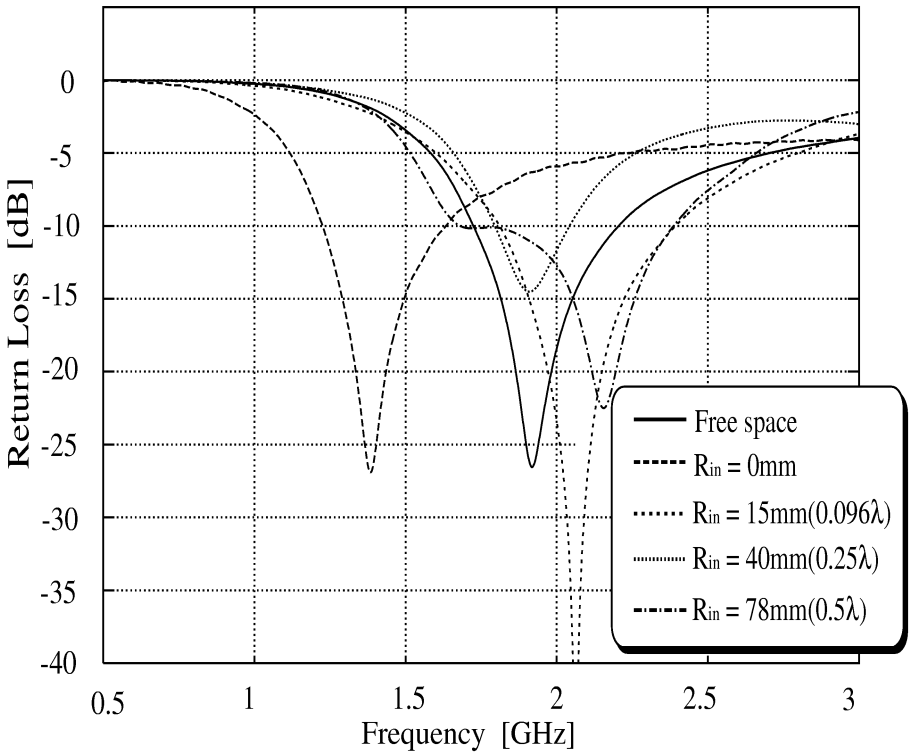

Figure 5.15: Return Loss Characteristic due to Radius of Cylindrical Radome($f_r = 1.92[GHz], \epsilon_r = 3.0$)

Figure 5.15 shows return loss characteristics due to radius of cylindrical radome. We notice that curve of $R_{in} = 0.5\lambda_0$ shows that there is another resonant point at higher frequency region. This is the reason of wide bandwidth ratio when $R_{in} > 0.5\lambda_0$. Figure 5.16 shows the input impedance in case of $R_{in} = 80[mm](0.51\lambda_0)$. Wide bandwidth can be observed from the smith chart. Figures 5.17 - 5.19 show the radiation pattern in this case. Same radiation patterns are obtained in two central frequencies.

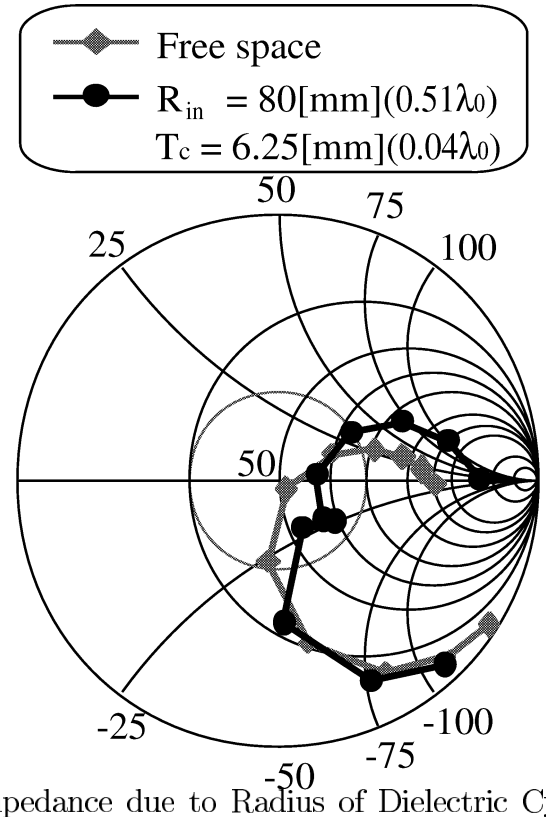

Figure 5.16: Input Impedance due to Radius of Dielectric Cylindrical Radome($f_0 = 1.92[GHz], \epsilon_r = 4.0, T_c = 6.25mm(0.04\lambda_0)$)

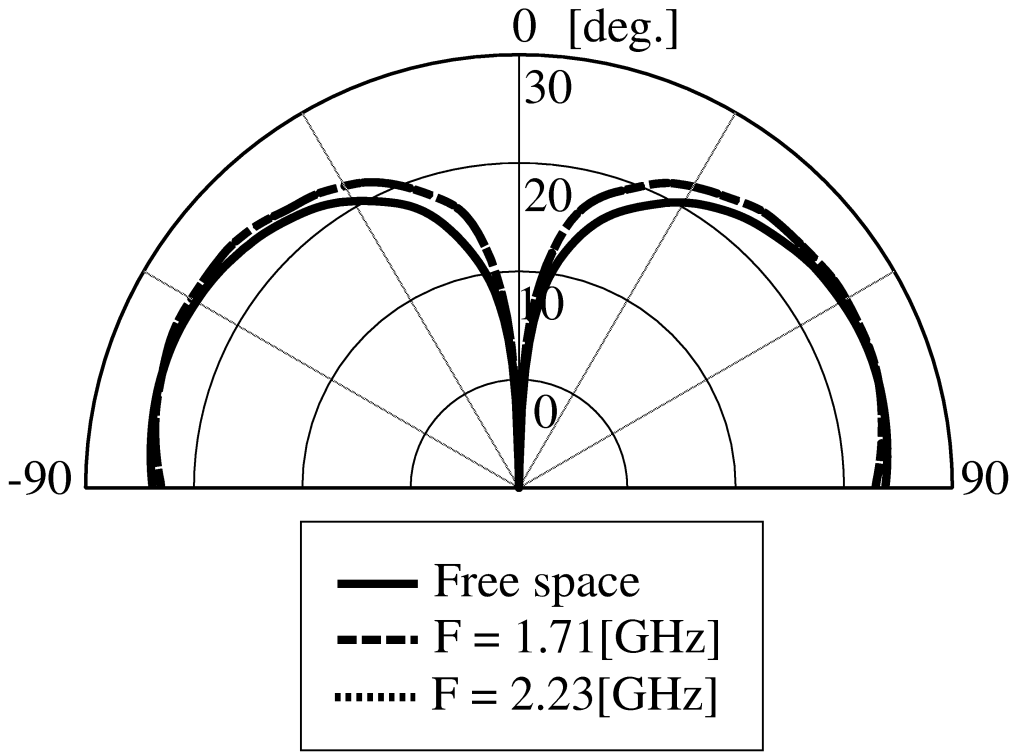

Figure 5.17: Radiation Pattern in ZX plane($\epsilon_r = 4.0, R_{in} = 80mm(0.51\lambda_0), T_c = 6.25mm(0.04\lambda_0)$)

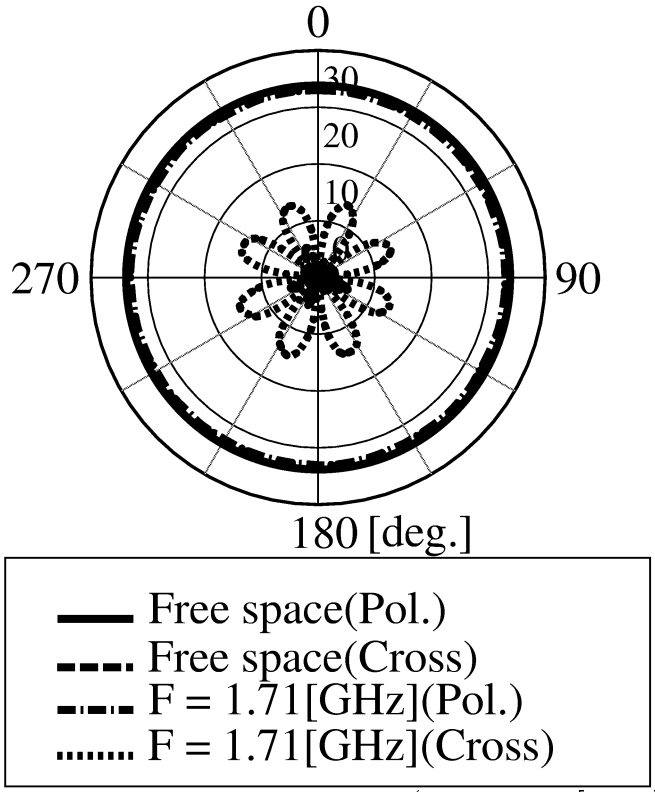

Figure 5.18: Radiation Pattern in XY plane($F = 1.71[GHz], \epsilon_r = 4.0, R_{in} = 80mm(0.51\lambda_0), T_c = 6.25mm(0.04\lambda_0)$)

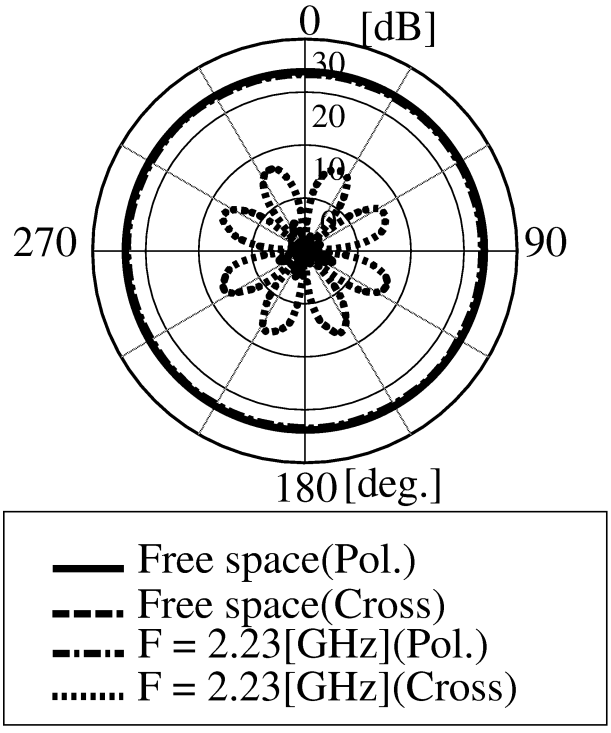

Figure 5.19: Radiation Pattern in XY plane($F = 2.23[GHz], \epsilon_r = 4.0, R_{in} = 80mm(0.51\lambda_0), T_c = 6.25mm(0.04\lambda_0)$)

Conclude the influence of radome's radius, the input characteristics change greatly due to radius. An orthodox way to evade this influence is to install the radiation element away from dielectric radome. But from the measurement and simulation results, we found that the bandwidth ratio become wider in certain parameters. If we count the radome's influence in design's early stage, we can use this characteristics to achieve the purpose of design a thinner antenna.

5.2.3 Thickness of radome(T_c)

Next, we calculated the input characteristics due to thickness of cylindrical radome(T_c). we select the central frequency of element only(without radome) f_0 as the reference. Figure 5.20 shows central frequency f_c normalized by reference level, characteristics of f_c/f_0 due to thickness of radome(T_c). And Fig. 5.21 shows bandwidth ratio of VSWR < 2.0 due to T_c. Dash lines show at level of 26% is bandwidth ratio of without radome case.

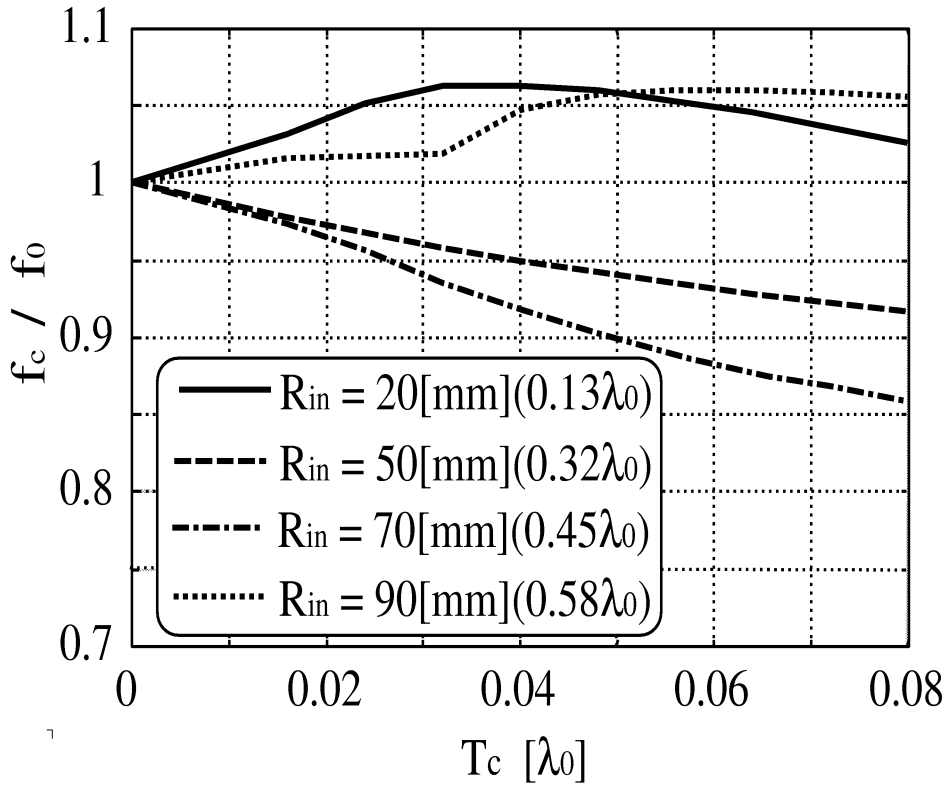

Figure 5.20: Central Frequency due to Thickness of Dielectric Cylindrical Radome($f_0 = 1.92[GHz], \epsilon_r = 4.0$)

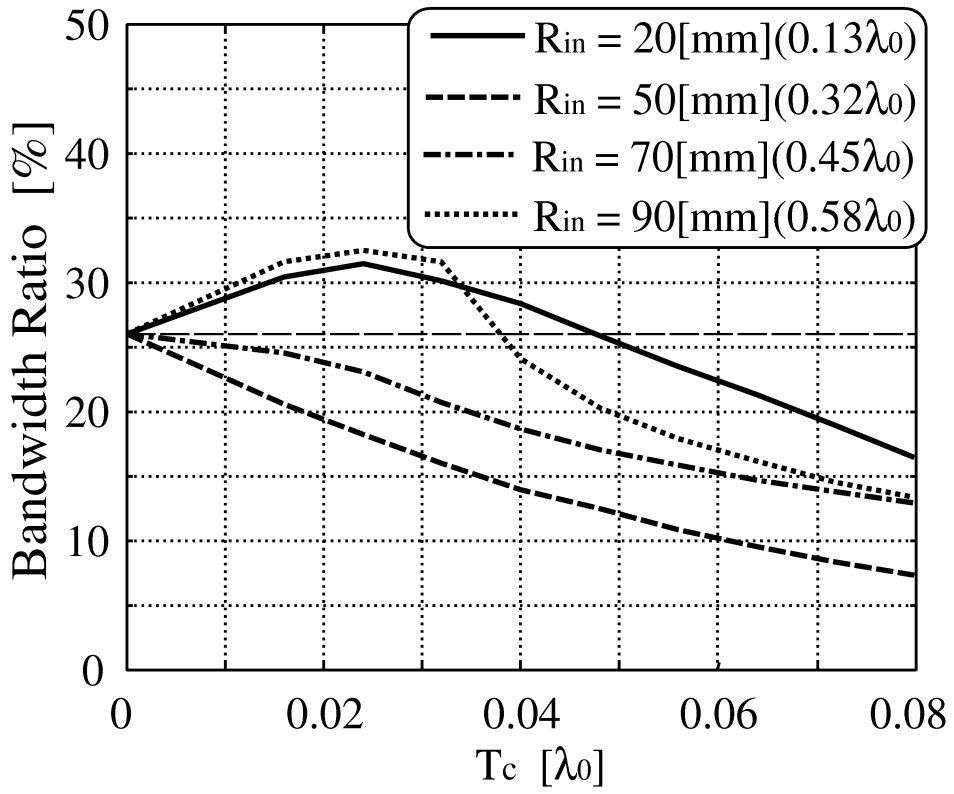

Figure 5.21: Bandwidth Ratio due to Thickness of Cylindrical Radome ($f_0 = 1.92[GHz], \epsilon_r = 4.0, VSWR <= 2.0$)

As shown in Fig. 5.20, we notice that as thickness of dielectric radome(T_c) increase, central frequency shift to lower region($f_0/f_r > 1.0$) when R_{in} are $0.32\lambda_0$ and $0.45\lambda_0$. And the radiation element resonant at high frequency region ($f_0/f_r > 1.0$) when R_{in} are $0.13\lambda_0$ and $0.58\lambda_0$. At the same time, the bandwidth ratio shows the same tendency as central frequency(Fig. 5.21). When R_{in} are $0.13\lambda_0$ and $0.58\lambda_0$, the bandwidth ratio is larger than the case of element only($T_c = 0$). After the peak appears at $T_c \approx 0.03\lambda_0$, as the thickness increased, central frequency shift to the lower region, and bandwidth ratio decreases gradually as thickness(T_c) increase.

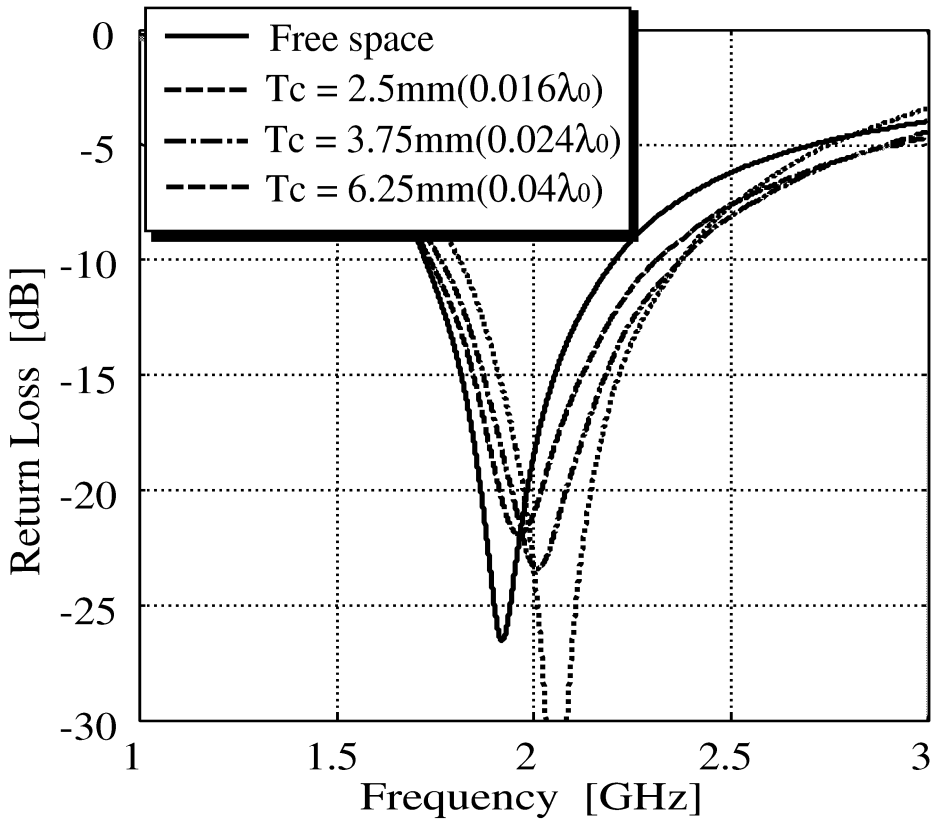

Figure 5.22: Return Loss due to Thickness of Dielectric Cylindrical Radome($f_0 = 1.92[GHz], \epsilon_r = 4.0, R_{in} = 20mm(0.13\lambda_0)$)

Figures 5.22 and 5.23 show return loss characteristics due to T_c when R_{in} are 20[mm]$0.13\lambda_0$ and 80[mm]$0.51\lambda_0$. From these figures, we notice that there is only one resonant point when radome's radius (R_{in}) is small(Fig. 5.22). For a thin dielectric radome(Fig. 5.23), same result can be obtained only when radome's thickness is small. When $T_c = 0.04\lambda_0$, the second resonant point appears at higher frequency region.

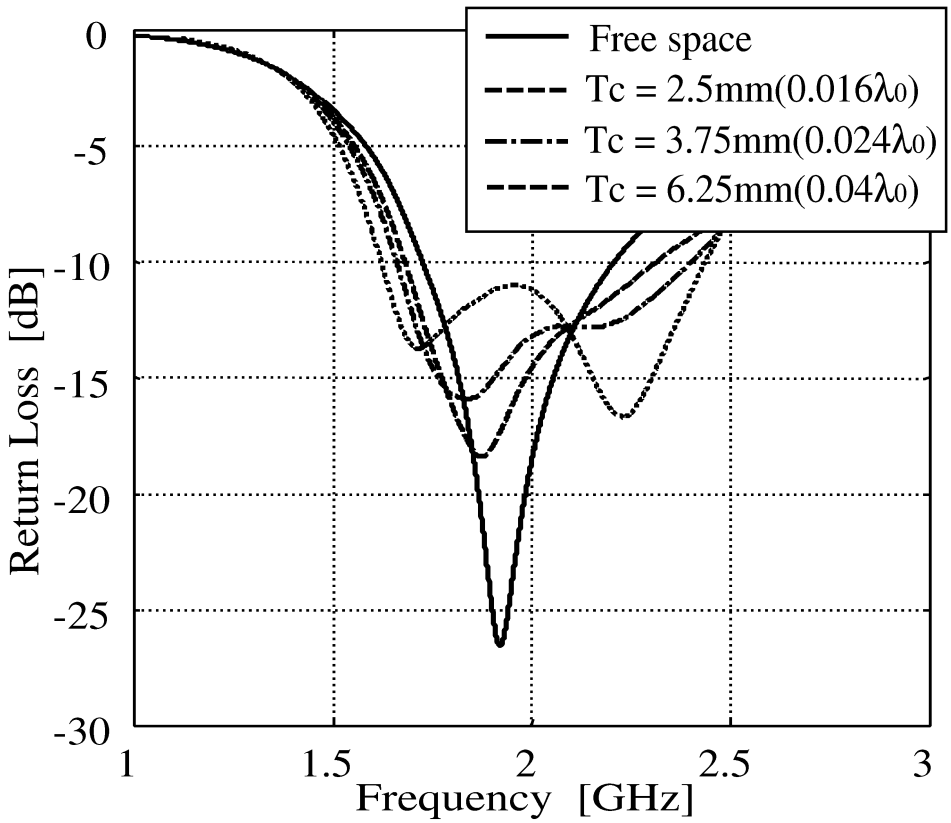

Figure 5.23: Return Loss due to Thickness of Dielectric Cylindrical Radome($f_0 = 1.92[GHz], \epsilon_r = 4.0, R_{in} = 80mm(0.51\lambda_0)$)

It is well know that because the wavelength propagated in dielectric material is shorter than in the free space, dielectric material will cause a lower frequency and narrower bandwidth compare to without radome case. But from curves be shown in Figs. 5.20 and 5.21, we notice that central frequency raise up to a level of 1.05 times higher than without radome case. And the bandwidth ratio also reaches to 1.3 times as wide as without radome case.

As conclude, input characteristics is easily influenced by thickness of cylindrical radome.

5.2.4 Permittivity of Radome (ϵ_r)

Finally, we calculated the input characteristics due to permittivity constant of cylindrical radome(ϵ_r). Figures 5.24 and 5.26 show comparison of ϵ_r when T_c is 5mm($0.032\lambda_0$). Same tendency as Figs. 5.8 - 5.9 can be observed on each curves.

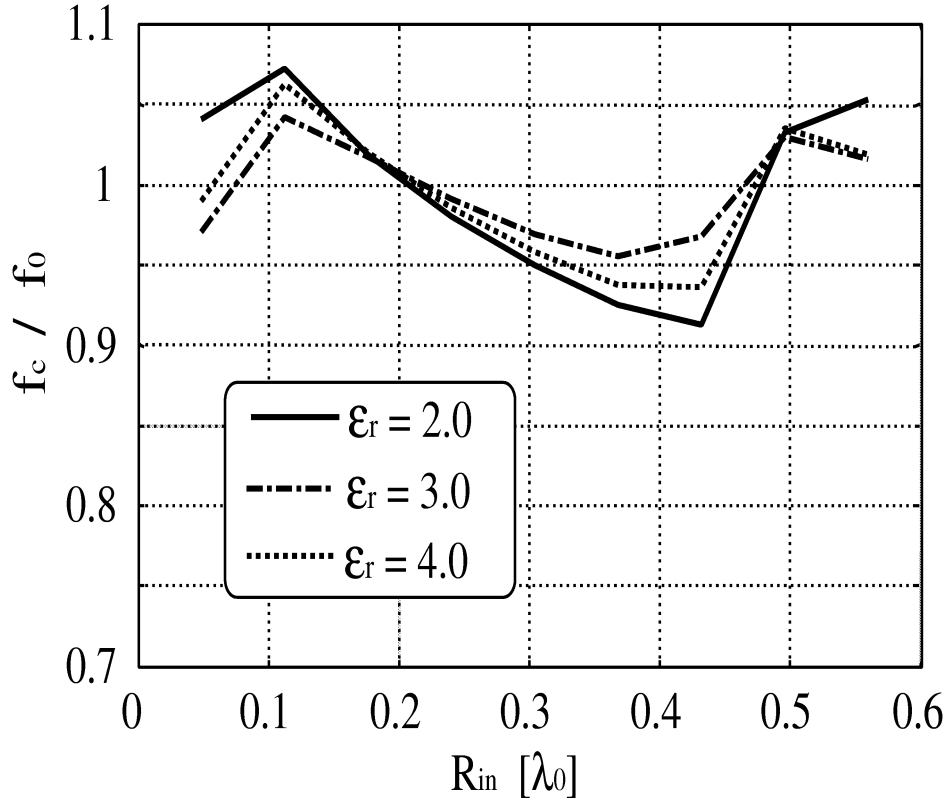

Figure 5.24: Central Frequency due to Radius of Cylindrical Radome($f_0 = 1.92[GHz], T_c = 5[mm](0.032\lambda_0)$)

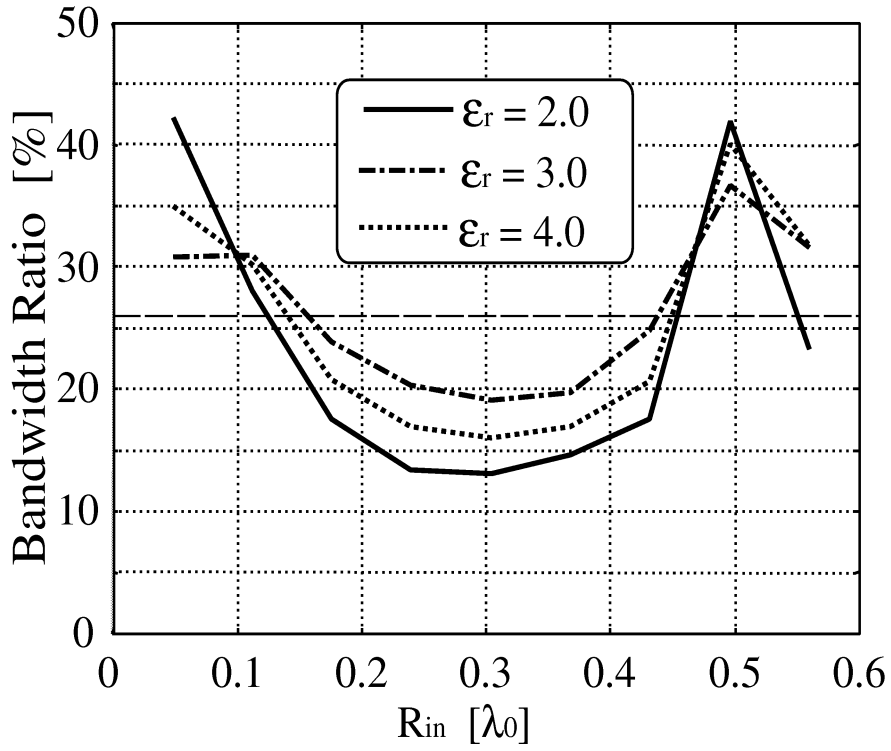

Figure 5.25: Bandwidth Ratio due to Radius of Cylindrical Radome($f_0 = 1.92[GHz], T_c = 5[mm](0.032\lambda_0), VSWR <= 2.0$)

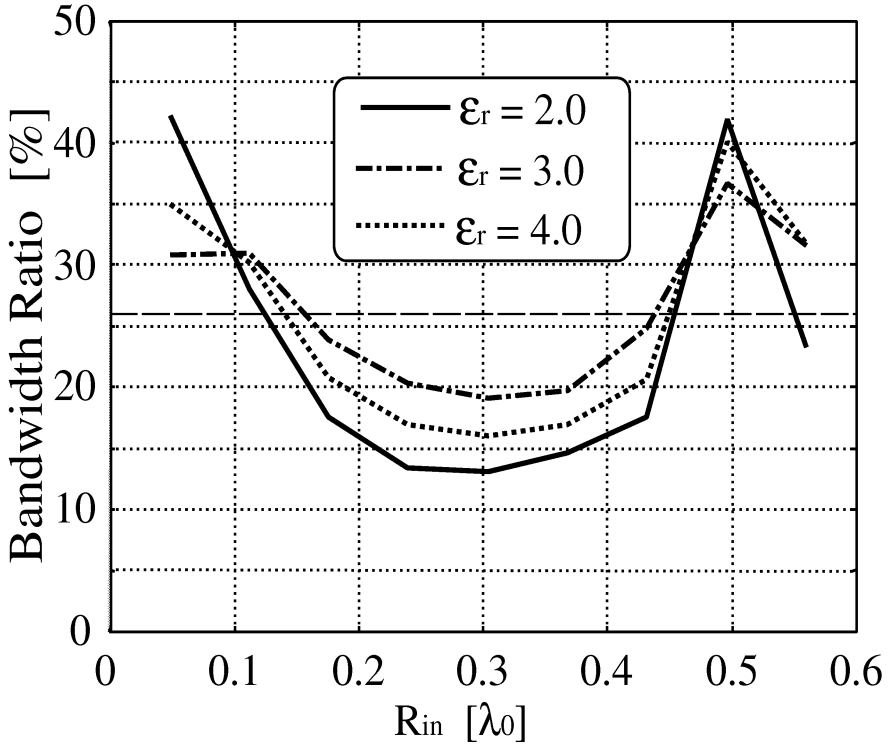

Figure 5.26: Bandwidth Ratio due to Radius of Cylindrical Radome($f_0 = 1.92[GHz], T_c = 5[mm](0.032\lambda_0), VSWR <= 2.0$)

From figures, we notice peak appears on each curves, and as ϵ_r lower, the peak level on curves become higher. Input characteristics is under the influence of permittivity dielectric radome easily.

5.3 Input and Radiation Characteristic due to Radiation Element's Location

Interaction between radiation element and dielectric radome is known as a complicated problem. In design and development of mobile communication's base station antenna, because the frequency band till now is low to ignore the influence of dielectric radome, there isn't big problem occurred. But the next generation system, which is famous known as IMT-2000, because the frequency band is around 2GHz, it is necessary to count the effect of radome in antenna's design. And the far field radiation pattern of antenna with dielectric radome also will change from the case of element only. It is necessary to investigate the change of antenna's input characteristic and radiation pattern due to cylindrical radome.

In previous subsection, in order to estimate the basic characteristic due to cylindrical

radome, we reported input characteristic of $\lambda/4$ monopole antenna due to parameters(radius, thickness, permittivity constant) of dielectric cylindrical radome.

To reduce the influence of cylindrical radome, install radiation element away from dielectric radome is usually adopted. But this will lead increases of radius and weight of radome directly. For base stations that is installed at the outdoor environment, the suitable characteristic on corrosion resistance and loading because of wind pressure are required. In this paper, we investigate input and radiation characteristics of print dipole antenna with reflector due to installation location in cylindrical radome. And from the measurement result, we propose the most suitable installation way of radiation element and the most effective radius of radome.

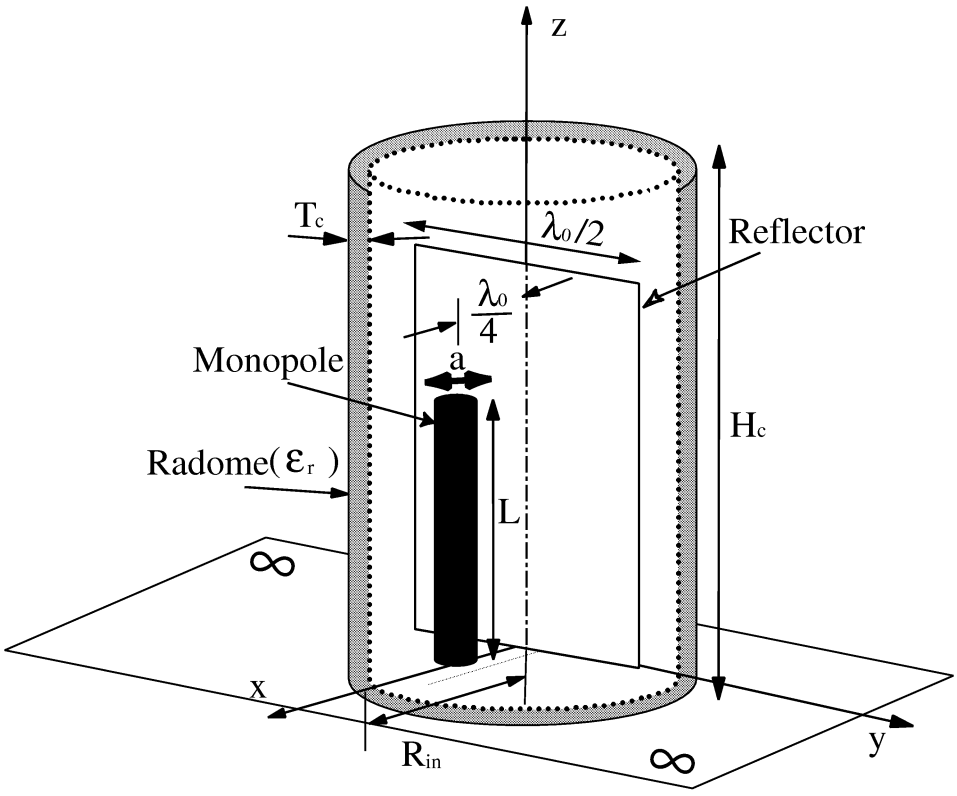

Figure 5.27: Measurement model

Figure 5.27 shows the measurement model. Radiation element is constructed by printed dipole antenna on a substrate($\epsilon_r = 2.6$) and reflector with $\lambda/2$ in width. The resonant frequency of r adiation element is around 2.0GHz. And the HPW(Half Power Width) is around 120^o. The radiation element is installed in a cylindrical radome($\epsilon_r = 4.7$). Thickness of dielectric radome(T_c) is 4[mm]. Radius of radome(R_{in}) are 46[mm] and 76[mm], respectively. The parameter *Offset* is defined as radiation element's location. By moving the radiation element parallel to the x-axis, input and radiation characteristic due to installation location can be obtained. Value of *Offset* > 0 and

Offset < 0 mean the radiation element is located on the positive and negative direction of x-axis, respectively.

By using parameters as mentioned previously, the measurement is carried out. Figures 5.28 and 5.32 show the return loss characteristics due to *Offset* when radius of radome (R_{in}) are 46[mm] and 76[mm]. We notice that both resonant frequency and bandwidth change greatly in most cases.

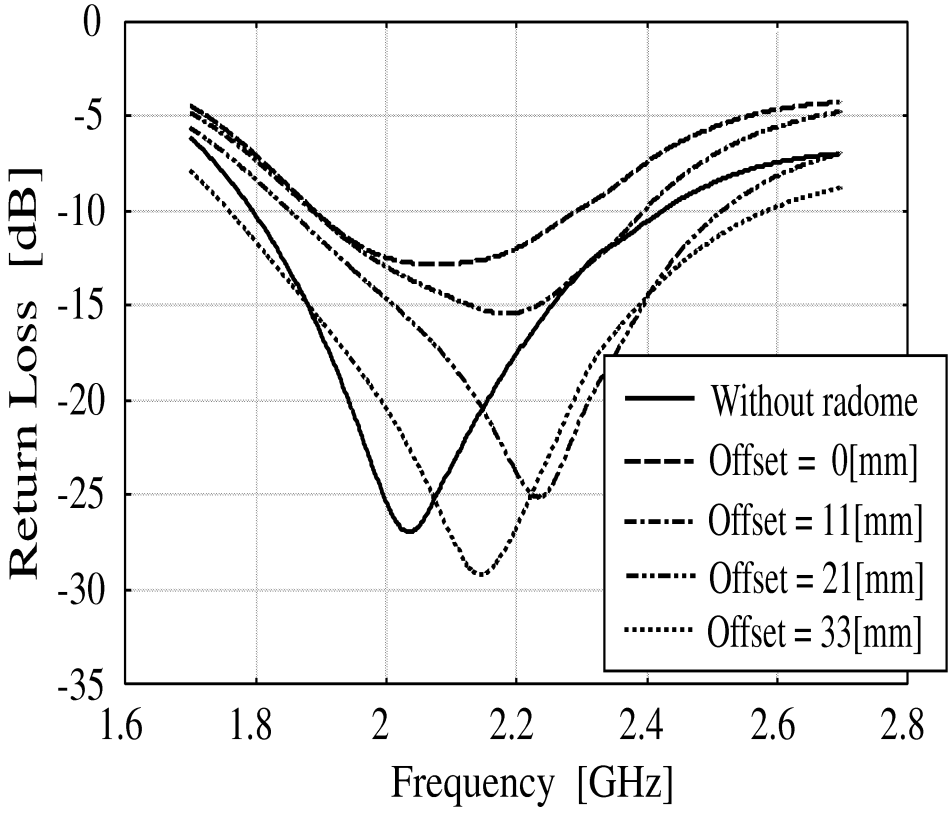

Figure 5.28: Return Loss Characteristic due to Offset from center of Radome($f_r = 2.0[GHz], \epsilon_r = 4.7, R_{in} = 46mm(0.31\lambda_0)$)

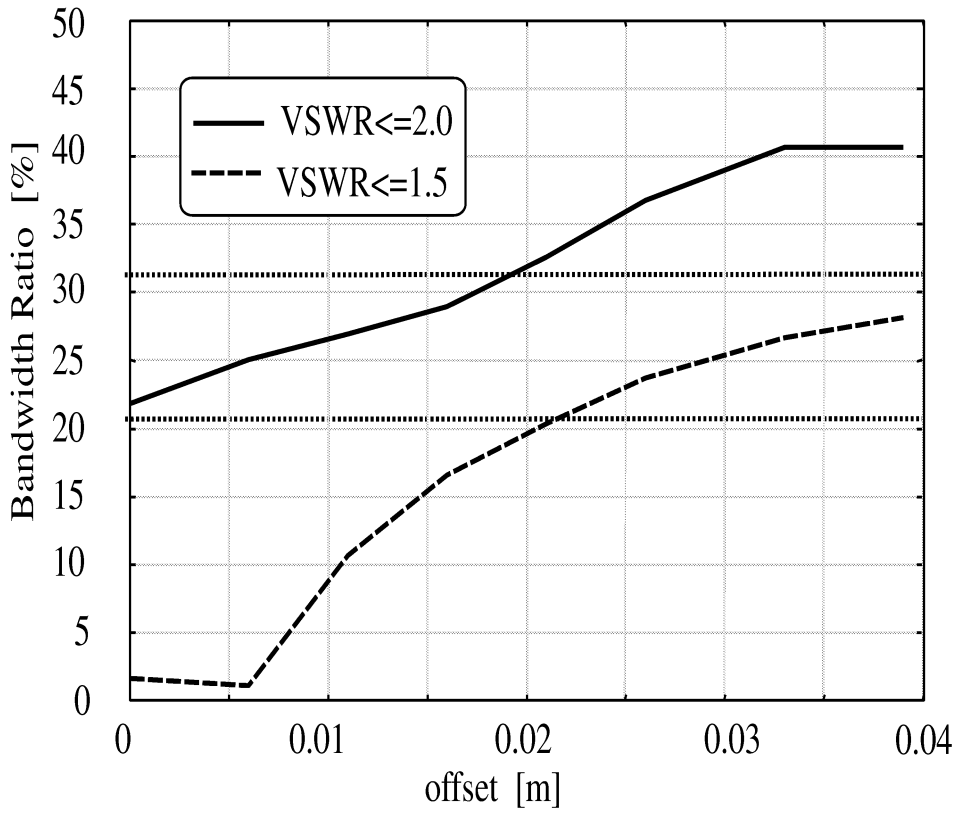

Figure 5.29: Bandwidth Ratio due to Offset from center of Radome($f_r = 2.0[GHz], \epsilon_r = 4.7, R_{in} = 46mm(0.31\lambda_0)$)

In order to estimate the input characteristic, the bandwidth ratio of VSWR < 2.0 and VSWR < 1.5 is examined. The bandwidth ratio is defined as $(f_{high} - f_{low})/f_0$. Figures 5.29 and 5.33 show the bandwidth ratio due to *Offset* when radius of radome (R_{in}) are 46[mm] and 76[mm]. Dash lines show at level of 32% and 21% are bandwidth ratio of without radome case. In order to examine the change of half power width(HPW) due to *Offset*, we select the half power width of element only(without radome) HPW_r as the reference.

From the result of cylindrical radome has a small radius (Fig. 5.29), we notice that as the increase of *Offset*, in other words, as we move the radiation element toward the inside wall of radome, the bandwidth ratio is increasing. And when *Offset* is larger than 0.02[m], the bandwidth ratio that is over the level of without radome case is obtained. The case of we install radiation element near the inside wall of radome got the largest bandwidth ratio. The reason is considered that dielectric radome resonate with radiation element when we install radiation element near by the radome. Next the radiation characteristic is carried out. Figures 5.30 and 5.31 show H-plane radiation pattern and half power width HPW_0 normalized by reference level, characteristic of HPW_0/HPW_r due to *Offset*. From figures, we notice that as *Offset* increase, HPW_0 also increases. This result indicates that the dielectric radome resonate with radiation

element when we move element toward the inside wall of radome.

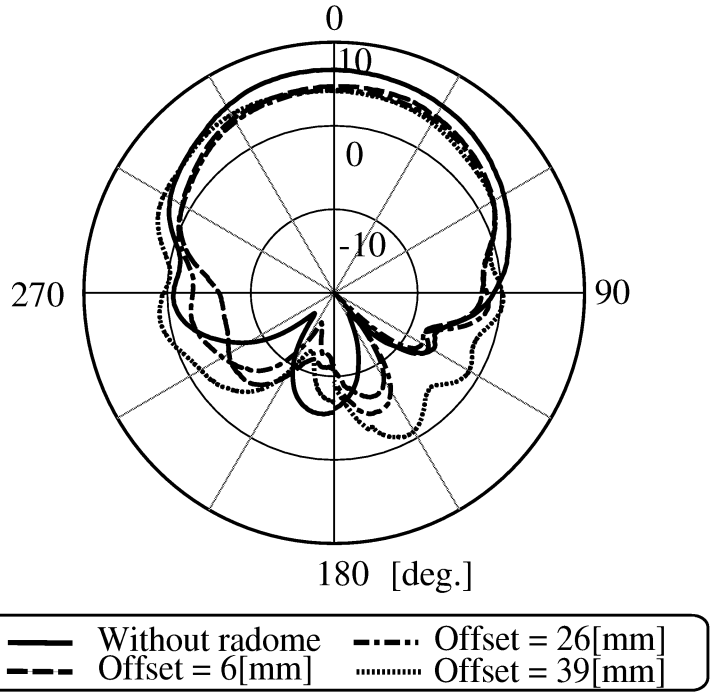

Figure 5.30: Radiation Pattern of x-y plane($f_r = 2.0[GHz], \epsilon_r = 4.7, R_{in} = 46mm(0.31\lambda_0)$)

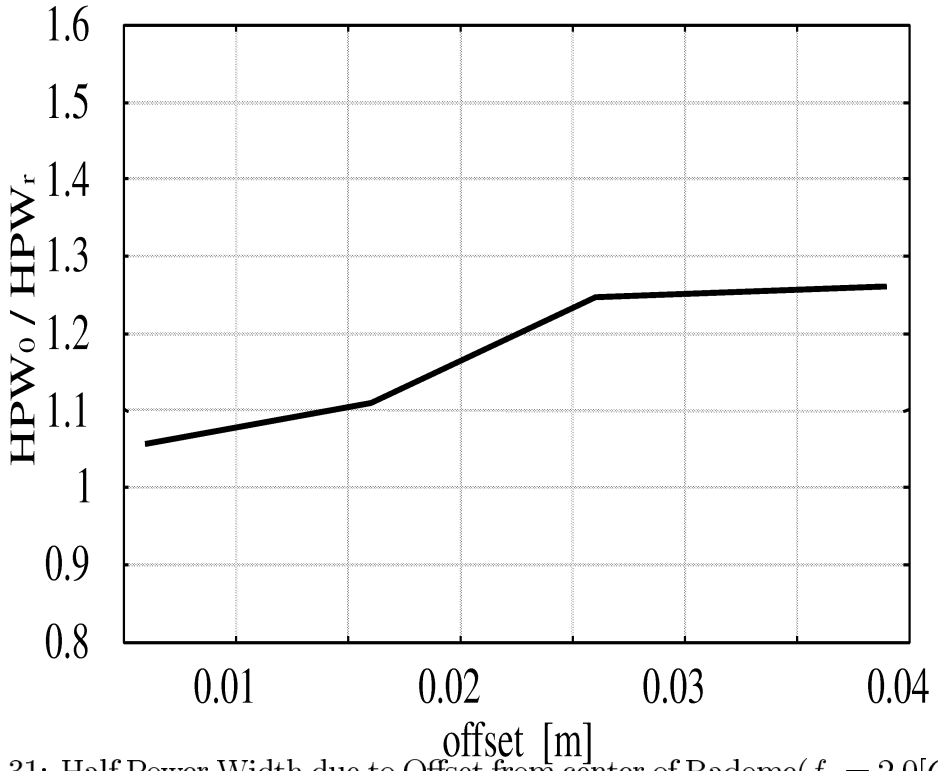

Figure 5.31: Half Power Width due to Offset from center of Radome($f_r = 2.0[GHz], \epsilon_r = 4.7, R_{in} = 46mm(0.31\lambda_0)$)

Next, measurement of case of cylindrical radome has a large radius is carried out. We examine cases of radiation element installed on positive and negative direction of x-axis. From result of the location is on negative direction of x-axis($Offset < 0$), we notice that bandwidth ratio obtains a higher level compare to the case of radiation element is on the center position ($Offset = 0$). And case of bandwidth ratio larger than without radome case are also observed(Fig. 5.33). From results of radiation pattern(Fig. 5.34 and Fig. 5.36), same changes are observed. The reason is considered that when we install radiation element on negative direction of x-axis, distance between element and side wall is enough small to lead resonant of radome. And when we focus the input and radiation characteristic of case of we install radiation element on positive direction of x-axis(Fig. 5.33, 5.35 and 5.36), we got as same result as case of radome that has a smaller radius.

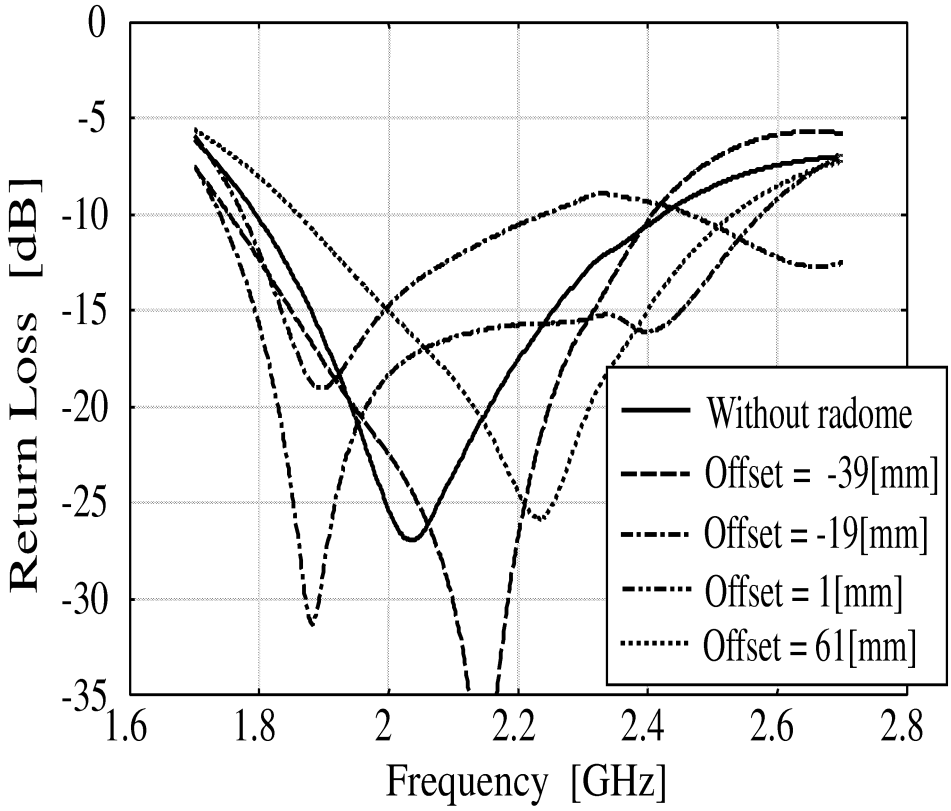

Figure 5.32: Return Loss Characteristic due to Offset from center of Radome($f_r = 2.0[GHz], \epsilon_r = 4.7, R_{in} = 76mm(0.51\lambda_0)$)

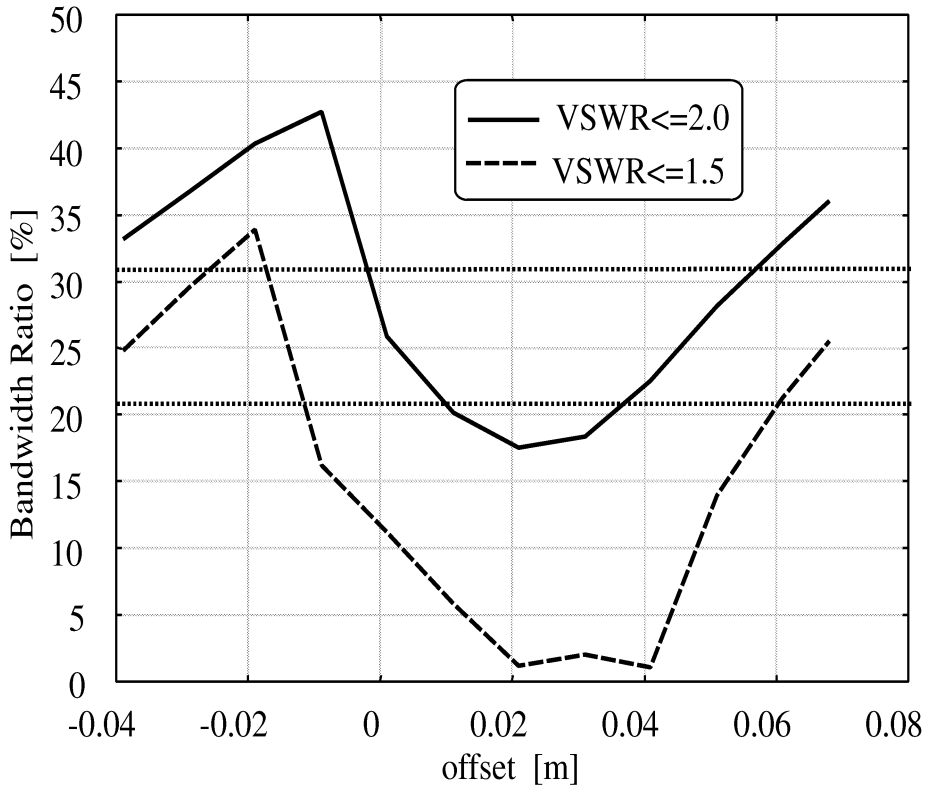

Figure 5.33: Bandwidth Ratio due to Offset from center of Cylindrical Radome($f_r = 2.0[GHz], \epsilon_r = 4.7, R_{in} = 76mm(0.51\lambda_0)$)

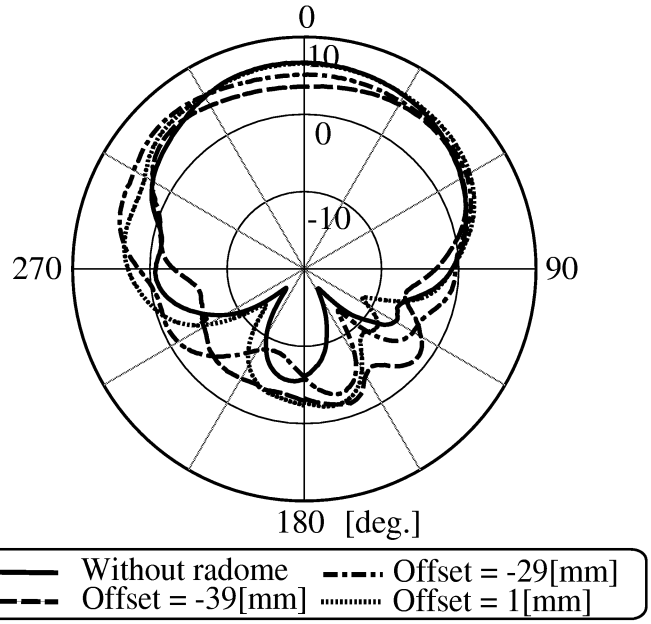

Figure 5.34: Radiation Pattern of x-y plane($f_r = 2.0[GHz], \epsilon_r = 4.7, R_{in} = 76mm(0.51\lambda_0)$)

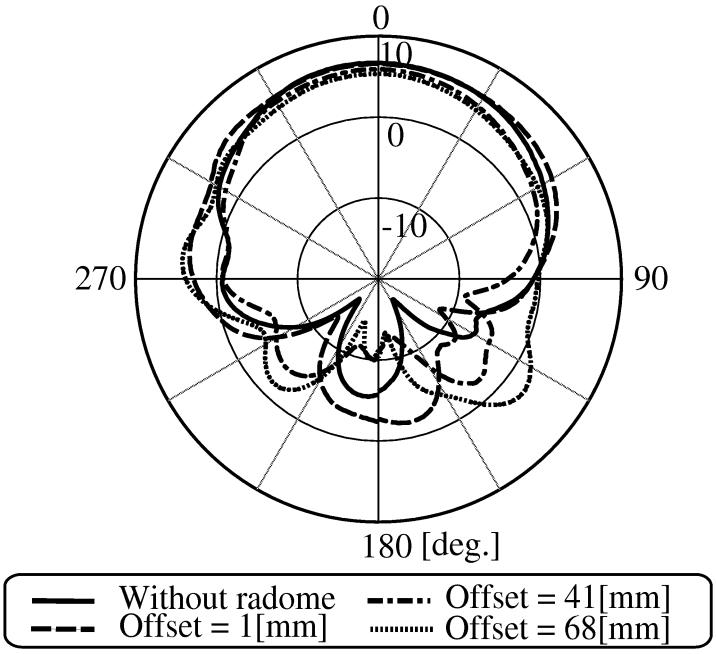

Figure 5.35: Radiation Pattern of x-y plane($f_r = 2.0[GHz], \epsilon_r = 4.7, R_{in} = 76mm(0.51\lambda_0)$)

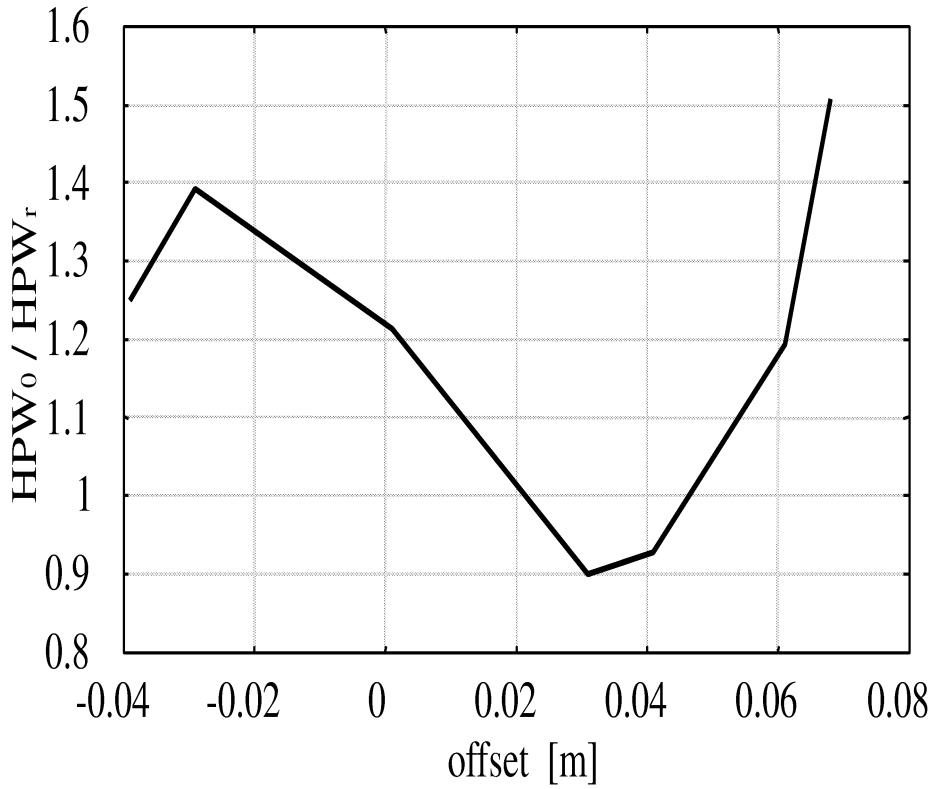

Figure 5.36: Half Power Width due to Offset from center of Radome($f_r = 2.0[GHz], \epsilon_r = 4.7, R_{in} = 76mm(0.51\lambda_0)$)

It is well know that because the wavelength propagated in dielectric material is shorter than in the free space, dielectric material will cause a lower frequency and narrower bandwidth compare to without radome case. But from curves be shown in this paper, we notice that the bandwidth ratio reaches to high level compare to without radome case when we install radiation element near by the radome. So we conclude that the most suitable installation location of element is inside wall of dielectric radome. And the radius of cylindrical radome also can be reduced greatly.

5.4 2GHz Band Sector Antenna

In the next generation system, which is famous known as IMT-2000, the frequency band is around 2GHz. It is expected that higher frequency band will be adopted in further mobile communication systems. The interaction between radiation element and dielectric radome must become increasingly a factor that can't be ignored. And the far field radiation pattern of antenna with dielectric radome also will change from the case of element only. It is necessary to count the influence of radome in antenna's design. Investigation of the change of antenna's input characteristics and radiation pattern due to cylindrical radome is required.

To investigate the interaction between radiation element and dielectric radome, some previous works are reported [3][21][22]. As far as our knowledge, there is no published work on the influence of radome at mobile communication system.

The purpose of this study is to investigate input and radiation characteristics of antenna due to parameters of dielectric cylindrical radome. In previous section, we reported the input characteristics of omni antenna due to cylindrical radome. But sector antennas occupy an important position in base station antennas. It is necessary to investigate the radome effect for sector antennas. In this paper, we investigate the input and radiation characteristic of 2GHz band 120^o beam antenna due to radome's parameter.

5.4.1 Simulation Model and Parameters

To clarify the mechanism of radome effect, FDTD Simulation [2][3] is considered as the most suitable. It becomes a large analysis problem if we handle the radiation element and dielectric radome simultaneously by FDTD method. The high performance three-dimensional FDTD algorithm by using non-uniform mesh that allows flexible cell size to improve the accuracy of modeling and reduce the computation resource is adopted in this study.

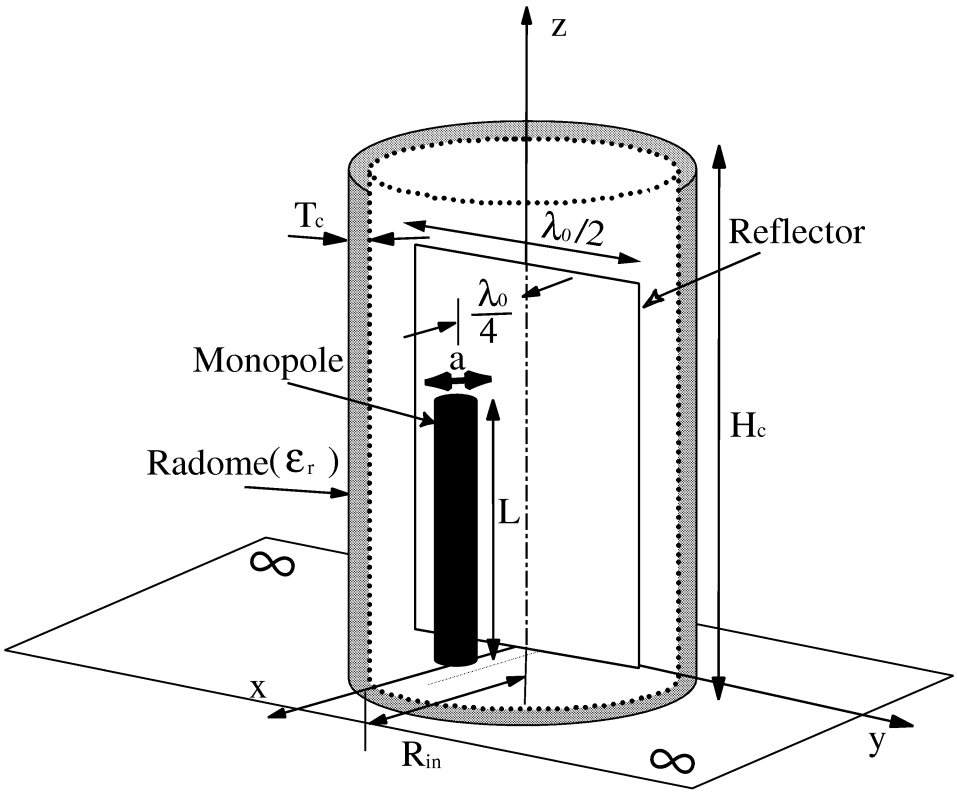

(a) 120^o Sector Antenna with Cylindrical Radome

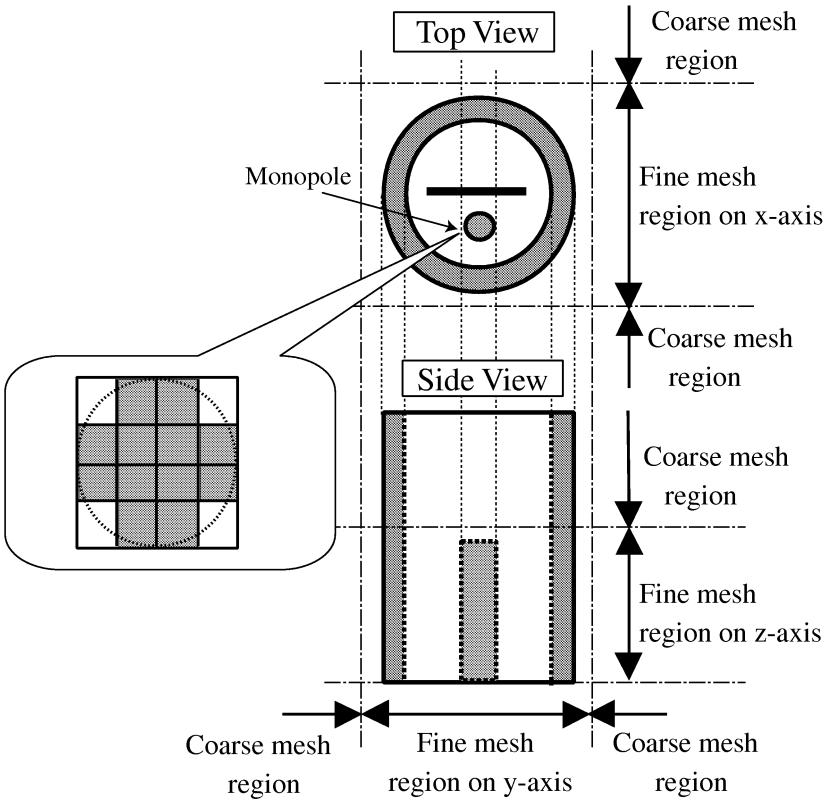

(b) FDTD Mesh Division

Figure 5.37: FDTD Simulation Model

Table 5.3: Parameters for FDTD analysis (Case of $f_0 = 2.03$[GHz])

Length of monopole (L)	34 [mm]
Thickness of monopole (a)	5 [mm]
Height of cover (H_c)	125 [mm]
Radius of cover (R_{in})	47.5 - 120.7[mm] ($\approx 0.32\lambda_0$ - $0.82\lambda_0$)
Thickness of cover (T_c)	2.5, 3.75, 5[mm] ($\approx 0.016\lambda_0$ - $0.032\lambda_0$)
Permitivity of cover (ϵ_r)	1.0(Free space), 2.0 - 6.0
Computation space	$0.8[m] \times 0.8[m] \times 0.4[m]$ ($\approx 5\lambda_0 \times 5\lambda_0 \times 2.5\lambda_0$)
Cell size	$[I]$ $\Delta_{fine} = 1.25[mm]$ ($\approx \lambda_0/125$) $[II]$ $\Delta_{coarse} = 11.25[mm]$ ($\approx \lambda_0/14$)
Iteration	6000
Incident wave	Gaussian pulse
Absorbing Boundary Condition	Mur's 2nd approx.

Figure 5.37(a) shows the simulation model in this study. Reflector($\lambda_0/2$ in width) is installed in the middle of radome. Radiation element is placed at a distance of $\lambda_0/4$ from reflector. In without radome case, the half power width is approximately 120^o. In simulation, the imaging plane that has infinite size is used to reduce the computation volume. Changing the length of element can allow us obtain the measurement and simulation results from 800[MHz] to 2.4[GHz]. By changing parameters of radius, thickness and permittivity constant of radome, input impedance due to radome parameters can be given.

Figur 5.37(b) and Table 5.3 show mesh division and parameters of FDTD simulation. The thickness of monopole is also under consideration.

5.4.2 Input and Radiation Characteristics by Radome Parameters

Using parameters be previously mentioned, the calculation of radiation characteristics are carried out. Figure 5.38 shows comparison of horizontal plane's radiation pattern. Curves on Fig. 5.38 show that the half power width kept 120^o when radius(R_{in}) is 81.6[mm]($0.55\lambda_0$). But when R_{in} is 47.5[mm]($0.32\lambda_0$), the half power width spread out from -90^o to 90^o. This shows the complexity of radome effect.

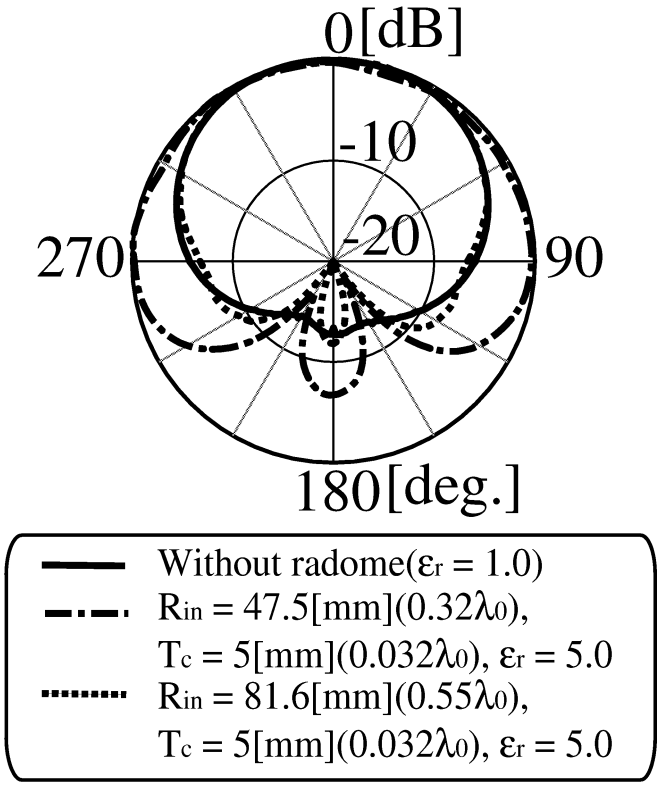

Figure 5.38: Comparison of Radiation Patter(E_θ)(f_0=2.03[GHz])

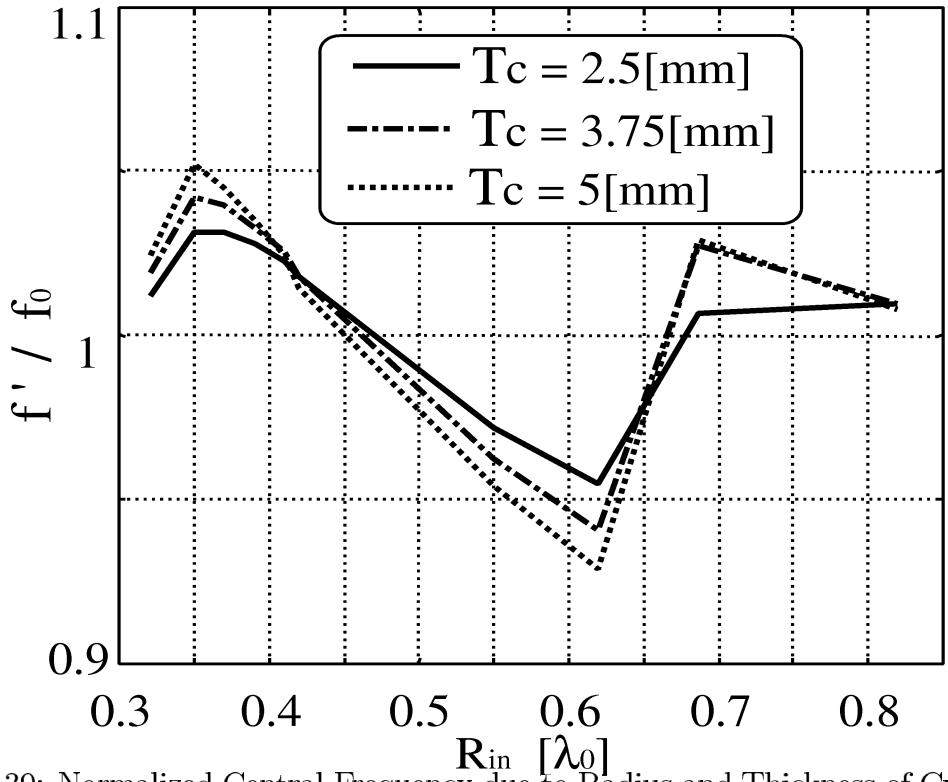

Figure 5.39: Normalized Central Frequency due to Radius and Thickness of Cylindrical Radome($f_0 = 2.03[GHz], \epsilon_r = 5.0$)

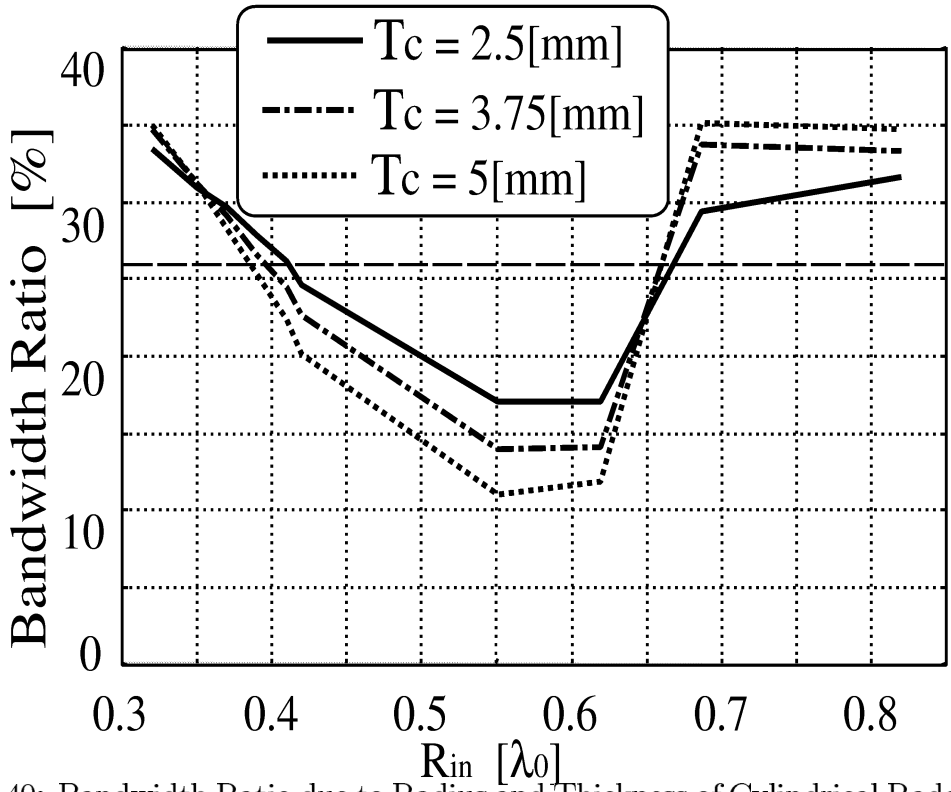

Figure 5.40: Bandwidth Ratio due to Radius and Thickness of Cylindrical Radome($f_0 = 2.03[GHz], \epsilon_r = 5.0, VSWR <= 2.0$)

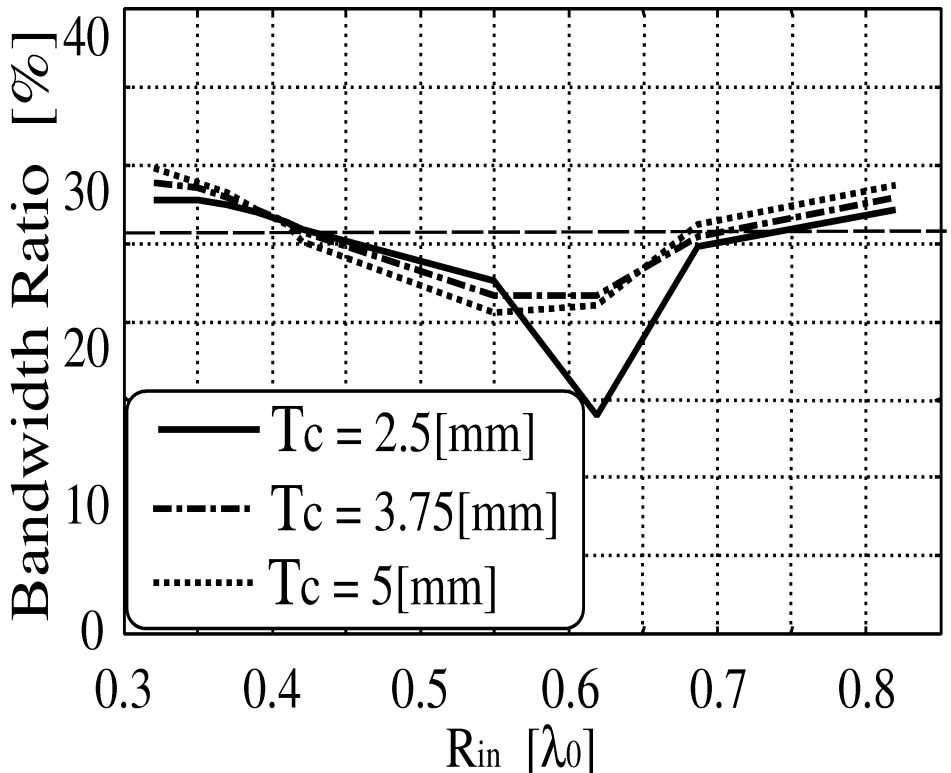

Figure 5.41: Bandwidth Ratio due to Radius and Thickness of Cylindrical Radome($f_0 = 2.03[GHz], \epsilon_r = 2.0, VSWR <= 2.0$)

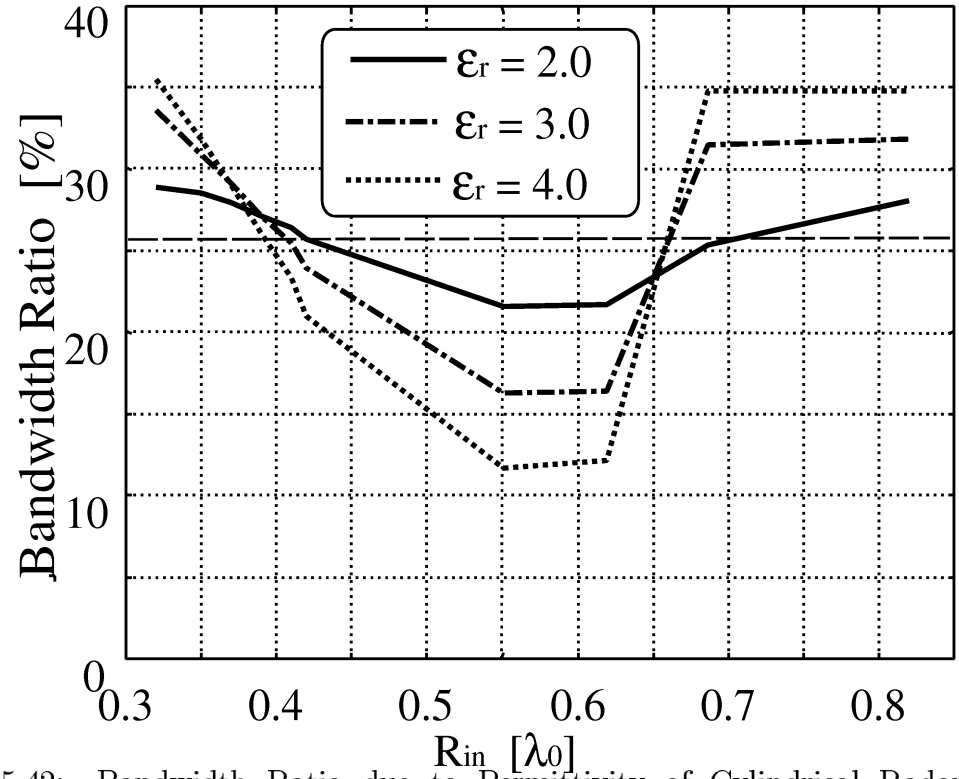

Figure 5.42: Bandwidth Ratio due to Permittivity of Cylindrical Radome($f_0 = 2.03[GHz], T_c = 3.75[mm](0.024\lambda_0), VSWR <= 2.0$)

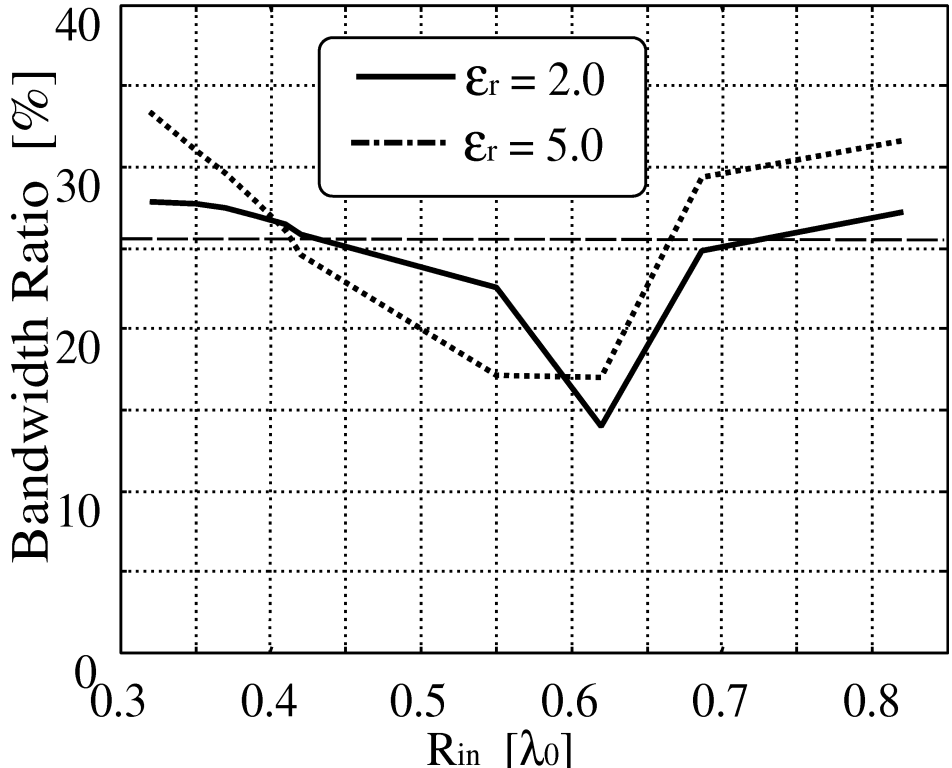

Figure 5.43: Bandwidth Ratio due to Permittivity of Cylindrical Radome ($f_0 = 2.03[GHz], T_c = 2.5[mm](0.016\lambda_0), VSWR <= 2.0$)

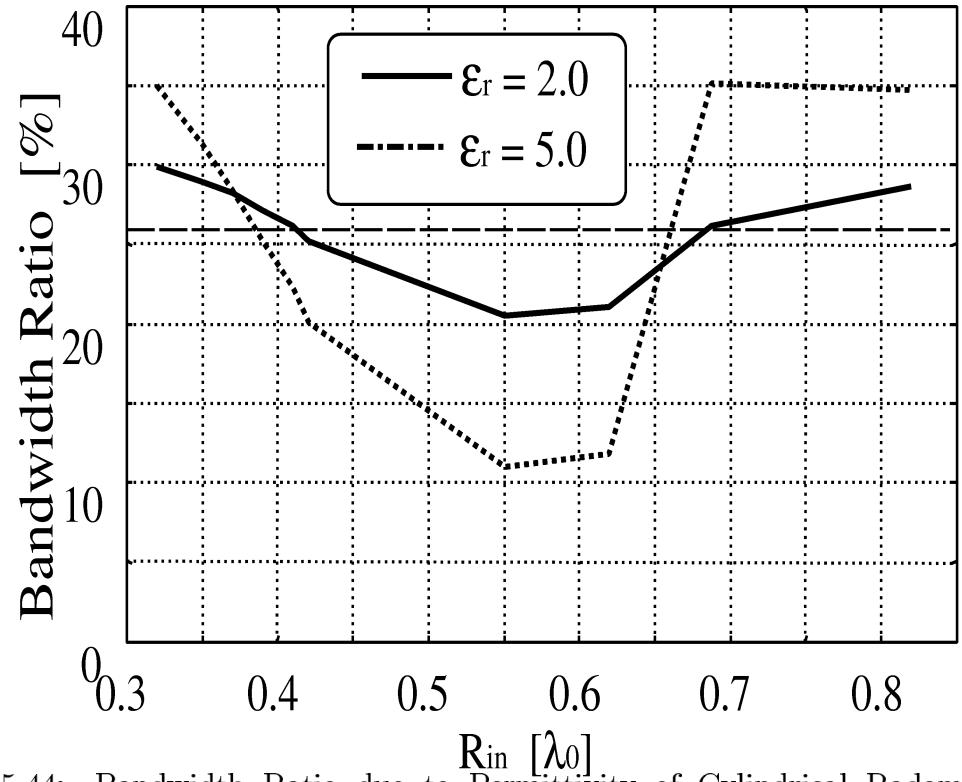

Figure 5.44: Bandwidth Ratio due to Permittivity of Cylindrical Radome ($f_0 = 2.03[GHz], T_c = 5[mm](0.032\lambda_0), VSWR <= 2.0$)

To clarify the mechanism of this problem, investigation of input characteristics due to cylindrical radome's parameter is carried out. In order to estimate the characteristics, we select the central frequency and bandwidth ratio of element only(without radome) f_0 and BW_0 as the reference. The ratio f_c/f_0 shows the central frequency f_c normalized by reference value f_0. Bandwidth ratio of VSWR < 1.5 and VSWR < 2.0 are observed.

First of all, the input characteristics due to radius of radome(R_{in}) is carried out. Figures 5.39 and 5.40 show normalized central frequency and bandwidth ratio due to R_{in}. Dotted line shows in 26% is the bandwidth ratio of without radome case. From the figure, we notice that wider bandwidth compared to without radome case obtained when R_{in} is less than $0.37\lambda_0$ and larger than $0.66\lambda_0$. Same result was got when permittivity of radome(ϵ_r) is 2.0 (Fig. 5.41).

When we focus the thickness of radome(T_c), we found that thin radome changes slowly compare to thick radome. The difference is especially obvious when ϵ_r is high.

Compare the Fig. 5.40 to Fig. 5.41, we found bandwidth ratio changed with different gradient when we change the ϵ_r. Figure 5.42 shows bandwidth ratio due to ϵ_r when T_c is 3.75[mm] ($0.024\lambda_0$). From curves on figure, it is clear that higher permittivity radome case shows larger gradient on bandwidth ratio's characteristics.

Generally, increase radome's radius can be considered as a useful way to avoid the radome's influence. From above results, bandwidth ratio widen when we increase the radius(R_{in}). But we also found it will lead the spread of half power bandwidth. The

reason is considered as radome's resonance. And same conclusion can be given in thin radome case, too. As the conclude, To find the best parameters for high performance, it is necessary to count the input characteristics and radiation characteristics simultaneously.

5.5 Conclusions

In this chapter, we first reported the characteristics of 2GHz omni antenna's input impedance due to parameters of cylindrical dielectric radome. From results of we change the thickness, radius, permittivity constant of radome, we conclude that input impedance is easily influence by parameters of radome.

The input impedance matching should count the effect of radome, in particularly at the high frequency region. And better performance compared to without radome case also can be expected when we reduce the radius of dielectric radome. We propose to count the radome's effect in design's early stage, which can lead to achieve the base station antenna's miniaturization.

At second section of this chapter, we reported input and radiation characteristic of printed dipole antenna with 120^o beam covered with cylindrical radome due to installation location in radome. From measurement results, we conclude that input impedance is easily influence by parameters of radome. The most suitable installation location of element is near by inside wall of dielectric radome. And the radius of cylindrical radome can be reduced greatly.

In the last section of this chapter, we investigated the antenna-radome interaction between 2[GHz] band 120^o beam antenna and cylindrical radome. From the result, it is clear that input and radiation characteristics change greatly due to distance between radiation element and cylindrical radome. It is necessary to count the radome effect in antenna's design.

Chapter 6

Summary and Conclusions

The objective of this study is to improve the efficiency and possibility of FDTD analysis. This dissertation discussed the following.

- Solution for discontinue junction between coarse mesh and fine mesh region;
- Investigation of NUM-FDTD's computation error;
- Simulation of antenna with fine structure partly by using NUM-FDTD;
- Investigation of antenna-radome interaction.

The fast and efficient FDTD method by using non-uniform mesh is presented in this paper. By using an assumed magnetic component and linear interpolation, the simple algorithm can be used to reduce computation resources and to improve its accuracy simultaneously.

In chapter 3, as the result of examination of computation error due to mesh size ratio and fine mesh region, we conclude that small numerical error can be obtained when we determine the fine mesh region based on electrical volume of object.

In chapter 4, we calculated several kinds of antenna that have fine structure partly compare to main part of antenna. The following results are obtained.

The basic linear antenna – monopole antenna, is simulated by NUM-FDTD. By applying small cell size at length direction of monopole antenna. Computation error of resonant frequency is reduced. In FDTD analysis, cell size is required to be certainly small in dielectric problem. Notch antenna loaded with dielectric material's simulation is the case of we apply NUM-FDTD to dielectric problem. In small pager's base station antenna's analaysis, we extened NUM-FDTD to 3 kinds of different mesh can be allow in simulation. Antenna's structure is modeled precisely, an accracy analysis is obtained. Using NUM-FDTD, miniaturization of top loaded low-profile monopole antenna is carried out. From results of we change parameters and shape of matching post, it is clear that different resonance existed due to distance between feed pin and matching post.

And optimum shape of matching structure is proposed. Another simulation of circular polarized patch antenna with cross-shaped slit is carried out. We investigated antenna's miniaturization by adding 4 slits on a square patch antenna. Increase the length of slit leads an obvious decrease of eigenvalue k_0a, which indicate antenna's miniaturization. And the input impedance can be arranged to have an appropriate value to match the load impedance if we change position of feed point. Further miniaturization is investigated by using a cross-shaped slit instead of slit. The eigenvalue k_0a is reduced 48.9%(f_0 =2.52[GHz]). Using degeneracy separation method, a circular polarization is achieved.

By applying smaller mesh size on fine structure, precise simulation is carried out by less computation resource. Non-uniform mesh FDTD algorithm is suitable for small antenna's optimization.

In chapter 5, investigation of antenna-radome interaction is carried out. The following results is obtained.

we first reported the characteristics of 2GHz omni antenna's input impedance due to parameters of cylindrical dielectric radome. From results of we change the thickness, radius, permittivity constant of radome, we conclude that input impedance is easily influence by parameters of radome. The input impedance matching should count the effect of radome, in particularly at the high frequency region. And better performance compared to without radome case also can be expected when we reduce the radius of dielectric radome. We propose to count the radome's effect in design's early stage, which can lead to achieve the base station antenna's miniaturization.

Next, investigation of input and radiation characteristic of printed dipole antenna with 120^o beam covered with cylindrical radome due to installation location in radome is carried out. From measurement results, we conclude that input impedance is easily influence by parameters of radome. The most suitable installation location of element is near by inside wall of dielectric radome. And the radius of cylindrical radome can be reduced greatly.

Last, we investigated the antenna-radome interaction between 2[GHz] band 120^o beam antenna and cylindrical radome. From the result, it is clear that input and radiation characteristics change greatly due to distance between radiation element and cylindrical radome. It is necessary to count the radome effect in antenna's design.

Acknowledgments

I wish to express my gratitude to my sincerest acknowledgment to my supervisor Associate Professor Hiroyuki Arai for his continuous guidance throughout this work.

I gratefully acknowledge Professor Masahiro Toki, Professor Yasuo Hirose, Professor Yasuo Kokubun and Associate Professor Toshihiko Baba with Yokohama National University for their useful advices and discussions.

I am indebted to Dr. Yoshio Ebine of NTT DoCoMo Inc. for his valuable suggestions and encouragement.

I would express my appreciation to the members of Associate Professor Arai's group of Yokohama National University.

I express the respect to my parents, my parents-in-law for their mental support.

Finally, I acknowledge my husband, Hiroyuki and son, Tomohiro for their strong support.

Bibliography

[1] K.S. Yee, "Numerical Solutions of Initial Boundary Value Problems Involving Maxwell's Equations in Isotropic Media," *IEEE Trans. Antennas & Propagt.*, vol. AP-14, pp.302-307, May. 1966.

[2] K.S. Kunz and R.J. Luebbers, "The Finite Difference Time Domain Method for Electromagnetics," *CRC Press*, 1993.

[3] A. Taflove, "Computational Electrodynamics – The Finite-Difference Time Domain Method," *Artech House*, 1995.

[4] Fusco, M., "FDTD algorithm in curvilinear coordinates," *IEEE Trans. Antennas & Propag.*, vol.AP-38, pp.76–89, Jan. 1990.

[5] S.S. Zivanovic, K.S. Yee and K.K. Mei, "A subgridding method for the time-domain finite-difference method to solve Maxwell's equations," *IEEE Trans. Microwave Theory & Tech.*, vol.39, no.3, pp.471–479, Mar. 1991.

[6] E.M. Daniel and C.J. Railton, "Fast finite difference time domain analysis of microstrip patch antennas," *Proc. IEEE AP-S Int. Symp.*, pp.414–417, London Canada, June 1991.

[7] A.C. Cangellaris, "Time-domain finite methods for electromagnetic wave propagation and scattering," *IEEE Trans. Magn.*, vol.27, no.5, pp.3780–3785, Sep. 1991.

[8] K. Li, C.F. Lee, S.Y. Poh, R.T. Shin and J.A. Kong, "Application of FDTD method to analysis of electromagnetic radiation from VLSI heatsink configurations," *IEEE Trans. Electromagnetic Compatibility*, vol.35, no.2, pp.204–214, May 1993.

[9] S. Xiao and R. Vahldieck, "An improved 2D-FDTD algorithm for hybrid mode analysis of quasi-planar transmission lines," *Proc. 1993 MTT-S*, pp.421–424, 1993.

[10] M. Okoniewski, E. Okoniewska and M.A. Stuchly, "3D sub-gridding algorithm for FDTD," *Proc. IEEE AP-S Int. Symp.*, vol.1, pp.232–235, June 1995.

[11] M.J. White, M.F. Iskander and Z.L. Huang, "Development of a multigrid FDTD code for three-dimensional applications", *IEEE Trans. Antennas & Propag.*, vol.AP-45, no.10, pp.1512–1517, Oct. 1997.

[12] T. Kondo, K. Kaneta, K. Sakurai, M. Ando, N. Goto, "A Conformal Planar Antenna for Mobile Communications," *IEICE Technical Report*, AP87-98, pp. 39-44, 1987.

[13] H. Arai, H. Iwashita, N. Toki and N. Goto, "A Flat Energy Density Antenna System for Mobile Telephone," *IEEE Trans. Behicular Technology*, vol. 40, No. 2, pp.483-486, 1991.

[14] S. Sekine, T. Uno, K. Sawaya and S. Adachi, "Theoretical Analysis of Disc-Loaded Folded Monopole Antenna," *The Trans. of IEICE*, vol. J71-B-II, No. 11, pp.1244-1247, 1988.

[15] Sato, Kawakami, Ikeda, Ogawa, "," *IEICE General Conf.*, pp. 799, 1983.

[16] K. Endo, H. Arai and M. Toki, "Analysis of Disc-Loaded Antenna with Matching Posts by Diakoptic Theory," *The Trans. of IEICE*, vol. J74-B-II, No. 11, pp.594-598, 1991.

[17] K. Hiramatsu, K. Sawaya and S. Adachi, "Analysis of Disc-Loaded Low-Profile Monopole Array Antenna," *IEICE Technical Report*, AP90-39, pp.51-57, 1990.

[18] H. Ochi, E. Yamamoto, Q. Chen and K. Sawaya, "Moment Method Analysis of Antennas Composed of Conducting Wires and Plates," *The Trans. of IEICE*, vol. J79-B-II, No. 9, pp. 566-573, 1996.

[19] J. Yang, T. Iijima and S. Tokumaru, "Multiplates: Low Profile Antennas," *The Trans. of IEICE*, vol. J80-B-II, No. 12, pp. 1050-1057, 1997.

[20] T. Ito, W. Chujo, M. Tokizawa and M. Fujita, "Experiment of Small-sized Microstrip Antenna with Deep Notches", *1988 Autumn National Convention Record of IEICE*, B-32, Sep. 1988.

[21] S. R. Rengarajan and E. S. Gillespie. JR., "Asymptotic Approximation in Radome Analysis," *IEEE Trans. Antenna & Propag.*, vol. 36, No. 3, pp. 405 - 415, March 1988.

[22] R. Orta, R. Tascone and R. Zich, "Performance Degradation of Dielectric Radome Covered Antennas," *IEEE Trans. Antenna & Propag.*, vol. 36, No. 12, pp. 1707 - 1713, Dec. 1988.

Publication list

Following lists contain the related publications of this dissertation.

Papers

1. H. Jiang and H. Arai, *"Analysis of Computation Error in Antenna's Simulation by Using Non-Uniform Mesh FDTD"*,
   IEICE Transactions on Communications, Vol. E83-B, No.7, pp.1544-1553, July 2000.

2. H. Jiang and H. Arai, *"FDTD Analysis of Low Profile Top Loaded Monopole Antenna"*,
   IEICE Transactions on Communications (submitted in 2001).

IEICE Technical Report

1. H. Jiang, K. Fujimori, H. Arai and Y. Ebine(NTT Docomo Inc.), *"Ray Tracing Analysis of Propagation Characteristics in Tunnels"*,(in Japanese)
   IEICE Technical Report, AP 96-71, pp.35-42, November 1996, Yamaguchi.

2. H. Jiang and H. Arai, *"Calculation Errors due to Mesh Size and Analysis Region on FDTD Analysis Using Sub-cell Technique"*,
   IEICE Technical Report, AP 98-8, pp.7-12, May 1998, Akita.

3. H. Jiang and H. Arai, *"FDTD Analysis of Disk Loaded Monopole Antenna with Matching Posts"*,
   IEICE Technical Report, AP 99-36, pp.9-16, June 1999, Tokyo.

4. H. Jiang, H. Arai and Y. Ebine(NTT DoCoMo Inc.), *"Input Characteristic of $\lambda/4$ Monopole Antenna Covered with Circular Cylinderical Radome"*,
   IEICE Technical Report, AP 99-244, pp.53-58, March 2000, Xi'An, China.

5. H. Jiang, H. Arai and Y. Ebine(NTT DoCoMo Inc.), *"Monopole Antenna using Resonance of Cylindrical Radome"*,(in Japanese)
IEICE Technical Report, AP 2000-159, pp.49-54, January 2001, Nagasaki, Japan.

International Conferences

1. H. Jiang, K. Fujimori, H. Arai and Y. Ebine(NTT DoCoMo Inc.), *"Propagation Characteristics and Uplink Diversity Effect for Tunnel Booster System"*,
International Symposium on Recent Advances in Microwave Techniques Proceeding 1997, pp.207-210, August 1997, Beijing, China.

2. H. Jiang and H. Arai, *"Fast and Efficient FDTD Analysis Using Non-Uniform Mesh for Small Antenna"*,
IEEE International Symposium on Antenna and Propagation 1998, Vol. 2, pp.1242-1245, June 1998, Atlanta, USA.

3. H. Jiang and H. Arai, *"3D FDTD Analysis by Using Non-Uniform Mesh"*,
1998 International Conference on Microwave and Millimeter Wave Technology Proceedings, pp.947-950, August 1998, Beijing, China.

4. H. Jiang and H. Arai, *"Calculation Error due to Fine Mesh Region on FDTD Analysis by using Non-Uniform Mesh"*,
1998 IEEE Asia Pacific Microwave Conference, Vol. 3, pp.1405-1408, December 1998, Yokohama, Japan.

5. H. Jiang and H. Arai, *"Analysis of Pacth Antenna with Short Pin by Using Non-Uniform Mesh FDTD"*,
1999 IEEE Antennas and Propagation Society International Symposium, Vol. 1, pp.610-613, July 1999, Orlando, USA.

6. H. Jiang and H. Arai, *"FDTD Simulation of Top Loaded Low-Profile Monopole Antenna"*,
1999 Asia Pacific Microwave Conference, Vol. 1, pp.150-153, December 1999, Singapore.

7. H. Jiang, H. Arai and Y. Ebine(NTT DoCoMo Inc.), *"FDTD Analysis of Input Characteristic of Monopole Antenna Covered with Cylindrical Radome"*,
2000 IEEE Antennas and Propagation Society International Symposium, Vol. 3, pp.1480-1483, July 2000, Utah, USA.

8. H. Jiang, H. Arai and Y. Ebine(NTT DoCoMo Inc.), *"Input and Radiation Characteristics of 120° Beam Antenna Covered with Cylindrical Radome"*,

Proceedings of The 2000 International Symposium on Antennas and Propagation, Vol. 1, pp.297-300, August 2000, Fukuoka, Japan.

9. H. Jiang, H. Arai, *"FDTD Simulation for Small Antenna Geometries by Using Non-Uniform Mesh Algorithm"*,
   Proceedings of Eleventh International Conference on Antennas and Propagation, Vol. 2, pp.408-411, April 2001, Manchester, U.K.

10. H. Jiang, H. Arai and Y. Ebine(NTT DoCoMo Inc.), *"Antenna-Radome Interaction of 2GHz Band 120 degrees Beam Antenna"*,
    2001 IEEE Antennas and Propagation Society International Symposium, Vol. 3, pp.66-69, July 2001, Boston, USA.

11. H. Jiang and H. Arai, *"Optimization of Circular Polarized Patch Antenna with Cross-shaped Slit"*,
    submitted to 2002 IEEE Antennas and Propagation Society International Symposium.

General Conference and Society Conference of IEICE (in Japanese)

1. H. Jiang, K. Fujimori, H. Arai and Y. Ebine(NTT Docomo Inc.), *"Propagation Characteristics Inside Tunnel Excited by Outside Antenna"*,
   1997 General Conference of IEICE, B-1-41, March 1997, Osaka.

2. H. Jiang, K. Fujimori, H. Arai and Y. Ebine(NTT Docomo Inc.), *"Polarization Characteristics Inside Tunnel Excited by Outside Antenna"*,
   1997 Society Conference of IEICE, B-1-35, September 1997, Tokyo.

3. H. Jiang and H. Arai, *"3D FDTD Analysis by Using Non-uniform Mesh"*,
   1998 General Conference of IEICE, B-1-79, March 1998, Kanagawa.

4. H. Jiang and H. Arai, *"A Study on FDTD Computation Error due to Fine Mesh Region by using Non-Uniform Mesh (NUM-FDTD)"*,
   1998 Society Conference of IEICE, B-1-88, September 1998, Yamanashi.

5. H. Jiang and H. Arai, *"Analysis of Pacth Antenna with Short Pin by Using Non-Uniform Mesh"*,
   1999 General Conference of IEICE, B-1-117, March 1999, Kanagawa.

6. H. Jiang and H. Arai, *"Analysis of Pager's Base Station Antenna by using Non-Uniform Mesh FDTD"*,
   1999 Society Conference of IEICE, B-1-73, September 1999, Chiba.

7. H. Jiang, H. Arai and Y. Ebine(NTT Docomo Inc.), *"Monopole's Input Characteristic due to Offset from center of Cylindrical Radome"*,
   2000 General Conference of IEICE, B-1-86, March 2000, Hiroshima.

8. H. Jiang, H. Arai and Y. Ebine(NTT Docomo Inc.), *"Radome Effect of 2GHz Band 120° Beam Antenna"*,
   2001 General Conference of IEICE, B-1-140, March 2001, Shiga.

9. H. Jiang and H. Arai, *"Optimization of Matching Structure for Top Loaded Monopole Antenna"*,
   2001 Society Conference of IEICE, B-1-100, September 2001, Tokyo.

10. H. Jiang and H. Arai, *"Circular Polarized Patch Antenna with Cross-shaped Slit"*, submitted to 2002 General Conference of IEICE.